MODELING VOLCANIC ASH TRANSPORT AND DISPERSION: EXPECTATIONS AND REALITY

René Servranckx and Peter Chen
Montréal Volcanic Ash Advisory Centre, Canadian Meteorological Centre,
Meteorological Service of Canada

FINAGLE's LAWS OF INFORMATION:
The information you have is not what you want
The information you want is not what you need
The information you need is not what you can obtain
The information you can obtain costs more than you want to pay

1. INTRODUCTION

1.1 Finagle's aphorisms capture the essence of the volcanic ash transport and dispersion modeling problem. Forecasting accurately the transport of airborne volcanic ash is a complex challenge. Yet, improvements in model formulation, a rapid increase in computing power combined with 24-hr real time monitoring meteorological operations have lead to significant improvements in the prediction of airborne volcanic ash. It would be unthinkable to operate today without the use of volcanic ash transport and dispersion models (VATDM).

1.2 The aviation community operates in a very precise and high accuracy environment. Aircraft flying at high speed are separated vertically by only a thousand feet. The time of landing thousand of kilometers away can be predicted to within a few minutes. This naturally leads users to have high expectations for VATDM, given their usefulness and recent successes.

1.3 Users expect VATDM to produce accurate information on where ash is or isn't present both in time and space. As importantly, they expect this information to be delivered in a timely matter.

1.4 What do these expectations mean from a modeling perspective and, more importantly, can VATDM meet them? The objective of this paper is to discuss these points (''reality check''), to present some of the limiting factors and to suggest some areas for improvement.

2. BASIC COMPONENTS OF THE PROBLEM

2.1 In its simplest form, the problem of accurately forecasting ash with VATDM can be expressed as having 3 distinct components:

- VOLCANIC ASH SOURCE
- METEOROLOGY
- TRANSPORT AND DISPERSION

2.2 The **VOLCANIC ASH SOURCE** component comprises all non-meteorological parameters that characterize a specific eruption or a volcanic ash cloud. For example, the volume / mass of ash released in the atmosphere, the duration of the eruption, the vertical and horizontal distributions of the ash around the volcano or in a detached volcanic ash cloud, the base and top of the ash cloud, particle size distribution, etc.

2.3 The **METEOROLOGY** component includes all meteorological parameters (wind fields, moisture, stability, etc.) that are predicted by NWP (numerical weather prediction) models.

2.4 The **TRANSPORT AND DISPERSION** component essentially combines inputs from the previous 2 components, though the use of VATDM, to displace and disperse the volcanic ash in the atmosphere as well as depositing it at the surface using various removal and deposition mechanisms.

3. TIMELINESS AND ACCURACY

3.1 Timeliness is the ability to quickly deliver the information. Its exact definition varies from one user to another according to specific needs. Accuracy is also a relative term for the same reasons. Its definition also depends on whether the approach is qualitative or quantitative.

3.2 In the context of aircraft operating at 700 knots, timeliness translates to having VATDM guidance delivered in a matter of minutes after notification of the eruption. At the same time, accuracy means that VATDM are expected to give precise and exact information on where ash is or isn't present in time and space.

3.3 In the context of the operational, real time application of VATDM, timeliness and accuracy are equally important for aircraft operations. Unfortunately, they are also somewhat counter posing. Timeliness implies that the guidance is made available quickly. A prerequisite for accuracy is that accurate data and information must first be collected and checked before being fed to the VATDM. This however takes time.

3.4 Attaining a balance between timeliness and accuracy is not easy. It can however be helped by quickly issuing a first run based on whatever information is available initially and default source term parameters for the rest. Subsequent runs and updates are then done as new information becomes available.

3.5 Putting aside the timeliness issue, it is clear that the accuracy of the guidance produced by the transport and dispersion component, through the use of VATDM, is highly dependent on the quantitative accuracy of the volcanic ash source and meteorology components that feed it. In short, an accurate quantitative time / space forecast of airborne volcanic ash can not be achieved without accurate quantitative

information from the volcanic ash source and meteorology components.

3.6 The expectations for VATDM to produce accurate information on where ash is located in time and space can be expressed quantitatively in the modeling context in the form ''the volcanic ash concentration at latitude / longitude X in Y hours after the start of the eruption will be Z micrograms of ash per cubic meters at an altitude of W feet''.

3.7 What are the factors that limit or restrict attaining accurate quantitative forecasts of airborne volcanic ash? They are discussed in the next section.

4. LIMITING FACTORS

4.1 Some of the limiting factors for the **VOLCANIC ASH SOURCE** component include:

4.1.1 Eruption parameters are largely unknown and / or poorly quantified. This is especially true for the real time response but also, in many cases, long after the eruption has ended. Large uncertainties exist in the estimate of the total amount of ash released, the time and duration of the eruption, the vertical and horizontal distribution of the ash. Even the height to which the plume rises is at times hard to determine, for example when ice or water clouds are present.

4.1.2 Because many of the world's active volcanoes are located in uninhabited regions, the rapid detection and location of volcanic eruptions are often problematic. In this regard, and aside from limited monitoring instruments such as seismological and infrasound, satellite remote sensing techniques (hot spot identification, ash signature, etc.) are used. However there are practical problems limiting their reliability and coverage (e.g. cloud cover, satellite coverage, signal contamination, detection schemes, day versus night application, etc). Simply put, the remote sensing instruments and tools currently available are not capable of producing an accurate quantitative measurement of the 3D space and time structure of airborne volcanic ash. Even when data are available (for example, estimates of the total volcanic ash mass loading estimated from satellite imagery), there is little or no information on the vertical distribution.

4.1.3 Objective measurements (wind tunnel experiments) of the threshold concentration at which volcanic ash becomes a ''significant" threat to engines or other components of aircraft have not been done. It is likely that the threshold value would vary with type of engine and aircraft. From a scientific point of view, it would be important to conduct such studies but is not clear, from an operational perspective, how this information might be used to improve the VATDM, given the numerous other remaining uncertainties.

4.1.4 A report on the brief and inadvertent encounter of a NASA DC-8 research airplane with a diffuse volcanic cloud 35 hours Mt. Hekla, Iceland erupted in February 2000 provides a fascinating insight on how very low concentrations of volcanic ash can apparently still be damaging (Grindle and Burcham, 2003). The flight crew noted no change in cockpit readings, but the sensitive research instruments onboard the plane detected the diffuse cloud of ash and sulfur dioxide. During the next 3 days, seven other research flights were done in the same region of the Arctic. The sensitive research instruments again recorded traces of the volcanic ash / SO2 cloud but much more diffuse than in the first encounter. Subsequent inspections to the plane lead to the removal and overhaul of the engines at a cost of $3.2 million. Apparently, damage can occur with very little ash.

4.1.5 Because of uncertainties of the source term, the VAACs' guidance charts err on the side of safety and depict hazardous zones relative to low threshold values. This may at times overestimate the actual extent of the volcanic ash cloud. While this approach is prudent from a VAAC perspective, it may be problematic for the Meteorological Watch Offices issuing SIGMETs, and equally for the primary users: air traffic controllers and the airline companies. Decisions based on SIGMETs, while primarily for safety arguments, can also have major economic and other operational implications.

4.1.6 The criterion for displaying volcanic ash on the guidance charts is based on a "visual ash cloud" (ICAO, 1998). Yet, there is no quantitative or scientifically-based definition of what constitutes a visual ash cloud. This problem has been raised on a number of occasions, including international meetings, but there is no simple way of defining it. A visual ash cloud as sighted by a pilot may be different from that detected by a satellite or predicted by a model. Even with an objective definition of ''visual ash cloud'', it is very likely that a single value for all situations would not exist. For a specific situation, the value is likely to change also in time and space. This is especially true for a long lived event where the atmospheric transport would disperse the ash over a large domain. Forecasters can play with contouring of the predicted ash plume or use "ash reduction" schemes for the model source term eruption parameters. The VAAC meteorologist can also adjust the threshold value defining the model output ash plume and the corresponding contouring on the charts based on real time data. Unfortunately, these modifications may at times introduce additional uncertainties and complications for non-specialist users trying to interpret the ash charts.

4.1.7 Eruption heights are often reported in flight levels given its general use by the aviation community. Flight levels are based on what is know as the ''standard atmosphere'' and rely on a number of assumptions. Because of this, there can be significant differences between the flight level reported by an aircraft and the true height with respect to the ground or sea level.

4.2 For the **METEOROLOGY** component, some of the limiting factors are:

4.2.1 The horizontal resolution of Numerical Weather Prediction (NWP) models typically range from a few kilometers for a limited domain / high resolution model to 100 kilometers for global models.

4.2.2 NWP models use a certain number of discrete levels (typically in the range 25 to 60) to represent the vertical component of the atmosphere. This means that meteorological

parameters at a level other than the model levels have to be deduced in one way or another (interpolation, averaging of 2 model levels, etc). Also, there are more levels in the lower portion of the atmosphere. Typically, half of the levels or so are found below 600 hPa.

4.2.3 The fundamental vertical coordinate of most NWP models is pressure (SIGMA and ETA coordinates). The conversion of the wind and temperature fields to flight levels or heights is based on a number of assumptions that have limitations.

4.2.4 The earth's surface features (topography) in NWP models are adjusted to a scale that is consistent with the horizontal and vertical resolution of the models. A very high, steep mountain will therefore be represented as a smoothed, rounder and flatter surface in the NWP model topography. This of course depends on the specific resolution of a model but, as a general rule, there are always differences between reality and what the model sees. A concrete, but somewhat extreme example of this: the topography of the Regional GEM model of the Meteorological Service of Canada for one of its recent operational configurations (24 kilometers horizontal resolution; 28 vertical levels) had its highest surface point in Alaska at 2640 meters. Yet in reality the highest peak, Mount McKinley, reaches 6194 meters!

4.2.5 Accuracy of the predicted fields: Our knowledge of the initial conditions in the atmosphere is incomplete due to a number of factors (limited observational data, errors in measurements, data cut-off deadlines, etc). We are faced with the problem of creating a sufficiently accurate picture of the state of the atmosphere at the outset of the forecast process. Errors introduced at the beginning of the forecast will propagate and amplify at each forecast interval, gradually eroding its accuracy and usefulness. In some situations, a small difference in the initial atmospheric conditions can produced significant differences in the forecasts. While NWP models are generally quite good in their predictions for the initial 24 to 48 hours, some atmospheric flows and patterns are much harder to predict accurately than others.

4.2.6 Another area of errors in NWP models results from a type of approximation called ‘’parameterization’’. It can be defined as the representation, in a dynamic model, of physical effects in terms of admittedly oversimplified parameters, rather than realistically requiring such effects to be consequences of the dynamics of the system. It is done to take into account the large-scale effects of phenomena that are too small to be picked-up at the model's resolution or too complex to be represented exactly. For instance, individual thunderstorms are too small to be forecasted by the model; yet in order to be useful the model must still produce a good approximation of the effects of thunderstorms on large-scale precipitation and temperature patterns. To be successful, the model must integrate an understanding of many different phenomena and their interactions: wind fields; how energy received from the sun is absorbed and transformed by oceans, the ground, the air, and the clouds; how water vapor condensates into clouds and how droplets of water turn to rain, ice and snow; etc. Thus, errors in handling one type of phenomenon can propagate to other parts of the model, or amplify errors in other model sub-systems.

4.3 Limiting factors for the **TRANSPORT AND DISPERSION** component:

4.3.1 The limiting factors presented in sections 4.1 and 4.2 have a clear, direct and important influence on the accuracy of the transport and dispersion component. Many of the factors previously covered also apply to the transport and dispersion component. They will not be repeated here.

4.3.2 At the same time, VATDM also have limiting factors that can be considered as quasi-independent from the source term and meteorology components. For one, VATDM must formulate the source term in one way or another. Even if the source term parameters were perfectly known, the VATDM formulation of the source term would have to be parameterized.

4.3.3 Another limiting factor is that the VATDM, for a number of reasons, often operate on space / time grids that are different from the ones used by the NWP models. This involves a number of interpolations.

4.3.4 Wind fields contribute largely to the horizontal transport airborne volcanic ash but parameterization must be used to account for the dispersal, removal and deposition of ash in time and space.

4.3.5 Real time assimilation of airborne ash plume data is not done by models. This would improve the tracking of ash movement and spreading over longer time spans. The data assimilation techniques are routinely used for other meteorological variables such as wind, temperature and pressure. However, the problem of volcanic ash is more complex and quite similar to total ozone data assimilation. The problem is also compounded by the absence of quantitative data on the vertical and horizontal space and time structure of the ash cloud. Given the important differences in wind speed as a function of altitude, this vertical distribution is, in fact, critical to operational decisions.

4.3.6 The ability of VATDM to predict accurately is also dependent on actual atmospheric circulation and flow into which the volcanic ash is injected. Some flows will be conducive to maintaining an integral ash cloud for many days and hence at great distances from the eruption. These are likely to be easier to forecast.

4.3.7 Another factor to consider is how information is presented to the users. Many operational constraints restrict the type and amount of information that can realistically be provided, especially in real time. This is important because how one interprets information is highly dependant on a number of factors, including the tools and technology available to display the information, how the information is presented and how one looks at the information.

4.3.8 To illustrate this, we present two examples. First look at the image on the right and note how your perception of what it shows is changed once you start looking for faces

(www.banane.be/images.php). As another example, we look at some Canadian Emergency Response Model images showing the ''visual ash cloud'' 45 hours after the start of the Mt Cleveland Alaska eruption in February 2001. The 3 images are based on identical conditions for the volcanic ash source, the meteorology and the dispersion / transport (Simpson et al, 2001). The only difference is the threshold value to display the ''visual'' ash cloud boundary. The units are indicated on each image, in micrograms per cubic meter average volcanic ash concentration for the layer 20 to 35 thousand feet. Note how the perception of where ash is or is not present changes wit the display threshold.

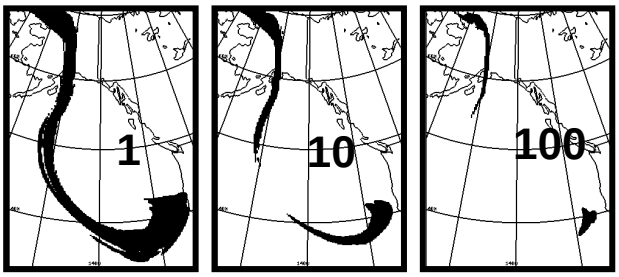

5. DISCUSSION / AREAS FOR IMPROVEMENT

5.1 The large number of uncertainties and limitations described in Section 4 may lead one to have doubts about the usefulness of the VATDM guidance. These are not founded. The qualitative verification of VATDM guidance based on satellite data and other tools has shown it to be of great value.

5.2 It would be unthinkable to operate today without VATDM. This is particularly true in an operational, real-time response context where timeliness in the delivery of the guidance is of key importance. Also, at times, the only guidance available is the one provided by VATDM. For example, we may not be able to detect volcanic ash with satellites when meteorological clouds are present. Also, satellite data may not be available in the area in interest.

5.3 The limitations also point out the importance of not using the guidance blindly. A careful interpretation of the guidance must be done by the user and this can not be done without a good knowledge of the limitations.

5.4 VATDM guidance and remote sensing techniques must be used together. Each can benefit from information provided by the other. But in addition, their simultaneous use is synergetic and sometimes even synergistic. For example, satellite data can help to better define what concentrations should be displayed on VATDM guidance while VATDM can help remote sensing detection by pointing out where ash is likely to be found. This synergy has been demonstrated on a number of occasions.

5.5 Clearly, any improvement that might reduce the uncertainties and limitations listed in section 4 would be beneficial. Listed below are some of the key elements that should be considered in order to maximize the improvements in VAFTD guidance:

5.5.1 Source term – eruption parameters: The reports of the Second and Third International Workshop on Volcanic Ash (Toulouse, May 1998 and September 2003) indicated that substantial improvements could be made in VATDM guidance if the source term estimates were improved. The basic question remains: is it possible to produce quantitative estimates of the source parameters for a specific eruption based on historical events, types of volcanoes, etc? What about the amount of ash released, the vertical and horizontal distributions, the particle size distribution, etc.? We seek the expertise of volcanologists to help answer these questions. If quantitative estimates can not realistically be produced, VATDM will simply continue to use some default parameters. A clear answer to these questions would help bring some closure to the subject.

5.5.2 Source term and Transport / Dispersion: The NASA DC-8 plane encounter with a diffuse volcanic cloud points to the fact that very small ash concentrations can produce damage and highlights he importance of a better definition of the source term. The encounter provides another example of a long-lived volcanic cloud. From a modeling perspective, it raises the question of how far out into the future can VATDM predictions be still considered reliable - even if the meteorological inputs have been updated along the way. For the purpose of immediate alerting, perhaps this is irrelevant. But if unconditional ash-avoidance is the rule, predictions beyond 72-hours would still be relevant - i.e. as long as there is ash, there should be an interest. Obviously, the predictions could be made over longer time periods and with more reliably / credibly if we could assimilate airborne ash information.

5.5.3 Source term - Remote sensing and detection of ash: Any technological advancement that might lead to a better quantitative estimate of airborne volcanic in the horizontal and vertical would have great benefits for VAFTD.

5.5.4 Source term – Assimilation of volcanic ash data: Some exploratory work on volcanic ash assimilation has already been done. For example, Siebert et al. 2002 used the basic idea that the vertical wind shear in the atmosphere (e.g. change of wind speed and / or direction with height) leads to different transport paths of the cloud (or parts of it) at different initial heights. The movement of the ash cloud diagnosed from satellite data and images could then

possibility be used to infer its vertical displacement and hopefully even a vertical distribution. Exploratory work is also being done elsewhere, for example at the NOAA Air Resources Laboratory. How much can be achieved in this area is highly dependant on improvements in the area of remote sensing (section 5.5.3). The reality is that real-time assimilation of volcanic ash data in a meteorological analysis using an objective numerical procedure remains a complex problem that will not be solved quickly.

5.5.5 Meteorology – NWP models: The improvement of NWP models is an ongoing process. Major NWP Centers regularly implement operational modifications to their analyses and forecast systems as a result of advancements in the areas of remote sensing, data assimilation, parameterization, computing power, etc. The vertical, horizontal and temporal resolutions of NWP models are also increased on a regular basis.

5.5.6 Meteorology and Transport / Dispersion – Ensemble forecasting: We already discussed the fact that the guidance skill diminishes with forecast time because of the growth of inevitable uncertainties in the initial conditions, and because numerical models describe in only an approximate way the exact laws of physics. Ensemble Forecasting provides a practical tool for estimating how these errors could affect the guidance. The basic principle is to produce many runs with NWP models and / or VATDM, using slightly different initial conditions to simulate errors in measurements, different parameterization schemes, etc. The results of the ensemble members are then averaged. It has been shown that this way of proceeding produces better guidance than what is obtained by looking at the results of a single model run. Furthermore, a measure of confidence in the average can be obtained from what is called the ''spread'' of the ensemble. It is a measure of how similar or different the various members (i.e. runs) are. A small spread indicates that the runs are similar while a large spread signals large differences. This is important because we know that the accuracy of the guidance is greater when the ensemble spread is small. Ensemble forecasting is already done operationally by major National Weather Centers in the area of NWP models but has not been yet attempted for VATDM. This might be an interesting avenue to explore. At the same time, the timeliness question would also need to be evaluated if ensemble forecasts were done, given that many runs need to be executed.

6. CONCLUSION

This paper presented the main factors that influence and sometimes limit VATDM. Despite the limitations and uncertainties, VATDM have proven to be of great value, to the point where it would be unthinkable today to operate today without them. At the same time, users must be aware of the limitations when using VATDM outputs. Another important point is that VATDM can not be used blindly. In fact, there is a synergistic benefit in using VATDM in conjunction with other sources of information.

REFERENCES

ICAO, 1998: International Civil Aviation Organization International Standards and Recommended Practices - Meteorological Service for International Air Navigation - Annex 3 to the Convention on International Civil Aviation (July 1998), 92 pp.

Grindle, T.J. and F. W. Burcham, 2003: Engine Damage to a NASA DC8-72 Airplane from a High-Altitude Encounter with a Diffuse Volcanic Ash Cloud. NASA/TM-2003-212030, August 2003, 27 pages. (www.dfrc.nasa.gov/DTRS/2003/PDF/H-2511.pdf)

Siebert, P., A. Frank and R. Servranckx, 2002: Satellite Data Assimilation for Volcanic Ash Forecasts. Poster presented at the European Geophysical Society General Assembly, Nice, France, April 2002. (A PDF version is available on request).

Simpson, James J., Hufford, Gary L., Pieri, David, Servranckx, René, Berg, Jared S., Bauer, Craig: The February 2001 Eruption of Mount Cleveland, Alaska: Case Study of an Aviation Hazard, Weather and Forecasting 2002 17: 691-704.

DISCREPANCIES BETWEEN SATELLITE DETECTION AND FORECAST MODEL RESULTS OF ASH CLOUD TRANSPORT: CASE STUDY OF THE 2001 ERUPTION OF MT. CLEVELAND VOLCANO, ALASKA

David J. Schneider, USGS-Alaska Volcano Observatory, Anchorage, AK, USA
Rene Servranckx, Environment Canada, Montreal VAAC, Montreal, Canada
Jeff Osiensky, National Weather Service, Anchorage VAAC, Anchorage, AK, USA

Volcanic ash transport and dispersion models are used in conjunction with satellite image data to forecast the movement of potentially hazardous volcanic ash clouds. Although these sources of information typically agree, discrepancies do occur. These discrepancies cause difficulty in accurately forecasting ash movement, especially in cases wherein model results indicate the presence of ash but none is detected in satellite data. A case study of the February 19, 2001 eruption of Mt. Cleveland volcano, Alaska is presented utilizing results from the CANERM dispersion model and GOES satellite images. For this eruption, the extent of volcanic ash predicted from ash transport and dispersion models was much larger than the extent detected in satellite image data. A discussion of the operational forecast decisions and information releases that were made during this eruption will illustrate the challenge faced in these instances: Whether to issue warnings based solely on model results or solely on satellite data.

ASSESSING VOLCANIC ASH HAZARD BY USING THE CALPUFF SYSTEM

Sara Barsotti[(1)], Augusto Neri[(1)], and Joe Scire[(2)]
[(1)] Centro di Modellistica Fisica e Pericolosità dei Processi Vulcanici,
Istituto Nazionale di Geofisica e Vulcanologia, via Della Faggiola 32, 56126 Pisa, Italy
[(2)] Earth Tech Inc., Concorde, MA USA

1. Introduction

Nowadays the presence of volcanic ash in the atmosphere represents a serious risk for the aviation. A large number of volcanoes is indeed situated near main commercial and civil air routes; for examples the regions of North-West America, Alaska, and the Kamchatka Peninsula. In Europe, the problem is probably less relevant than in other parts of the world. However, just in the last few years, the explosive activity of Mt.Etna, Sicily (Italy), has focused the attention of volcanologists and air traffic operators to the problem of an active volcano located very close to two international airports (Catania and Sigonella) as well as to the city of Catania and many other towns.

Although this problem has drawn the attention of the scientific community for many years, a reliable instrument for forecasting ash cloud movements and, therefore, for avoiding plane encounters does not exist yet (Williamson, this issue). To this aim a number of computer codes able to describe the temporal and spatial evolution of the ash plume have been developed worldwide in the last 15 years. Some of them are actually in use at the Volcanic Ash Advisory Centers (VAACs), such as CANERM (which is operative at the Canadian Meteorological Centre), MEDIA (operative at Toulouse Meteo France), NAME (operative at London Met Office) and VAFTAD (developed by NOAA ARL and in use at the Washington and Anchorage VAACs). CANERM (Simpson et al., 2002) is a 3D Eulerian model used for medium- and long-range transport which assumes a virtual source described by a distribution of mass in the vertical direction. Similarly, MEDIA (Piedelievre et al., 1990) is an Eulerian atmospheric transport/diffusion model focused on the long-range dispersal of particles ejected from a source at a given altitude. Vice versa, NAME (Watkin et al., this issue) is a Lagrangian particle model that can work on either regional or global scales and is able to consider areal as well as point-like sources. Finally, VAFTAD (Heffter and Stunder, 1993) is a 3D time-dependent Eulerian model which needs the maximum height reached by the volcanic column to model the source, as input. In addition to those used at the VAACs a few more models have been developed for or applied to the problem of volcanic ash. For instance, the well-known model PUFF, (Searcy et al., 1998), currently used at the University of Tsukuba (Japan) in collaboration with the Japan Meteorological Agency and at the U.S. National Weather Service, Alaska, describes the movements of a collection of discrete ash particles representing a sample of the eruption cloud by using a Lagrangian scheme and treating the source as a virtual pre-assigned vertical distribution of mass. Similarly, HYSPLIT (Draxler and Taylor, 1982, Draxler and Hess, 1998), developed at the NOAA Air Resources Laboratory describes, by a Lagrangian approach, the evolution of puffs (containing material particles with diameters up to 30μm) without taking account of buoyancy effects. Finally, FALL3D (Costa and Macedonio, this issue), is an Eulerian advection/diffusion code, developed at Osservatorio Vesuviano-INGV, that uses a virtual point-like or vertical source of mass on air, and that was specifically designed for the estimation of in-air ash concentration and ground deposition at medium and long distances from the source.

From such a brief summary it is clear how most of the dispersal models in use are relevant only to medium- and long-distance dispersal areas and do not account for the influence of volcano orography on the wind flow field. In addition, none of the above models describes the dynamics of the buoyant volcanic plume thus making the definition of the virtual source quite subjective.

The aim of this work is to present a new modelling system, called CALPUFF, able to describe the movements of the ash cloud, as well as the in-air ash concentration and ground deposition, generated by a given source (Scire et al., 2000). As several other codes used in volcanological applications, CALPUFF has been originally developed as an air quality modelling code for transport of pollutants and then applied to several other environmental problems. The CALPUFF System is composed of three main parts; the geophysical pre-processor, the meteorological processor (named CALMET) and the Lagrangian dispersal model (named CALPUFF). The dispersal model treats the ash cloud as a discrete series of packets of particles, or *puffs*, which are advected by the prevailing winds and, at the same time, diffuse in

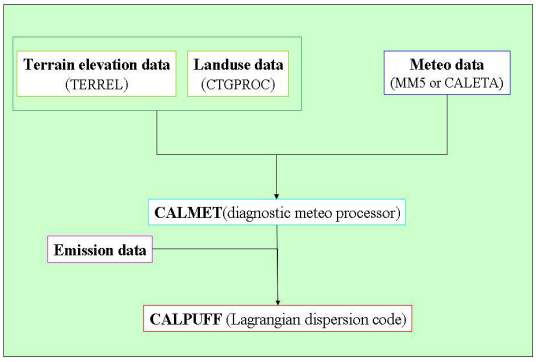

Figure 1. The flowchart of the CALPUFF System as used in our simulations.

the atmosphere. In addition, CALPUFF is able to describe the dynamics of the rising buoyant plume, and therefore the altitude of the virtual source, through the solution of a full non-Boussinesq form of the transport equations. Finally, CALPUFF can describe the ash dispersal dynamics using very refined computational grids (with a final resolution up to 1 km or less), while keeping the execution time very short (of the order of minutes). In the following sections the main features of the system and a first application to a real eruption will be presented.

2. The CALPUFF System

With the terms "CALPUFF System" here we mean the whole numerical procedure that from meteorological and geophysical input data computes the concentration of the ejected material in the atmosphere and at the ground. The CALPUFF system was developed by the Earth Tech Inc. in the '90 and it is available on line at the website http://www.src.com/calpuff/calpuff1.htm. CALPUFF is a quite complex model composed of a great number of sub-processors. Figure 1 shows the basic configuration of the modelling system as we have used it in our study. The procedure starts with the elaboration of the geophysical information, as terrain elevation and land-use data. This procedure is run only once after the choice of the computational domain is made. The geophysical data are then processed by two different programs in order to make them readable to another pre-processor (named MAKEGEO) that merges all the data and produces a single geophysical file for the meteorological processor CALMET.

In parallel with the elaboration of the geophysical data, the processing of the meteorological data occurs in order to provide CALMET of the necessary input data every three hours. The meteorological processor CALMET is a diagnostic code; this means that it computes the values of the meteorological variables on a finer grid without solving the time-dependent equation of motion. CALMET, in particular, works on two steps that refine and correct an initial guess field typically provided by a prognostic code. In the first step the initial data are interpolated on a grid usually much finer than the one used in the mesoscale models and the effects of the local orography are accounted for. In the second step, data collected at the ground or at upper air stations, when available, are considered in order to correct the computed wind field through an objective analysis that assigns appropriate weight to each data. The output provided by CALMET contains the wind field and the other micro-meteorological variables hourly and on a grid in a terrain-following coordinate system with a vertical and horizontal user-defined resolution. This file, together with the one containing the data related to the source, is fed as input to the core of the system: the CALPUFF dispersal model.

This is a Lagrangian dispersion code that treats the emitted material as a sequence of *puffs* each containing a discrete quantity of particles. Each hour a finite number of puffs are emitted and subjected to wind advection, vertical and horizontal diffusion and removal of material due to gravity as well as wet deposition. The user is then free to define a grid of receptors or choose discrete receptors at which concentration and ground deposition will be calculated. Before illustrating the way in which the code computes the ash concentration at a given receptor the treatment of the buoyant plume leaving the crater is briefly described.

CALPUFF is indeed able to handle an areal source which emits in the atmosphere hot material under the action of inertia and buoyancy. To this aim the code solves, each hour of simulation, the three equations of conservation of mass (eq.(a)), momentum (eq.(b)) and energy (eq.(c)) here expressed as (refer to the original work of Hoult and Weil (1972) for a detailed description of them):

$$\frac{d}{ds}(\rho U_{sc} r^2) = 2r\alpha\rho_a |U_{sc} - U_a \cos\varphi| + 2r\beta\rho_a |U_a \sin\varphi| \quad \text{(a)}$$

$$\frac{d}{ds}(\rho U_{sc} r^2 (u - U_a)) = -r^2 \rho w \frac{dU_a}{dz} \quad \text{(b)}$$

$$\frac{d}{ds}(\rho U_{sc} r^2 w) = g r^2 (\rho_a - \rho)$$

$$\frac{d}{ds}(\rho U_{sc} r^2 (T - T_a)) = \rho \frac{d\eta_a}{dz} w r^2 + \frac{Q}{c_p} r^2 \quad \text{(c)}$$

At this stage, only the hot gas of the plume has been considered in the above equations; this assumption will be removed in the future when the presence of particles will be explicitly considered. The code can also treat the case of non-steady emission of ash from the crater once an input file containing all the temporal variations of the source variables is provided.
Once the plume has reached its maximum height the puff description begins. At the emission point, localized at a given downwind distance from the vent and at an effective height above the ground as computed by the above described source model, the pyroclastic material is released as a series of puffs whose dynamics are described in a Lagrangian way.
During one sampling time step (the time interval at which the ash concentration is computed) the puff diffuses and its contribution to the concentration at each receptor defined is calculated. The mathematical expression of this contribution is the following Gaussian function corrected to account for vertical and horizontal diffusion as well as for gravitational settling (Scire et al., 2000):

$$C = \frac{Q}{2\pi\sigma_x\sigma_y} g \exp[-d_a^2/(2\sigma_x^2)]\exp[-d_c^2/(2\sigma_y^2)] \quad \text{(d)}$$

The quantity of mass in the puff is represented by the variable Q and it varies with time because of the removal of material due to gravity. CALPUFF permits to describe the behaviour of different granulometric classes characterized by different diameters, densities, and, of course, settling velocities. However, the present version of CALPUFF is limited to the consideration of particles up to a few tens of microns. In eq. (d), d_a and d_c are the downwind and crosswind distances between the puff centre and the receptor, g is the so-called *vertical term* that takes into account the vertical diffusion due to the mixing lid, and the two sigmas represent the horizontal diffusion due to turbulent atmospheric motions, buoyancy and lateral dimension of the areal source.
Finally, it is worth noting that the CALPUFF System has been validated through extensive comparison of model predictions to experimental data such as the Cross-Appalachian Tracer Experiment (CAPTEX). Due to the very good performance of the model, the U.S. Environmental Protection Agency (Scire et al., 2000) has proposed the CALPUFF modelling system as a guideline model for regulatory application involving long-range transport and in-near field applications where non–steady-state effects may be important.

3. A first CALPUFF application to Mt.Etna, Sicily, Italy

A first application of the CALPUFF System, as it stands at this time, to a recent eruption of Mt. Etna has been carried out in order to a preliminary assessment of the capabilities and limits of the code. As a consequence this application has to be interpreted just as a first step of the research work we have planned in order to develop an appropriate version of CALPUFF System to be used for volcanic purposes.
The eruption of Mt. Etna we refer to started on 18th July 2001 and produced a quite intense explosive activity for about one week. This activity was characterized by an almost continuous injection of ash and lapilli in the atmosphere with the formation of ash columns up to about 5 km (Coltelli et al., 2001; Coltelli, this issue). As mentioned above, the ash and lapilli blanketed the city of Catania, producing major problems to the city airport, whereas the finer particles reached the coasts of Africa. The evolution of the ash cloud was closely observed and many satellite images are available for a first comparison with the model predictions.

3.1. Input data and computational parameters

Geophysical, meteorological, and source data were defined in order to carry out the dispersal predictions. Geophysical data were adopted from USGS. In detail, GTOPO global data and global land-use data with a resolution of about 900 m were implemented. SRTM data for terrain elevation were also implemented producing very similar results. As far as the meteorological data, two different datasets were used: one provided by NOAA and the other one by ECMWF. Both datasets had a spatial resolution of 2.5*2.5 degrees and a temporal resolution of 6 hours (both of them were produced by reanalysis studies). This double choice was actually due to our interest in investigating the sensitivity of CALPUFF results on meteorological data. Finally, in Table 1 are reported the vent data used as input data and boundary conditions for the solution of eqs. (a)-(c) as well as the main puff parameters.
The computational domain is composed by 100*100 cells with a grid spacing of 2km and twelve vertical levels not uniformly spaced. It should also be noted that, so far, we have used CALMET in a no-observational mode, i.e. skipping the objective analysis described above.

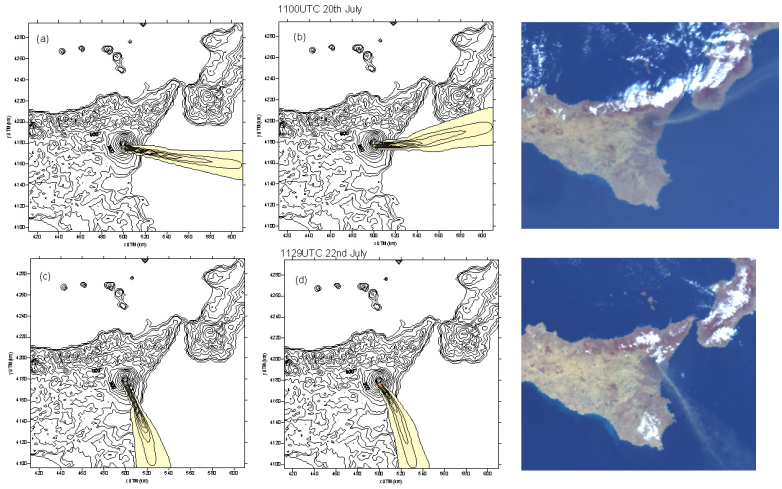

Figure 2. Comparison between CALPUFF modelling results and satellite images on July 20 (top) and July 22 (bottom).The first column refers to the NOAA meteo data, the second column to the ECMWF meteo data.
The minimum value chosen for the graphic is equal to 10^-7 kg/m^3

Table1. Vent input data and puff parameters as used in the simulations (Coltelli et al., 2001, IAVCEI 2004).

Vent velocity	25-75 m/s
Vent temperature	100-300 °C
Vent radius	25-75 m
Ground elevation	2550 m
Vent height a.g.	100 m
Emission rate	10^5 kg/s
Particle diameter	3-64 µm
Particle density	2500 kg/m^3

3.2. Main results

The following aspects of the dispersal process have been investigated by simulating the eruption over five days (starting at 00UTC 20th till 24UTC 24th of July): 1) the main large-scale features of the dispersal, 2) the sensitivity of results on the meteorological datasets used and 3) the model capability of describing the rising phase of the plume.
Model results, shown in form of animations, clearly describe the temporal evolution of the ash cloud that results to be mostly affected by the wind direction at the level of puff emission. The predicted dispersal direction is for long period consistent with observations. With full particular, observations indicate that, for all the 20th of July, the plume is directed in the N-E direction whereas it moves in the S-E direction for the remaining days interesting repeatedly the city of Catania and the Fontanarossa Airport. In addition, in the early morning of July 22 a plume bifurcation, which disappeared within few hours, was observed in satellite images.

Figure 2 shows an example of comparison between model predictions and observations with satellite images. Plots (a) and (b) refer to 11UTC of July 20, whereas plots (c) and (d) refer to 1130UTC of July 22. All plots show the cumulative concentration (kg/m^3), integrated over the vertical levels, as calculated by CALPUFF. In particular, plots (a) and (c) were generated using NOAA data, whereas plots (b) and (d) were generated using the ECMWF data. From the figure it is evident that the comparison is quite good for both datasets even though, for July 20, the data provided by ECMWF seem to produce results which agree more with the observations. In this case, a deeper analysis of the meteorological conditions showed that, even though at that time the heights of puff emission were very similar, some hours before, the difference in wind direction in correspondence with the emission heights was about 30 degrees.
The dynamics of the rising plume was also analysed due to its importance in the determination of the puff emission point. In particular, the temporal evolution of the effective height and the downwind distance of the emission point from the vent was investigated. Results showed that these two variables are strictly related - when one increases the other decreases - and strongly depend on meteorological conditions such as the mixing layer depth (that in turn depends on the hour of the day).
Finally, by using an appropriate set of receptors it was possible to investigate the spatial and temporal distributions of ash concentration in the atmosphere. In particular, the horizontal and vertical distribution along the dispersal axis was analysed. It was found that, even at constant emission rate, the observed variability, in time and distance from the vent, of the maximum ash concentration is strongly affected by

the temporal movements of the emission point as well as by the meteorological conditions and the turbulent processes that control the ash diffusion.

4. Conclusive remarks

In the light of the above described modelling capabilities and results obtained from its first volcanological application, the CALPUFF modelling system appears to be a very promising tool for the real-time monitoring and forecasting of ash dispersal dynamics produced by a weak plume. The possibility to describe the dynamics of the rising plume, to account for the volcano topography and direct measurements of meteorological conditions, to work with a user-defined spatial resolution, to obtain results in near real-time, are some of its more attractive features. In addition, the ability of reproducing correctly the large-scale evolution of the ash cloud movements underlies the efficiency of the meteorological processor CALMET in generating a reliable wind field even using a low resolution meteorological input data. However, the sensitivity analysis on the meteorological dataset highlights the importance of using high-resolution meteo data, as well as an accurate description of plume rise, in order to get a correct prediction of ash dispersal. Future works should also focus on the extension of the code to the modelling of coarse ash and lapilli in order to describe the more proximal fallout.
Finally, it is worth mentioning that an effective progress in the modelling and forecasting of ash dispersal appears strictly tied to the definition of accurate volcanological datasets to be used in model validation studies as well as to the carrying out of real-time measurements of the plume.

Acknowledgements
This work has been partially supported by Dipartimento di Protezione Civile, Gruppo Nazionale per la Vulcanologia, Italy, Framework Programme 2000-2003, project no. 9, and by Ministero dell'Istruzione dell'Università e della Ricerca, Italy, FIRB project no. RBAU01M72W.

References

Coltelli M., 2004: Recent Etna's explosive eruptions threaten seriously aviation in central Mediterranean region, Proc. *2nd International Conference on Volcanic Ash and Aviation Safety*.

Coltelli M., Del Carlo P. and Macedonio G., 2001: The plume of the 2001 eruption of Etna: observation, modelling and impact on Catania airport operations, Proc. *Assemblea Generale del Gruppo Nazionale per la Vulcanologia.*

Costa A. and Macedonio G., 2004: FALL3D: A numerical model for volcanic ash dispersion in the atmosphere. Proc. *2nd International Conference on Volcanic Ash and Aviation Safety*.

Draxler R.R. and Taylor A.D., 1982: Horizontal dispersion parameters for long-range transport modelling, J. Appl. Met., 21, 367-372.

Draxler R.R and Hess G.D., 1998: An overview of the HYSPLIT_4 modelling system for trajectories, dispersion and deposition, Austral. Meteorol. Mag., 47, 295-308.

Heffter J.L and Stunder B.J.B., 1993: Volcanic ash forecast transport and dispersion (VAFTAD) model, Weath. Forecast., 8, 533-541.

Hoult D.P. and Weil J.C., 1972: A turbulent plume in a laminar crossflow, Atmos.Environ., 6, 513-531.

IAVCEI Tephra Group webpage 2004: www.soest.edu/IAVCEI-tephra-group/.

Piedelievre J.P., Musson-Genon L. and Bompay F., 1990: MEDIA- An Eulerian model of atmospheric dispersion: a first validation on the Chernobyl release, J. Appl. Meteor., 29, 12, 1205-1220.

Scire J., Strimaitis D.G. and Yamartino R.J., 2000: CALPUFF user's guide.

Searcy C., Dean K. and Stringer W., 1998: PUFF: a Lagrangian trajectory volcanic ash tracking model, J. Volcanol. Geotherm. Res., 80, 1-16.

Simpson J.J., Hufford G.L., Servranckx R., Berg J.S. and Bauer C., 2002: The February 2001 eruption of Mt. Cleveland, Alaska: Case study of an aviation hazard, American Meteorol. Soc., 17, 691-704.

Watkin S., Ryall D., Watkin H., Champion H., Wortley S. and Gait N., Volcanic ash monitoring and forecasting at the London VAAC, Proc. *2nd International Conference on Volcanic Ash and Aviation Safety.*

POTENTIAL OF THE ATHAM MODEL FOR USE IN AIR TRAFFIC SAFETY

[1]Christiane Textor, [2]Gerald GJ Ernst, [3]Michael Herzog, [4]Andrew Tupper

[1] Lab. Sciences du Climat et de l'Environnement, CEA-CNRS, Paris, France
[2] Geological Institute, University of Ghent, Krijgslaan 281/S8, B-9000 Gent, Belgium
[3] Dept. of Atmospheric, Oceanic, and Space Sciences, University of Michigan, Ann Arbor, USA
[4] Bureau of Meteorology, Darwin, Northern Territory, Australia, and School of Mathematical Sciences, Monash University, Victoria, Australia

Abstract

Numerical models used by the VAAC centers often fail to accurately predict volcanic ash dispersal, because they do not include sufficient information on the initial ash distribution in the proximity of the volcano. In addition, ash dispersal is assumed to be determined by the atmospheric background conditions only, and effects of the eruption on the ambient motions are neglected.

In this paper we present the eruption column model ATHAM (**A**ctive **T**racer **H**igh resolution **A**tmospheric **M**odel). This model simulates the processes within the eruption column, and the dispersal of the ash cloud on spatial scales of some hundreds of kilometers during some hours. We show the development of the ash cloud and of hydrometeors during a plinian eruption simulated with the ATHAM model.

ATHAM can be used to improve understanding of in-column processes, and of the initial ash distribution. Better initialization of the usual VAAC models will lead to more accurate forecasts of ash dispersal.

1. Introduction

Various numerical models are used by VAAC centers to forecast volcanic ash dispersal for air traffic safety (e.g., VAFTAD, NAME, CANERM, HYSPLIT, PUFF, etc.). These emphasize the role of background atmospheric motions and ignore the role of the eruption dynamics itself upon dispersal. The initial ash distribution close to the volcano is often not well known and has thus to be prescribed in a simplified, sometimes unrealistic way. These models tend to have a physically unsound source term description. Their forecasts often fail to accurately predict the extent of the volcanic ash cloud, even for small explosive eruptions (e.g., Hekla 2000 eruption, Iceland [*Grindle and Burcham*, 2002; *Grindle and Burcham*, 2003]), especially in the first six hours of spreading, with source errors propagated for the 12h+ forecasts. For full-blown plinian eruptions or any moderately explosive eruptions in weak winds, the models often fail to predict ash dispersal with satisfactory accuracy, because of imprecise observations of the initial plume height. On the other hand, the ATHAM model is a numerical eruption column model that predicts the rise of volcanic gases, ash and hydrometeors from the lithosphere to the height neutral buoyancy column, and the atmospheric dispersal of the plume during the eruption and some hours afterwards. The model is based on first physical principles and includes eruption dynamics, cloud meteorology and chemical aspects. ATHAM can be run quickly on a fast PC, has a flexible modular structure ideal for 1) testing against observations and 2) comparisons with simple numerical simulations and laboratory experiments. In the following, we will introduce the ATHAM model, and then show some results form numerical simulations.

2. Dynamics

ATHAM has been designed to simulate the dispersal of a volcanic eruption [*Graf et al.*, 1999; *Herzog et al.*, 1998; *Herzog et al.*, 2003; *Oberhuber et al.*, 1998]. The simulation time is some hours covering spatial scales of some hundreds of kilometers. ATHAM is a non-steady state, non-hydrostatic model. It solves the full set of Navier-Stokes equations for the multiphase system. Sound waves are included, because the flow can be supersonic in the high-density lower parts of the eruption column. Tracers (liquid and solid particles and gases) can occur in very high concentrations in the erupted gas-particle mixture. They act on the dynamics of the system by altering the mixture's density and heat capacity. The description of this system requires a large set of dynamic and thermodynamic equations for each component and the interactions between them. However, the gas-particle mixture can be assumed to be in thermal and dynamical equilibrium[1], on the condition that all particles are smaller than about a millimeter. Based on these assumptions, the

[1] Thermal equilibrium: All tracers have the same in-situ temperature. Dynamical equilibrium: The model does not resolve accelerations between tracers and gas. Tracers move with their terminal fall velocity, however, the mixture can be accelerated as a whole.

equations have only to be solved for volume mean quantities. For each active tracer one additional transport equation is needed that takes into account the tracer's fall velocity. Active tracers and dynamical variables are coupled through the bulk density and the heat capacity of the mixture.

To avoid conflicts with the model assumptions processes in the high pressure, hot temperature regime within and close to the crater cannot be resolved, and the topography of the volcanic vent has to be neglected. The simulations start just after pressure adjustment to atmospheric values, hence we do not prescribe any overpressure. Typically, decompression takes place within a vertical distance of some jet radii above the vent. Hence, we can neglect the topography of the volcanic crater and simply use a flat surface. Due to the low gas content of the erupting gas-particle-mixture, the temperature does not change significantly during decompression [*Woods and Bower*, 1995]. In an explosive eruption, the vertical velocity after decompression at the base of the eruption column is about twice the speed of sound for a freely decompressing jet. If the apex angle of the crater is small, the flow behaves like a high-speed supersonic flow in a divergent nozzle and the velocity can be even higher.

3. Turbulence

A turbulence closure scheme describes sub-scale turbulent processes in the eruption column [*Herzog et al.*, 2003]. Turbulent exchange coefficients are predicted for each prognostic quantity. The strong influence of buoyancy forces and vertical transports in the eruption column is represented by differentiating between horizontal and vertical turbulent exchange. Turbulent disequilibria are possible, and anisotropic effects are included in the formulation of turbulent kinetic energy. High tracer concentrations as well as supersonic effects at low Mach numbers are taken into account. The turbulent exchange coefficients are derived from a set of three coupled differential equations for the horizontal and vertical turbulent energy, and the turbulent length scale.

4. Cloud microphysics

The development of liquid and frozen meteorological clouds and precipitation is simulated. The effect of latent heat release on the dynamics is taken into account [*Graf et al.*, 1999; *Herzog et al.*, 1998; *Textor et al.*, 2004]. Two types of schemes can be alternatively used in ATHAM. The bulk scheme [*Herzog et al.*, 1998] predicts the mass mixing ratio of liquid and frozen hydrometeors, and is for suitable for the investigation of latent heat effects on the eruption column dynamics. The more complex two-ment-scheme [*Textor et al.*, 2004] predicts both the mass mixing ratio and the number concentration, and offers the possibility to simulate interactions between volcanic particles and hydrometeors. This scheme can be used to examine the microphysical properties of volcanic eruption clouds under different volcanic and environmental conditions.

5. Ash aggregation

In the current version of ATHAM, volcanic particles are assumed to aggregate as soon as they are coated with water or ice, with the hydrometeors acting as adhesive, thus forming larger hydrometeor-ash aggregates [*Textor et al.*, 2004]. The aggregation coefficients (describing the ratio of successful particle growth resulting from a theoretical particle collision) are approximated with the parameterizations commonly used in cloud microphysics. These values are modified with a simple function depending on the amount of hydrometeor available at the particle. The inclusion of this wet or icy aggregation process leads to more realistic sedimentation features.

6. Gas scavenging

The scavenging module calculates the dissolution of volcanic gases (SO_2, HCl, H_2S, and HBr) by liquid droplets and their incorporation into ice particles. The kinetics of the phase transfer and the subsequent dissociation in the liquid phase is considered as a function of the drop acidity. In addition, incorporation into ice particles is taken into account. Gaseous compounds enter the ice phase via co-condensation of water vapor and gases at growing ice. The concentration of volcanic gases in ice is then rather ruled by phase transfer kinetics than by the low equilibrium solubility. The redistribution of species contained in hydrometeors due to microphysical processes is included [*Textor et al.*, 2003a; *Textor et al.*, 2003b].

7. Model concept

The solution of the complete Navier-Stokes equation is computed on a Cartesian Arakawa C grid [*Mesinger and Arakawa*, 1976] using a Eulerian method. An implicit time stepping scheme is used (Cranck-Nicholson, 25% forward, 75% backward). A parallel iteration of the dynamic quantities accounts for the temporal coupling of the equations with updated density. The conservation of mass and momentum is explicitly guaranteed by applying the flux

form for the equations of motion and continuity of the tracers. The time step is automatically adapted to satisfy the Courant-Friedrichs-Lewy criterion (with CFL<= 0.8) and typically varies between 0.1 and 10 sec. A grid stretching allows using a higher spatial resolution in the model center than at the boundaries. The grid distances increase from some hundreds of meters to some kilometers. The Neumann boundary condition (fixed derivatives, open for sound waves) is applied at the lateral boundaries. We use a fixed bottom, including tracer deposition as lower boundary condition. Pressure and temperature anomalies are damped in the upper model levels.

The ATHAM model can be run in fast, two-dimensional versions for sensitivity studies. The first version in Cartesian coordinates represents a vertical slice of the three-dimensional model. The use of second two-dimensional version in cylindrical coordinates allows for a more realistic dilution of the eruption column in an atmosphere at rest, but cross-wind effects cannot be studied. The most realistic three-dimensional version has been parallelized for efficient use on multi-processor computers [*Herzog et al.*, 2000].

The ATHAM model is written in a modular structure. It is easy to add additional modules of different levels of complexity for specific investigations.

8. Simulations with the ATHAM model

For the simulation we present here, the ATHAM model was initialized with horizontally homogeneous profiles of temperature, relative humidity and wind representative for a tropical atmosphere, as shown in Figure 1.

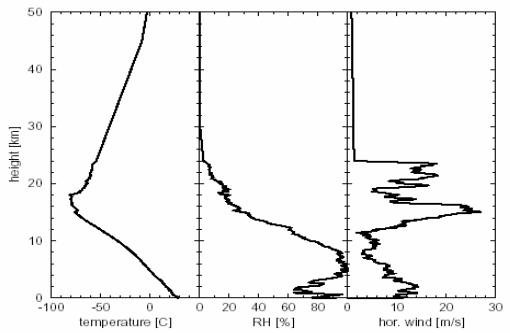

Figure 1: Atmospheric background conditions taken from [*McClatchey et al.*, 1972].

A plinian eruption of 60 min was simulated [*Herzog et al.*, 2003]. The model domain was 250x200x50 km3, with 127x107x127 grid points. Typical plinian conditions prescribed at the eruption column base are given below.

- Mountain height: 2500m,
- Width of eruption column base: 300m,
- Temperature: 1073 K,
- Gas fraction: 6 % by mass,
- Water vapor fraction of tot. gas: 50% by mass,
- Bulk density of the gas particle mixture: 3.1 kg/m3,
- Vertical velocity at eruption column base: 250 m/s,
- Mass eruption rate: ~5.55 107 kg/s,
- Particle density: 2000 kg/m3,
- Three particle classes, 1/3 by mass each,
- Particle diameter: 10, 200, and 4000 μm.

Figure 2 shows results from a three dimensional simulation (see also [*Herzog et al.*, 2003]) at three different times for volcanic ash and for hydrometeors. The ash plume is observed from 10-km altitude, that of the hydrometeors from somewhat lower. The background wind blows from the left side along the lines shown on the ground. The eruption column penetrates the tropopause at about 17 km after about 5 min of eruption. The average vertical velocity in the central rising zone is larger than 100 m/s. An orographic cloud, which is partly entrained into the plume, can be seen on the right of the eruption column between 5 and 10 km in figure 2b. An ice cloud forms in the umbrella region (figures 2b, 2d, and 2f). After 30 min of eruption, the three particle size classes occur at different heights, the umbrella region consists mainly of fine ash particles (figure 2c). Larger particles leave the umbrella region more quickly due to sedimentation, or do not even reach the height of neutral buoyancy. At 70 min of simulation, this separation of large particles from the fine ash and gases is even more evident (figure 2e). A large ice cloud has developed in the stratosphere. Most of the hydrometeors in the eruption column are in the frozen state (figure 2f).

9. Conclusions

In this paper, we have presented the concept of ATHAM model and the modules available for cloud microphysics, ash aggregation and scavenging of volcanic gases. In addition, codes for gas phase chemistry and for radiative transfer calculations exist [*Trentmann et al.*, 2003a; *Trentmann et al.*, 2003b]. We have shown results from a three-dimensional simulation of a plinian eruption in a tropical environment. These three-dimensional simulations remain to be carefully tested against volcanological observations. We plan to simulate a well-observed eruption and the first hours of ash dispersal under realistic ambient conditions. An earlier evaluation of results from the simpler two-dimensional, axis-symmetric

version confirmed that the results are relatively robust, and three-dimensional fire-simulations have been successfully tested against data [*Trentmann et al.*, 2002].

The ATHAM model has been used for the examination of specific processes and of the parameters controlling them within the rising eruption column, and during plume dispersal in the atmosphere. Applications included investigations on the influence of the ambient conditions on the plume development [*Graf et al.*, 1999], on cloud microphysics [*Herzog et al.*, 1998], gas scavenging [*Textor et al.*, 2003a; *Textor et al.*, 2003b] and on ash aggregation [*Textor et al.*, 2004].

Results from sensitivity studies using ATHAM provide insights into cloud and aggregation processes, and of ash removal within the eruption column (see extended abstract of A. Tupper et al. in this volume). These help to improve the source term matrix of the VAAC ash forecasting models and thus to more accurately forecast ash for air traffic safety.

10. References

Graf, H.-F., M. Herzog, J.M. Oberhuber, and C. Textor, The effect of environmental conditions on volcanic plume rise, *JGR*, *104*, 24309--24320, 1999.

Grindle, T., and F.W.J. Burcham, Even Minor Volcanic Ash Encounters Can Cause Major Damage to Aircraft, *ICAO journal*, *57* (2), 12-14, 2002.

Grindle, T., and F.W.J. Burcham, Engine Damage to a NASA DC8-72 Airplane From a High-Altitude Encounter With a Diffuse Volcanic Ash Cloud, *NASA/TM*, *2003-212030*, 27, 2003.

Herzog, M., H.-F. Graf, C. Textor, and J.M. Oberhuber, The Effect of Phase Changes of Water on the Development of Volcanic Plumes, *JVGR*, *87*, 55--74, 1998.

Herzog, M., J.M. Oberhuber, and H.F. Graf, A prognostic turbulence scheme for the non-hydrostatic plume model, *JAS*, *60*, 2783--2796, 2003.

Herzog, M., C. Textor, and M. Antonelli, Modelling Volcanic Eruption Plumes, *HPC News*, *13*, 2000.

McClatchey, R.A., R.W. Fenn, J.E.A. Selby, F.E. Volz, and J.S. Garing, Optical properties of the atmosphere, 3rd ed., 1972.

Mesinger, F., and A. Arakawa, Numerical methods used in atmospheric models, *GARP*, *17*, 1976.

Oberhuber, J.M., M. Herzog, H.-F. Graf, and K. Schwanke, Volcanic Plume Simulation on Large Scales, *J. Volcanol. Geotherm. Res.*, *87*, 29--53, 1998.

Textor, C., H.-F. Graf, M. Herzog, and J.M. Oberhuber, Injection of Gases into the Stratosphere by Explosive Volcanic Eruptions, *JGR*, *108* (D19), 10.1029/2002JD002987, 2003a.

Textor, C., H.-F. Graf, M. Herzog, J.M. Oberhuber, W.I. Rose, and G.G.J. Ernst, Volcanic Particle Aggregation in Explosive Eruption Columns Part I: Hydrometeor-Ash Particle Growth in Volcanic Eruption Column Part II: Numerical Experiments, *submitted to Journal of Volcanological and Geothermal Research*, 2004.

Textor, C., P.M. Sachs, H.-F.Graf, and T.H. Hansteen, The 12,900 yr BP Laacher See eruption: estimation of volatile yields and simulation of their fate in the plume, in *Volcanic Degassing*, edited by C. Oppenheimer, D. Pyle, and J. Barclay, Geological Society, London, Special Publications, 2003b.

Trentmann, J., M.O. Andreae, and H.-F. Graf, Chemical processes in a young biomass-burning plume, *JGR*, *108* (D22), 10.1029/2003JD003732, 2003a.

Trentmann, J., M.O. Andreae, H.-F. Graf, P.V. Hobbs, R.D. Ottmar, and T. Trautmann, Simulation of a biomass-burning plume: Comparison of model results with observations, in *JGR*, pp. 10.1029/2001JD000410, 2002.

Trentmann, J., B. Früh, O. Boucher, T. Trautmann, and M.O. Andreae, Three-dimensional solar radiation effects on the actinic flux field in a biomass burning plume, *Journal of Geophysical Research*, *108*, 4558, 2003b.

Woods, A.W., and S. Bower, The decompression of volcanic jets in craters, *EPL*, *131*, 189--205, 1995.

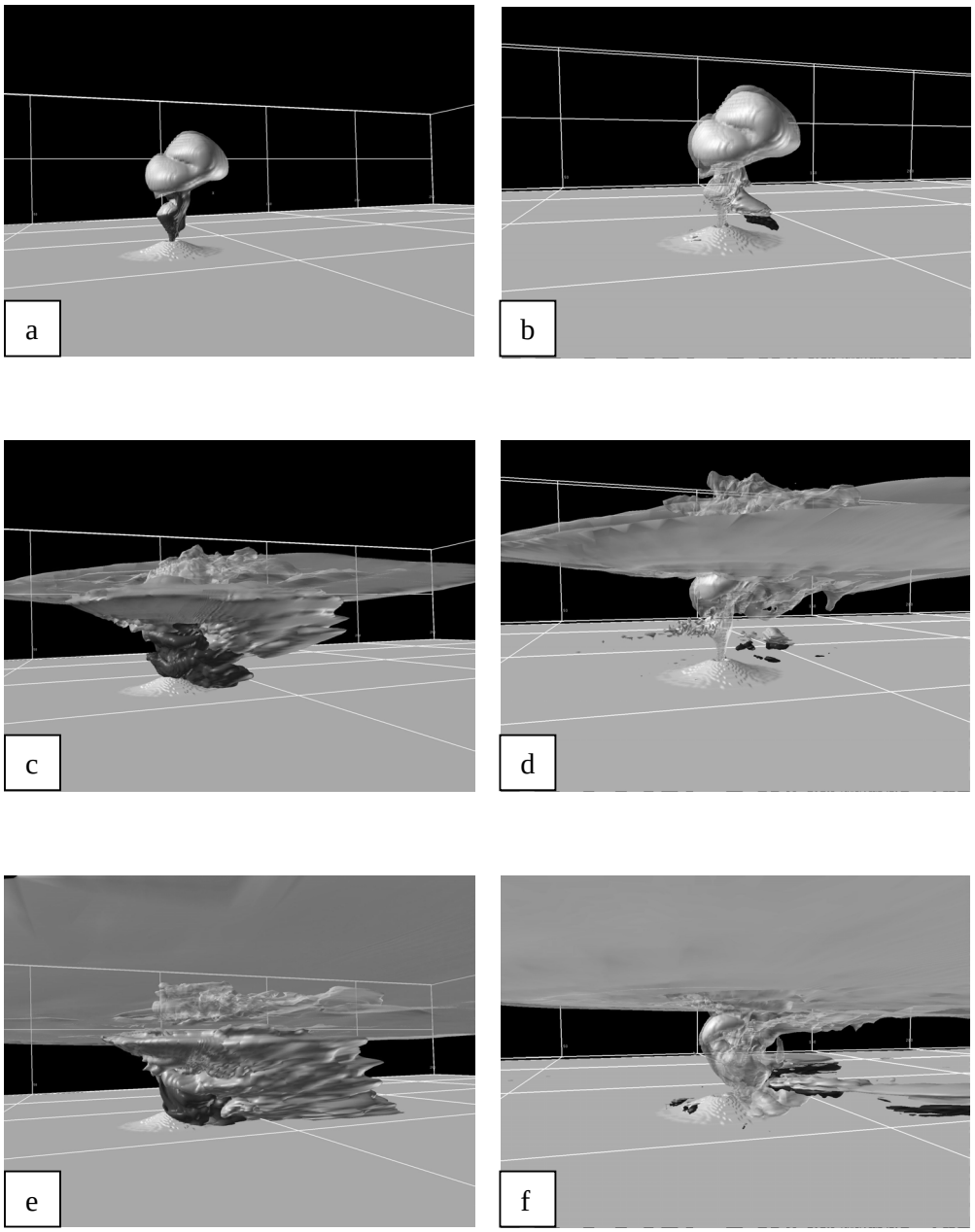

Figure 2: Simulation of a volcanic eruption with the three dimensional version of ATHAM LIT. The plots show the eruption columns of total ash (size classes: light gray: 10, gray: 200, dark gray: 4000, all in [µm] diameter) on the left hand side (figures 2a, 2c, 2e), and of finest ash and hydrometeors (light gray: 10 µm ash, gray: ice, dark gray: liquid water) on the right hand side (figures 2b, 2d, 2f). Three time levels are given (top: 5 min (figures 2a and 2b), middle: 30 min (figures 2b and 2d), and bottom: 70 min (figures 2e and 2f)). Only a fraction of the model domain is depicted; the pale lines at the ground and in the background indicate distances of 50 km in the horizontal and 25 km in the vertical direction. Visualizations by Michael Boettinger, Deutsches Klimarechenzentrum, Hamburg, Germany.

VOLCANIC ASH AND AEROSOL DETECTION VERSUS DUST DETECTION USING GOES AND MODIS IMAGERY

Bernadette Connell
Cooperative Institute for Research in the Atmosphere, Colorado State University
Fort Collins, Colorado, USA
connell@cira.colostate.edu

Abstract

Case examples of the various volcanic ash/aerosol and dust aerosol detection techniques utilizing infrared wavelengths in the 8-12 µm region are presented for the moderate resolution imaging spectroradiometer (MODIS) imagery and compared with available products from the geostationary operational environmental satellite (GOES) imagery. Information gained by using the short wavelength region (3-4 µm) will also be presented. A question that is posed, and partially answered is: How is ash, sand or aerosol detected with the various channel combinations?

Introduction

Volcanic eruptions are extremely variable in intensity and composition, they are difficult to predict, and they are hazardous. Because of this they are often difficult to measure directly and it is difficult to track their emissions. Examples are limited. Dust and ash tend to be comprised of silicates and it is expected that remote sensing techniques for detection to be similar. Volcanic eruptions are often associated with sulfur based aerosols while blowing dust is not.

Within this paper, easy to implement techniques are utilized for detecting volcanic ash and aerosol and dust using GOES and MODIS imagery. The easy to implement techniques use channel differencing of brightness temperature or a "normalized" radiance difference product. A volcanic ash and a dust example highlight a few of the many subtle aspects of detecting ash and dust. Because of the variability of the eruption event and variability of the weather, no one detection technique will work 100% of the time. The brightness temperature (BT) difference: 11.0 - 12.0 µm works the best in distinguishing ash from meteorological clouds under ideal conditions. This technique will be used to compare against techniques from the other channels in the shortwave and longwave infrared region.

Techniques

Prata (1989a, 1989b) used the brightness temperature (BT) difference between the bands centered near 11.0 and 12.0 µm to detect ash while Shenk and Curran (1974) used this difference to detect dust storms. The BT11.0 – BT12.0 is generally negative for ash and dust and positive for ice and water clouds.

The use of the 3.9 µm channel for detection of ash has been demonstrated by Ellrod et al. (2003) and has been shown by Ackerman (1989) for the detection of dust. The 3.9 µm channel senses solar radiation as well as emitted radiation; hence the imagery is interpreted differently during the day than at night. For the daytime scenes, scattering by particles of shortwave radiation enhances the reflectance. For water particles, the reflectance is inversely proportional to the drop size. Small water droplets are strongly reflective, larger ice particles are less reflective. Volcanic ash and dust samples show higher reflectance in the 3.9 µm region than in the 10.7 or 12.0 µm regions (Schneider and Rose, 1994; Salisbury and Walter, 1989). The reflectance is estimated by: $R3.9 - R3.9_{(BT10.7)}$. The emitted radiance component at 3.9 µm is estimated using the planck function with the measured BT10.7. This is then subtracted off the measured radiance at 3.9 µm.

At night, the detection of an optically thick cloud with the 3.9 µm channel is difficult, particularly for temperatures colder than -40C, where instrument noise becomes large and overwhelms the signal. For optically thin clouds, transmission plays and important role and the BT3.9 – BT10.7 is positive for ash cloud (Ellrod et al., 2003). The

BT3.9-BT10.7 at night is generally positive for ice cloud and negative for water cloud. In summary for the 3.9-10.7 products, during the day ash and dust have a signature similar to that observed for water cloud. At night, ash and dust have a signature similar to that observed for non-opaque ice cloud.

Baran et al. (1993) and Ackerman and Strabala (1994) looked into the use of the 8.3 µm channel on the high resolution infrared sounder (HIRS) system for the detection of H_2SO_4 aerosol from the Pinatubo eruption. Over oceans there is a small negative BT8.3 – BT12.0 background signature due to moisture. The BT8.3 – BT12.0 becomes more negative for H_2SO_4 aerosol, and also becomes more negative for an increase in atmospheric water vapor. The BT8.3-12.0 is positive for ice.

For dust, Ackerman (1997) found that increasing the optical depth increases BT8-BT11 over clear sky conditions. A thick optical depth results in positive BT8-BT11. Wald et al. (1998) simulated the MODIS capabilities of the detection of mineral dust over desert using the 8.0 - 12.0 µm region. Using various particle sizes of quartz and varying the optical depth, they found that the BT12.0 – BT 8.0 was the smallest (ie. negative) (positive for BT8.0 – BT 12.0) for 2 µm particles and small optical depth and was positive for large optical depth, taking on the signature of the quartz sand background. All authors mentioned in this paragraph discuss the difficulties encounter over land surfaces where diurnal temperature variations and variable surface emissivities affect BT8.

Examples

The eruption of the Popocatepetl volcano in Mexico on 22-23 January 2001 was chosen because the eruption started later in the day on the 22nd, providing a brief example of the reflectance seen in the 3.9 µm channel, with drifting ash continuing through the night when the first MODIS imagery is available. According to the volcanic ash advisory issued by the Washington Volcanic Ash Advisory Center, the explosive event started at approximately 22:15 UTC on 22 January 2001. Figure 1 shows the erupting plume at 22:45 UTC. The outline of the plume is shown on the visible imagery in Figure 1a. The stratus cloud to the east is also labeled. In the reflectance product (figure 1b), enhanced reflectance is noted for the eruption plume and appears brighter than

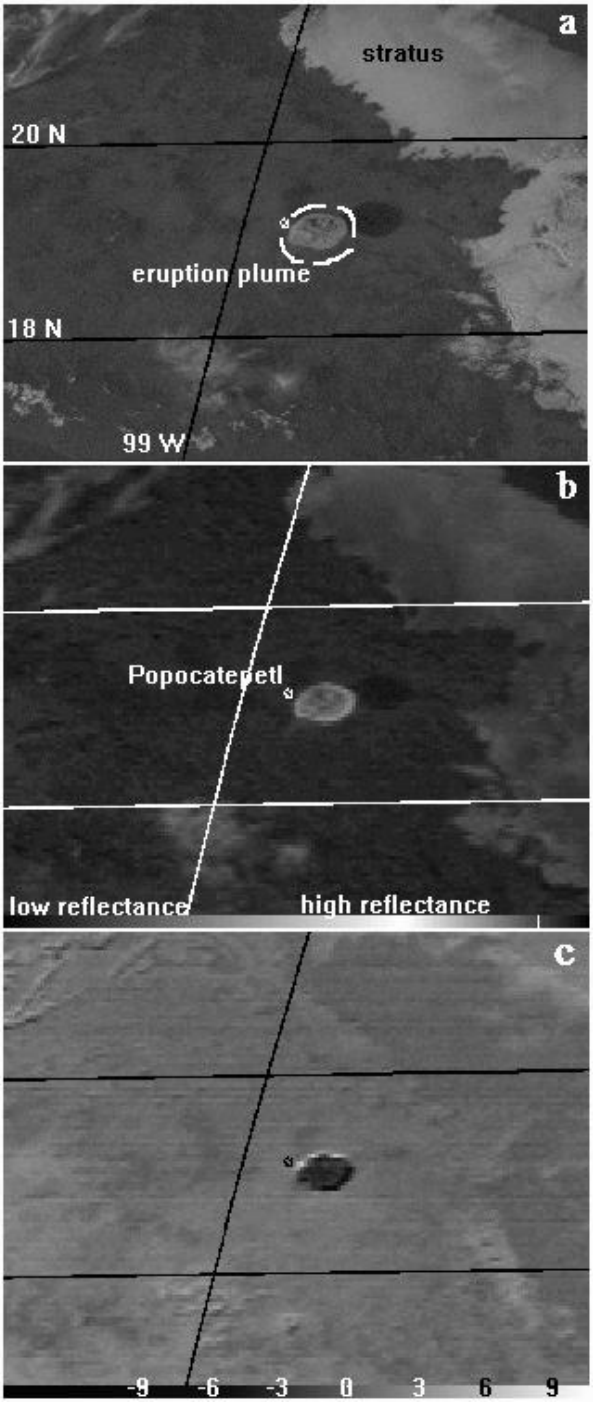

Figure 1. GOES imagery showing the erupting plume from the Popocatepetl volcano in Mexico on 22 January 2001 at 22:45 UTC. a) visible imagery, b) reflectance product using the 3.9 and 10.7 µm imagery, and c) BT10.7-BT12.0

the stratus cloud. The cloud shape resembles a convective cloud and would normally appear darker because of the presence of less reflective ice particles. The BT10.7-BT12.0 product (figure 1c) shows negative values for the plume with the most negative value (-7.7) along the southeastern edge where the plume is thinner.

A night scene of the eruption plume is displayed in figure 2. The GOES imagery (figure 2 a, b) are from 04:45 UTC on 23 January 2001, and the MODIS Terra imagery (figure 2 c, d) are from 04:50 UTC. The pattern of the GOES and MODIS BT11-BT12 shown in figure 2a and 2c are very similar. The GOES product produced more negative differences in background regions as well as in various parts of the plume. The differences were generally relatively small (0.5C) as in the circled regions x and y, but got as large as 2.0C in circled region Z (-5.5C for GOES and -3.3C for MODIS. At this point it is unclear as to whether the differences are a result of the sampling differences associated with different spectral coverage, spatial coverage, or viewing angle. The GOES 10.7 channel has a bandwidth of 10.2-11.2 µm, while the MODIS 11.0 µm channel has a bandwidth of 10.78-11.28 µm. The GOES 12.0 µm channel has a bandwidth of 11.5-12.5 µm, while the MODIS 12.0 µm channel has a bandwidth of 11.77-12.27 µm.

The GOES BT10.7-BT3.9 shown in figure 2b shows the plume quite well. In this case it is because of the contrast of the plume with the brighter lower level stratus and ground surface. Tracking of the plume with the GOES imagery

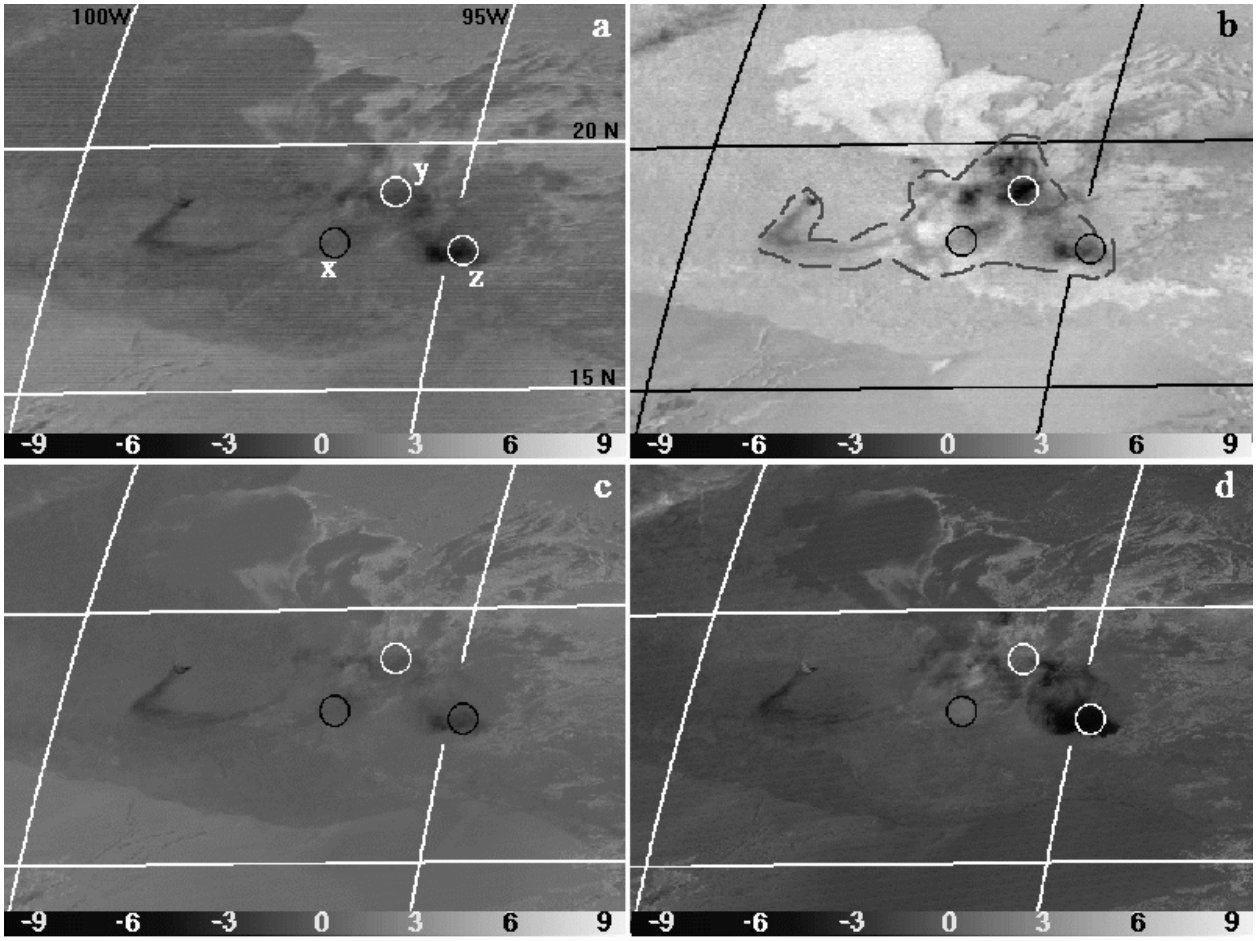

Figure 2. Satellite imagery products showing the erupting plume from the Popocatepetl volcano in Mexico on 23 January 2001, GOES at 04:45 UTC and MODIS Terra at 04:50 UTC. a) GOES BT10.7-BT12.0, b) GOES BT10.7-BT3.9, the dashed line indicates the plume outline c) MODIS BT11.0-BT12.0, and d) MODIS BT8.5-BT12.0.

through time helped significantly in discerning various portions of the plume that are outlined in figure 2b. The BT8.5-BT12.0 image provides another view of the plume and its characteristics. It has many regions of negative difference similar to BT11.0-12.0 (figure 2c) and one region in particular indicated by circle z has much stronger negative differences (-14.0C). Regions circled as x and y show slightly positive differences. The modeling efforts referenced in the previous section suggest that the regions of positive differences in circles x and y contain smaller particles and small optical depth. The more negative differences observed in circle z reflect the presence of SO_2 and sulfates and a larger optical depth.

An example of blowing dust during the day is shown in figure 3 for 18 April 2004 at 19:30 UTC. The extent of the plume is highlighted with dashed lines in the MODIS BT11.0-BT12.0 (figure 3c) image. Both the MODIS and the GOES difference product for BT11-BT12 (figure 3c and 3a respectively) show similar values (most negative value = -2.5, average = -2.0 and -1.5 respectively) for the thicker part of the plume, represented by the circle labeled y. They also show similar values (1.0 and 0.0 = the most positive values respectively, average=-0.5) for the thinner portion of the plume labeled as circle x. The extent of the dust plume for these difference products agrees with that shown by the GOES reflectance product in figure 3b. In this product, the dust as well as low level water clouds appear more reflective. In contrast, the MODIS BT8.5-BT12.0 product shown in figure 3d represents the plume with values -1.0 – 0.0 in what appears to be the densest

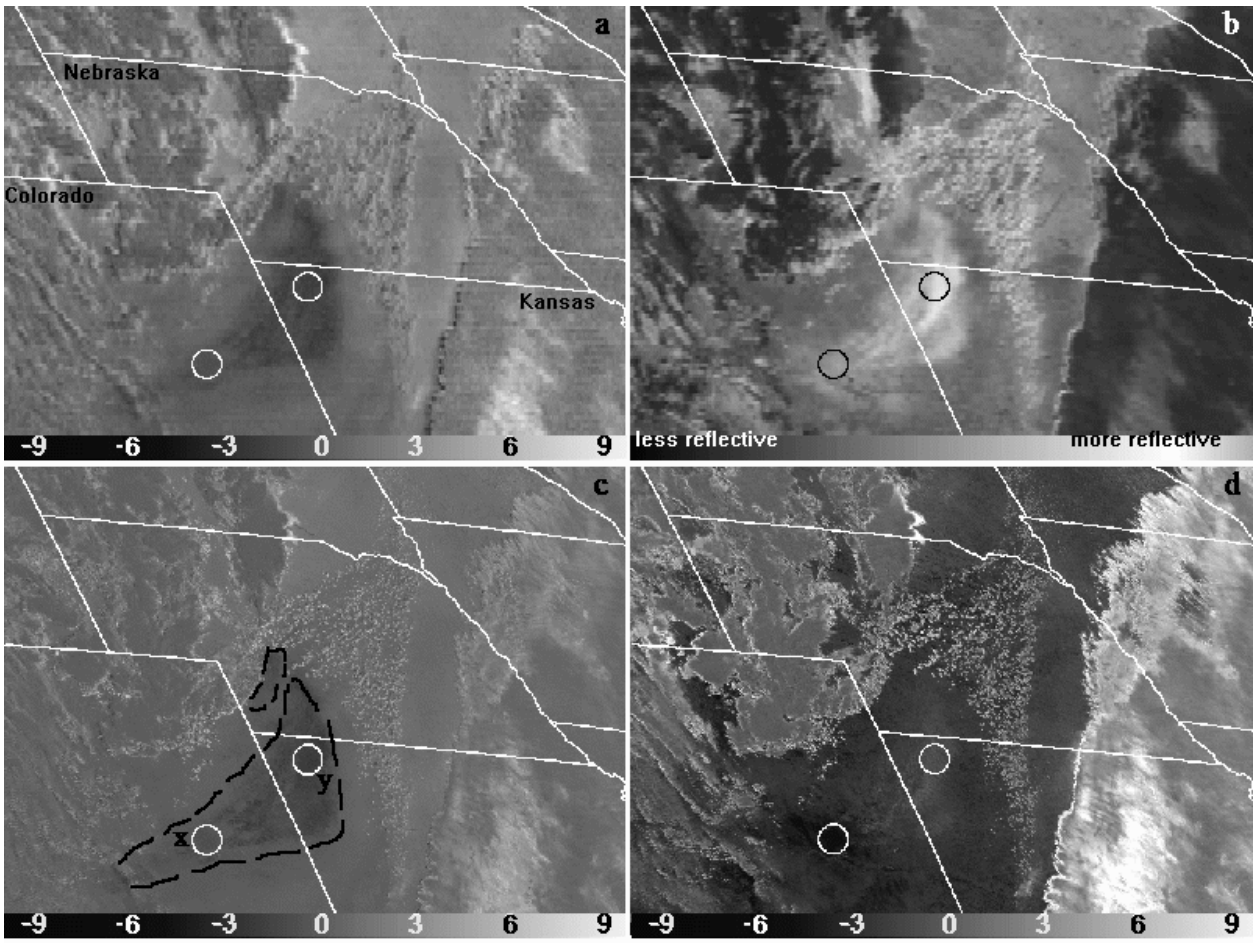

Figure 3. Satellite imagery products showing the dust plume extending from Colorado into Kansas and Nebraska on 18 April 2004, GOES and MODIS Aqua at 19:30 UTC. a) GOES BT10.7-BT12.0, b) GOES reflectivity product using the 3.9 and 10.7 channels c) MODIS BT11.0-BT12.0, the dashed line indicates the plume outline, and d) MODIS BT8.5-BT12.0.

region labeled as circle y. In the circled region labeled as x, the most negative value is -7.0 with an average value of -5.0. These observations are opposite what is expected from the modeling results referenced in the previous section. Further information is needed on the effect of surface emissivities, particle size, and opacity of the plume.

Summary

Blowing dust has characteristics similar to volcanic ash and techniques used for its detection can be extended to volcanic ash detection. The BT11-BT12 technique is the most widely used technique in the detection of volcanic ash. It has also been used with success in detection of blowing dust. There are many instances when the 3.9 µm products enhance the ash plume and blowing dust plumes. Even though the signature does not uniquely distinguish it from meteorological cloud, it can be used in conjunction with the other products to better delineate the extent of coverage.

The 8.5 µm channel is currently available on the MODIS satellites. It has the capability to detect SO_2 and sulfates as well as ash and dust. In general, the presence of SO_2 and sulfates will make the BT8.5-BT12.0 signal negative. The presence of small (2 µm) quartz dust (or ash) particles and a low optical depth will result in a positive BT8.5-BT12.0 signal. High optical depth results in a negative BT8.5-BT12.0, similar to viewing a quartz ground signal. The night volcanic ash case viewed here showed features that seemed to be consistent with both the presence of ash and aerosol. The day dust case had negative and positive regions that were not consistent with what was expected.

Since the detection of SO_2 and sulfates is desirable along with the detection of ash, further research is needed to determine regional sensitivities to the background surface emissivity and particle size as well as optical depth in the 8.5 µm region. This will help to develop a more robust and comprehensible product to be used in monitoring volcanic emissions.

Acknowledgements

This work is supported by NOAA Grant NA17RJ1228.
The MODIS data used in this study were acquired as part of the NASA's Earth Science Enterprise and archived and distributed by the Goddard Earth Sciences (GES) Data and Information Services Center (DISC) Distributed Active Archive Center (DAAC).

References

Ackerman, S. A., 1989: Using the radiative temperature difference at 3.7 and 11 µm to track dust outbreaks. *Remote Sens. Environ.* **27**:129-133.

Ackerman, S. A., 1997: Remote sensing aerosols using satellite infrared observations. *J. Geophys. Res.*, **102** (D14): 17,069-17,079.

Ackerman, S. A., and K. I. Strabala, 1994: Satellite remote sensing of H2SO4 using the 8- to 12- µm window region: Application to Mount Pinatubo. *J. Geophys. Res.*, **99** (D9): 18,639-18,649.

Baran, A. J., J. S. Foot, and P. C. Dibben, 1993: Satellite detection of volcanic sulphuric acid aerosol. *Geophys. Res. Lett.*, **20** (17):1799-1801.

Ellrod, G. P., B. H. Connell, D. W. Hillger, 2003: Improved detection of airborne volcanic ash using multi-spectral infrared satellite data. *J. Geophys. Res.*, **108** (D12): Art. No. 4356 Jun 21.

Prata, A. J., 1989a: Observations of volcanic ash clouds in the 10-12 µm window using AVHRR/2 data. *Int J. Remote Sensing*, **10**(4-5):751-761.

Prata, A. J., 1989b: Infrared radiative transfer calculations for volcanic ash clouds. *Geophsy. Res. Lett.*, **16**(11): 1293-1296.

Salisbury, J. W., and L. S. Walter, 1989: Thermal infrared (2.5-13.5 um) spectroscopic remote sensing of igneous rock types on particulate planetary surfaces. *J. Geophys. Res*., **94**, No. B7, 9192-9202.

Schneider, D. J., and Rose, W. I., 1994: Observations of the 1989-1990 Redoubt volcano eruption clouds using AVHRR satellite imagery. In: Volcanic ash and aviation safety: Proceedings of the First International Symposium on Volcanic Ash and Aviation Safety. U. S. Geological Survey Bulletin 2047, 405-418.

Shenk, W. E., and R. J. Curran, 1974: The detection of dust storms over land and water with satellite visible and infrared measurements. *Mon. Weather Rev.*, **102**: 830-837.

Wald, A. E., Y. J. Kaufman, D. Tanré, and B. –C. Gao, 1998: Daytime and nighttime detection of mineral dust over desert using infrared spectral contrast. *J. Geophys. Res.*, **103** (D24): 32,307-32,313.

Ice in Volcanic Clouds: When and Where?

William I Rose, Gregg JS Bluth and I Matthew Watson
Michigan Technological University, Houghton, MI 49931 USA

Volcanic clouds are suspensions of particles, analogous to meteorological clouds. In volcanic clouds the particles include volcanic ash, *hydrometeors* (raindrops, snow, hail, graupel, sleet, etc), sulfate aerosols and particles that are mixtures or conglomerations of all the other particle types present. *Ash fall* is analogous to rain, hail or snow, and consists of large ash particles in descent. Ash fall occurs most markedly from the high energy first stage of volcanic clouds, with or without precipitation, near the vent and soon (<1hr) after eruption (Rose et al, 2000). Volcanic clouds exhibit a second stage of evolution, lasting a day or so, where rapid physical and chemical changes occur and when ash fall occur and when ash fall (and precipitation) is muted and controlled by aggregation of ash particles too small to fall by themselves. A third stage of volcanic clouds lasts several more days and consists of drifting over hundreds or thousands of km and very slow fallout (Rose et al, 2003).

This paper explores published data from remote sensing and other sources concerning the existence of ice particles in volcanic clouds, to attempt to reveal patterns in its variability. We use data from a variety of satellite sensors and using several different algorithms for retrieval of information about ice, ash, sulfate and SO_2 (Table 1), applied to eruptions of the last few decades.

If one type of particle is dominant in the volcanic cloud, it is challenging to use these remote sensing algorithms to quantify the subordinate particles. We discuss in this paper cases when ice is the dominant particle type, when ash is dominant and when ash and ice are similar in mass proportions.

Table 1 Algorithms used for volcanic cloud sensing retrievals, see also Watson et al (2004)

Name	Sensor (s)	Objective	Reference(s)
2 band BTD	GOES, AVHRR, MODIS	Mass of fine (> 15 μm radius) ash, Particle size	Wen & Rose, 1994; Yu et al, 2002 (atmospheric corrections Rose et al, 1995 (ice retrievals)
8.6 μm SO_2	MODIS, ASTER	SO_2 mass	Realmuto et al, 1997
7.3 μm SO_2	MODIS, HIRS/2	SO_2 mass	Prata et al, 2003 (HIRS/2) Prata et al, in prep (MODIS)
UV SO_2	TOMS	SO_2 mass	Krueger et al, 1995
Multiband IR	MODIS	Fine ash, ice, sulfate masses	Yu & Rose, 2000

GOES = Geostationary Operational Environmental Satellite; AVHRR= Advanced Very High Resolution Radiometer; MODIS= Moderate Resolution Imaging Spectroradiometer; ASTER= Advanced Spaceborne Thermal Emission and Reflection Radiometer; TOMS= Total Ozone Mapping Spectrometer

Ice Dominant Volcanic Clouds
Rabaul, Papua New Guinea 1994

The Rabaul eruption was the event which made us realize that ice could be the dominant particle in volcanic clouds. The eruption came from dual vents on opposite sides of a caldera breached by the ocean and resulted in a 20 km high eruption cloud

which was detected by satellite sensors such as the polar orbiting AVHRR. Numerous conventional photographs from the Space Shuttle (http://www.geo.mtu.edu/volcanoes /rabaul/shuttle/) show that this cloud had a bright white color like a meteorological cloud. Infrared remote sensing showed that the cloud contained >2 MT of ice. Salty rain falls occurred in a wide arc N and NW of the volcano and there were wet ash and mud falls which contained sea salt, although ash could not be detected by satellite remote sensors. The Vulcan vent (the main source of the Rabaul eruptions) was itself breached, and so the ocean flowed directly into the active vent during eruption. Thus the ice in the great cloud may have largely been the result of evaporation of the ocean (Rose et al, 1995). Remote sensing also revealed that the Rabaul volcanic cloud contained relatively low levels of SO_2 (80 $\pm$ 50 kT), which suggested that ice sequestered much of the volcanic gas and removed it from the volcanic cloud by precipitation in the early stage of the volcanic cloud. Overall this example showed that ice could reduce the residence time of both ash and SO_2 in the volcanic cloud, an idea suggested by Pinto et al (1989).

Hekla, Iceland 2000

The Hekla eruption was a small (ash volume ~ 0.01 km3; total magma volume ~0.17 km^3 and mass about $3x10^5$ MT) fissure eruption of lava preceded by a brief (1-2 hr) explosive phase that produced an eruption cloud which suddenly reached 10-12 km. Meteorological radar was a useful monitoring tool to document the explosive eruption and the growth of ice in the volcanic cloud (Lacasse et al, 2004). The volcanic cloud was mapped by a variety of satellite sensors as it drifted N of Hekla toward Svalbard for 2 days (Rose et al, 2003). It was also traversed by a research aircraft with in situ atmospheric sensors. In spite of the small scale of the eruption, the Hekla volcanic cloud contained >1 MT of ice and 160-240 kT of SO_2. Ash was a minor component and was detected by remote sensors only in the first hour of the eruption (~100 kT or .1 Tg). The ice mass in the volcanic cloud declined by an order of magnitude before the aircraft encounter 35 hours after eruption (figure 1).

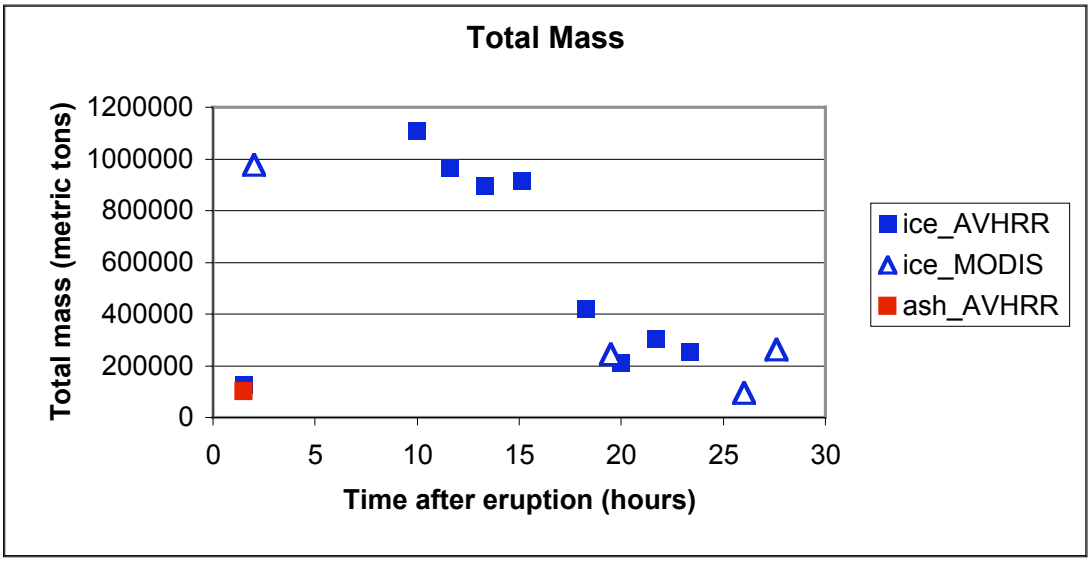

Figure 1: Time based determinations of particle masses determined using the multispectral IR retrieval of Yu & Rose (2000) for the Hekla Volcanic Cloud (Rose et al, 2003).

Examples where ice is clearly subordinate
Spurr, Alaska 1992
Crater Peak, Mount Spurr Alaska had 3 similar VEI=3 eruptions in 1992. Each resulted in a volcanic cloud which reached the lower stratosphere (~14 km asl) and had eruptive volumes of about 0.01-0.02 km^3 (Rose et al, 2001). All three events were studied with AVHRR sensors which enabled us to estimate masses of several hundreds of kilotonnes of fine (<15 μm radius) ash particles. These particle masses declined markedly during the first 18-24 hours due to aggregate formation and fallout. No ice could be detected with remote sensing in any of these clouds. We used atmospheric profile information and a numerical model called ATHAM which includes microphysical processes (Textor et al, 2003) to determine the likely amounts of ice in the Spurr volcanic clouds and found that the model results showed that ice concentrations in the Spurr Clouds were of the order of a few % of the fine ash concentrations. One factor that limits the ice is the low concentrations of H_2O in tropospheric air at high latitudes, which limits the entrained water vapor in the column. The low proportions of ice in Spurr volcanic clouds may limit the fallout of icy aggregates which accelerate ash removal in other clouds. We also note that the Spurr clouds did not show separation of ash and SO_2 (See discussion in Rose et al, 2001).

Cleveland, Alaska 2001
Cleveland is a stratovolcano 1730 m high located 1500 km SW of Anchorage in the east central Aleutians. With 11 eruptions since 1893 and ash eruptions in 1987 and 1994, it is relatively active. As it is unmonitored seismically and remote, satellite observations of thermal anomalies and eruption clouds play a vital role in monitoring (Dean *et al,* 2004). In 2001, Cleveland erupted on February 19, March 11 and March 19. On February 19, the largest of the three events produced ash eruptions that lasted 8-9 hours and which were observed by satellite sensors (GOES, AVHRR and MODIS) for 48 hours. The fine (<15 μm radius) ash masses in this volcanic cloud was found to be ~30 kT and the SO_2 mass was ~10 kT. There was a sight separation of ash and SO_2, suggesting that the SO_2 was emitted earlier and higher. No ice signal could be detected. The most important new observation about the Cleveland eruption was the enhanced sensitivity of the infrared detection from the large satellite zenith angles (Gu et al, in prep).

Other ice subordinate examples.
We have observed more examples of ash dominant volcanic clouds, such as Augustine, 1986 (Holasek & Rose, 1991) and Kluychevskoi, 1994 (Rose et al, 1995). We note that these examples are all at latitudes >40, which suggests that tropospheric water vapor, which is much higher at tropical latitudes, influences volcanic cloud ice through the entrainment process (Glaze et al, 19xx).

Subequal Proportions of ice and ash in volcanic clouds
Pinatubo, Philippines 1991
The largest eruption of the past 25 years, Pinatubo produced truly global scale atmospheric changes from its climactic eruption on 15 June 1991 (McCormick et al, 199x). About 80 MT of ice, about 50 MT of fine ash (<15 μm radius), and 18-19 MT of SO_2 were found in Pinatubo's huge volcanic cloud by Guo et al (2004a, 2004b). The coexistance of ice and fine ash makes retrieval using the two band BTD method of Wen & Rose difficult or impossible (Figure 2). This observation highlights an important issue for volcanic cloud detection, and provides a need for further development of multispectral infrared retrieval algorithms such as Yu & Rose (2000). The effects of ice in the Pinatubo cloud were marked: 1. SO_2 was apparently significant sequestered by ice (Figure 3) during the first day of atmospheric residence (Guo et al, 2004a) and 2. The ice and the ash fell out of the cloud quickly (about 90% removed in 3 days) and at very similar rates, suggesting that they fell out as ice/ash aggregates (Guo et al, 2004b).

Soufrière Hills, Montserrat, 26 December 1997
On 26 December 1997, the volcanic dome at Soufrière Hills, Montserrat collapsed catastrophically, producing a debris avalanche,

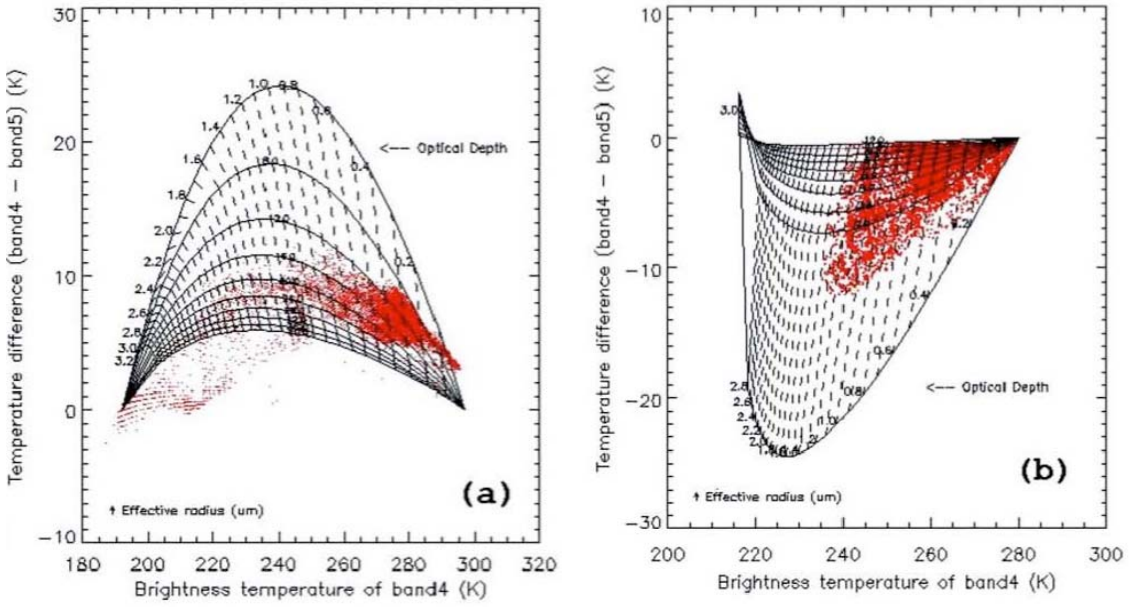

Figure 2: Brightness temperature difference (BTD) of band 4 (λ=11 μm) and Band 5 (λ=12 μm) data from AVHRR plotted against band 4 brightness temperature for two eruption clouds: a: Rabaul, 19, Sept, 1994, which was interpreted as ice dominant and b: Kluchevskoi, 1 October 1994, which was interpreted and ash dominant (Rose et al, 1995).

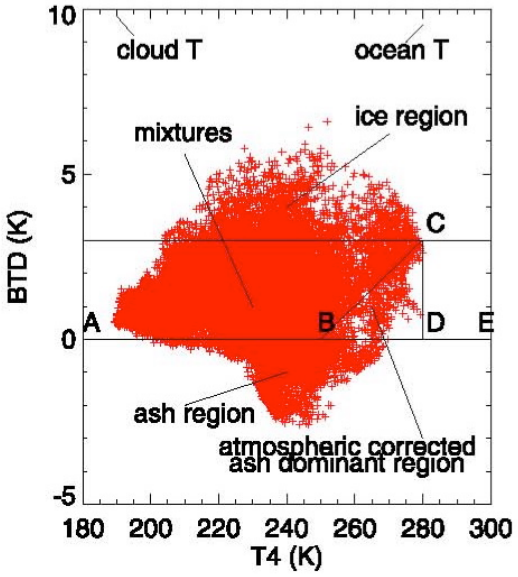

Figure 3: BTD plot, as in figure 2, but for the volcanic cloud of Pinatubo, 15 June 1991. This volcanic cloud is extremely variable and plots mainly in region labeled "mixtures", and only partly in the fields labeled "ash region" and "ice region". Compare with figure 2.

a pyroclastic density current and an ash cloud which rose to 15 km (Sparks et al, 2003). Because the density current carried hot andesite directly to the sea, the evaporation of the ocean led to the formation of a volcanogenic meteorological cloud, which also rose to stratospheric levels. The mapping of two stratospheric clouds and their particle masses (~45 kT fine ash (<15 μm radius) in the volcanic cloud; ~150 kT ice in the volcanogenic meteorological cloud) was demonstrated by Mayberry *et al* (2003). The two clouds overlapped in their two dimensional extent as they drifted SE for more than 6 hours.

El Chichón, Mexico 1982

The El Chichón eruption consisted of 3 large phases (the first and smallest on March 29 and the other two on April 4, 1982). The April 4 events produced a volcanic cloud which dramatically separated into a higher (22-26 km high) westward-drifting SO_2 rich volcanic cloud and a lower (19-21 km high) which contained most of the fine ash erupted (Schneider *et al*, 1999). The April 4 events produced ~ 7 MT of SO_2 and about 7 MT of fine ash (<15 μm radius) and the mass map of the cloud is obscured along its eastern edge (figure 4). By analogy with the Pinatubo example, we suggest that this is due to ice, which is present in proportions subequal to fine ash. The existence of ice may also explain the very rapid ash fallout observed by the satellite sensors, where >90% was lost in 3 days.

Conclusions

Ice is present in all cold volcanic clouds and this has important implications for hazards. For detection using infrared remote sensing, ice presence in the volcanic cloud interferes with volcanic ash, which means that the simplest detection schemes (2 band brightness temperature differencing) may be less sensitive or even ineffective.

Ice may be dominant, subordinate or subequal to ash in terms of mass in volcanic clouds and we have found good examples of each of these cases in the last 25 years. High latitude volcanoes are likely to be ice poor, perhaps because entrainment of tropospheric H_2O by the eruption column is limited by the drier high latitude troposphere.

Besides entrained tropospheric water vapor, sources of H_2O for volcanic cloud ice includes, magma, various hydrospheric reservoirs (ocean, crater lakes, glaciers, groundwater) and hydrothermal systems.

Ice in volcanic clouds enhances ash fallout by forming composite aggregates.

Ice forms immediately after eruption, and then decreases markedly by an order of magnitude in only a few days, apparently sublimating as well as precipitating from the drifting volcanic cloud.

Ice sequesters SO_2, and can remove it by precipitation or release it during sublimation, so that SO_2 masses in volcanic clouds have been observed to increase for 1-2 days after eruption.

References

Dean, K G, J Dehn, K R. Papp, S Smith, P Izbekov, R Peterson, C Kearney and A Steffke, 2004, Integrated satellite observations of the 2001 eruption of Mt. Cleveland, Alaska Journal of Volcanology and Geothermal Research Volume 135, Issues 1-2 , 15 July 2004, Pages 51-73

Glaze, LS, S M Baloga and L Wilson, 1997,Transport of atmospheric water vapor by volcanic eruption columns, Journal of Geophysical Research, D, Atmospheres 102, no. 5: 6099-6108

Guo, S, W I Rose, G J S Bluth and I M Watson, 2004, Particles in the great Pinatubo volcanic cloud of June 1991: the role of ice, Geochemistry, Geophysics, Geosystems, Vol 5, no 5 Q05003, doi: 10.1029/2003GC000655

Guo, S, GJS Bluth, W I Rose, I M Watson and A J Prata, 2004, Reevaluation of SO2 release of the climactic June 15, 1991 Pinatubo eruption using TOMS and TOVS satellite data, Geochemistry, Geophysics,

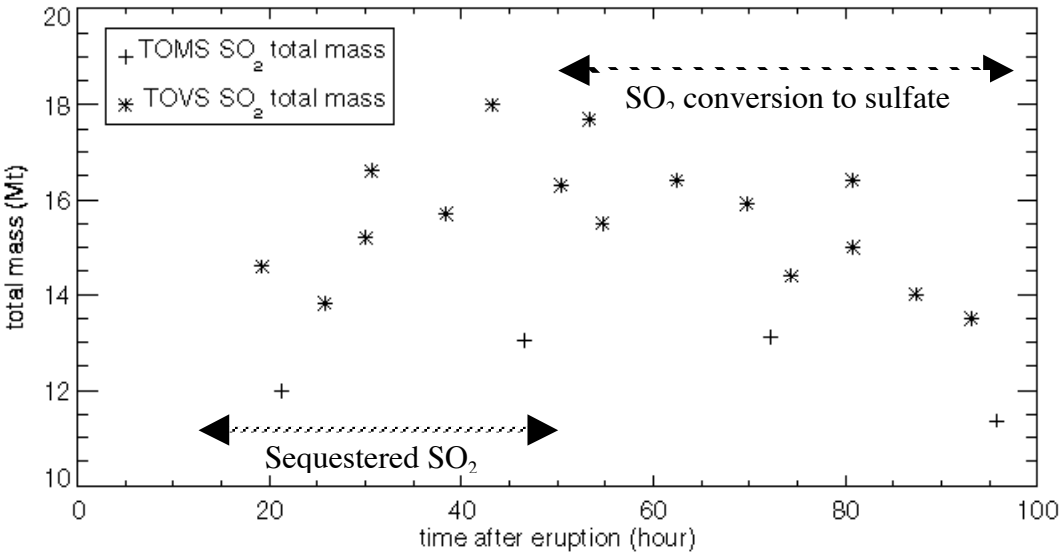

Figure 4: Plot of SO_2 mass retrievals for the 15 June 1991 eruption of Pinatubo, showing time periods where SO_2 sequestration is dominant and where SO_2 conversion is dominant. (from Guo et al, 2004b)

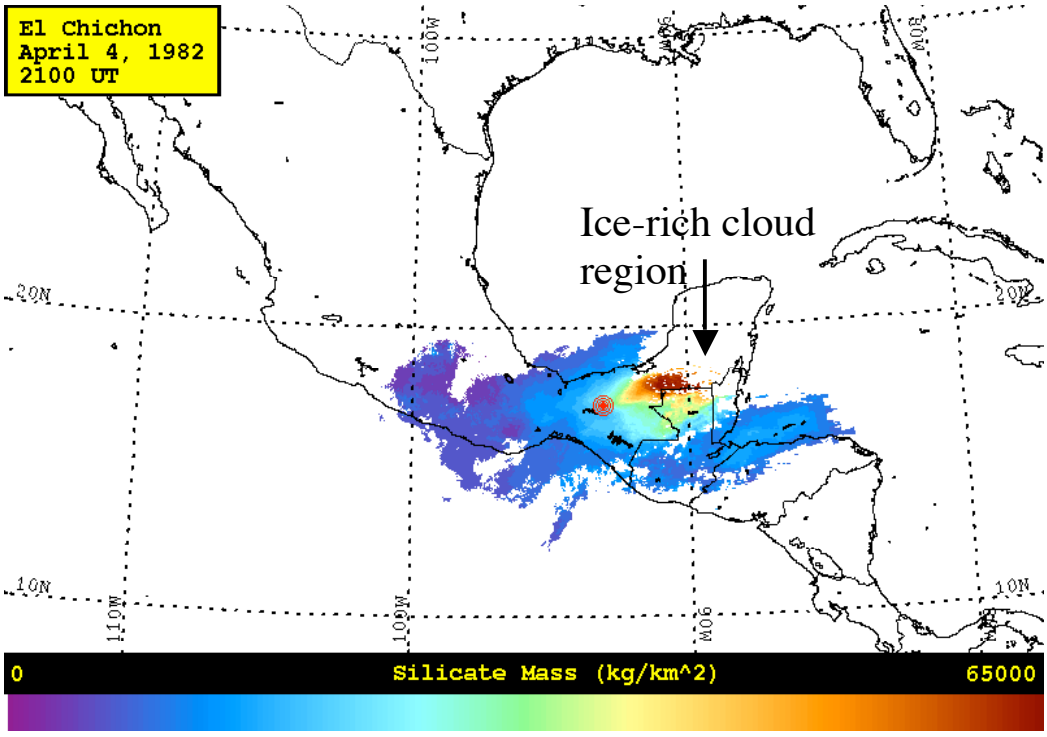

Figure 5: Map of fine ash (<15 μm radius) burden for the El Chichón eruption cloud of 4 April 1982, showing a region where the ash signal is masked by large ice masses. Note how contours of similar burden are terminated. From Schneider et al (1999).

Holasek, R. E., and W. I. Rose, 1991, Anatomy of 1986 Augustine Volcano eruptions as revealed by digital AVHRR satellite imagery, Bull. Volcanol., 53: 420-435.

Krueger A J, L S Walter, P K Bhartia, C C Schnetzler, N A Krotkov, I Sprod and G J S Bluth, Volcanic sulfur dioxide measurements from the Total Ozone Mapping Spectrometer (TOMS) instruments. *J Geophys Res 100:* 14057-14076, 1995.

Lacasse, C, S Karlsdóttir, G Larsen, H Soosalu, W I Rose and G G J Ernst, 2003, Weather radar observations of the Hekla 2000 eruption cloud, Iceland, Bulletin of Volcanology, 66:457-473.

Mayberry, G C, W I Rose and G J S Bluth, 2003, Dynamics of the Volcanic and Meteorological Clouds Produced by the December 26, 1997 Eruption of Soufrière Hills volcano, Montserrat, W.I., in The Eruption of Soufrière Hills Volcano, Montserrat, 1995-99, ed by T Druitt and P Kokelaar, Geological Society of London, Memoir 21: 539-555.

Pinto J P,, R P Turco and O B Toon, 1989, Self limiting physical and chemical effects in volcanic eruption clouds, J Geophys Res 94: 11165-11174.

Prata A J, W I Rose, S Self and D O'Brien, 2003, Global, long-term sulphur dioxide measurements from TOVS data: A new tool for studying explosive volcanism and climate, AGU Geophysical Monograph 139: Volcanism and the Earth's Atmosphere, ed by A Robock and C Oppenheimer, pp. 75-92. ISBN 0-87590-998-1

Realmuto, VJ, AJ Sutton and T Elias, Multispectral thermal infrared mapping of sulfur dioxide plumes - a case study from the East Rift Zone of Kilauea volcano, Hawaii, *Jour. Geophys. Res., 102:* 15057-15072, 1997.

Rose, W I, G J S Bluth and G G J Ernst, 2000, Integrating retrievals of volcanic cloud characteristics from satellite remote sensors--a summary, Philosophical Transactions of Royal Society, Series A, vol. 358 no 1770, pp. 1585-1606.

Rose, W I, G J S Bluth, D J Schneider, G G J Ernst, C M Riley and R G McGimsey 2001, Observations of 1992 Crater Peak/Spurr Volcanic Clouds in their first few days of atmospheric residence, J Geology, 109: 677-694.

Rose, W. I., D. J. Delene, D. J. Schneider, G. J. S. Bluth, A. J. Krueger, I. Sprod, C. McKee, H. L. Davies and G. G. J. Ernst, 1995, Ice in the 1994 Rabaul eruption cloud: implications for volcano hazard and atmospheric effects, Nature, 375: 477-479.

Rose, W I, Y Gu, I M Watson, T Yu, GJS Bluth, A J Prata, A J Krueger, N Krotkov, S Carn, M D Fromm, D E Hunton, G G J Ernst, A A Viggiano, T M Miller, J O Ballentin, J M Reeves, J C Wilson, B E Anderson D Flittner, 2003, The February-March 2000 eruption of Hekla, Iceland from a satellite perspective, AGU Geophysical Monograph 139: Volcanism and the Earth's Atmosphere, ed by A Robock and C Oppenheimer, pp. 107-132. ISBN 0-87590-998-1

Schneider, D. J., W. I. Rose, L. R. Coke, G. J. S. Bluth, I. Sprod and A. J. Krueger, 1999, Early Evolution of a stratospheric volcanic eruption cloud as observed with TOMS and AVHRR, J. Geophys. Res., 104; 4037-4050.

Sparks RSJ, J Barclay, ES Calder, RA Herd, J-C Komoroski, R Luckett, GE Norton L J Ritchie, B Voight and AW Woods, 2003, Generation of a debris avalanche and violent pyroclastic density current 0n 26 December 1997 at Soufriere Hills Volcano, Montserrat, in The Eruption of Soufrière Hills Volcano, Montserrat, 1995-99, ed by T Druitt and P Kokelaar, Geological Society of London, Memoir 21: 409-434.

Textor C, H-F Graf M Herzog and JM Oberhuber, 2003, Injection of gases into the stratosphere by explosive volcanic eruptions, J Geophys Res 108: No D19, 4606.

Watson, I. M., V. J. Realmuto, W. I. Rose, A. J. Prata, G. J. S. Bluth, Y. Gu, C. E. Bader and T. Yu, 2004, Thermal infrared remote sensing of volcanic emissions using the moderate resolution imaging spectroradiometer, J Volcanol Geoth Res 135: 75-89.

Wen, S and W I Rose, 1994, Retrieval of Particle sizes and masses in volcanic clouds using AVHRR bands 4 and 5, J. Geophys. Res., 99:5421- 5431.

Yu, T W I Rose and A J Prata, 2002, Atmospheric correction for satellite-based volcanic ash mapping and retrievals using "split window" IR data from GOES and AVHRR, J Geophys Res, 106: No D16, 10.1029.

Yu, T and W I Rose, 2000, Retrieval of sulfate and silicate ash masses in young (1-4 days old) eruption clouds using multiband infrared HIRS/2 data, AGU Monograph 116 --Remote Sensing of Active Volcanism, ed by P Mouginis-Mark, J Crisp and J Fink, pp. 87-100.

FIRST MEASUREMENTS OF VOLCANIC SULPHUR DIOXIDE FROM THE GOES SOUNDER: IMPLICATIONS FOR IMPROVED AVIATION SAFETY

Fred Prata[1],
Tony Schreiner[2], Tim Schmit[2],
Gary Ellrod[3],
[1]CSIRO Atmospheric Research, Aspendale, Victoria, Australia
[2]NOAA/NESDIS, Office of Research and Applications, Madison, WI, U.S.A.CIMSS, University of Wisconsin-Madison, Madison, WI 53706, U.S.A.
[3]NOAA/NESDIS, Office of Research and Applications, Camp Springs, Maryland, U.S.A.

Abstract

The GOES sounder is a multi channel imaging filter radiometer operating in the infrared to 15 μm, providing up to hourly data at 10x10 km^2 spatial resolution and covering large parts of the globe. The principal aim of the sounder is to provide vertical profiles of atmospheric temperature and moisture for global weather applications. Analysis of data acquired during the July, 2003 eruptions of Soufriere Hills, Montserrat, suggests that some of the channels can be used to detect upper tropospheric SO_2. We provide qualitative and quantitative assessments of GOES' ability to detect SO_2, illustrated with examples and suggest its advantages and limitations compared to other satellite measures of SO_2. Currently three GOES sounders are operational at longitudes: 134.85°E, 99.66°W, and 74.78°W. The temporal frequency and constant viewing angles of the GOES platform make them an ideal system for providing timely aircraft warnings of the presence of upper tropospheric/lower stratospheric SO_2, and consequently are useful for monitoring hazardous volcanic clouds.

Introduction

Satellite measurements of volcanic gases and particles (volcanic ash) are increasingly used by the aviation community to alert them of the possibility of a hazardous encounter. It is well recognized that an encounter with a volcanic ash cloud is likely to cause severe damage to jet engines with the likelihood of loss of power and ultimately loss of the aircraft and lives. A tragedy of this kind has not occurred, yet. However, jet aircraft continue to intercept ash clouds at alarming frequency. Many airline operators are cognisant of the dangers and take very conservative measures to avoid volcanic clouds, when their presence is known. This sensible action comes at the cost of increased mileage through re-routing and consequently airlines incur an economic penalty.

An encounter with a volcanic cloud is often first noticed by the pilot, cabin crew and passengers through the sensing of the presence of sulphur odours. The characteristic pungent odour of sulphur dioxide is an effective indicator. Occasionally, other signs of an ash encounter will be noticed; for example, "St Elmo's Fire", "smoke" in the cabin or observation of a darker than usual cloud. Later inspection of external surfaces will confirm whether an encounter has occurred. The severity of the encounter may require expensive engine checks or repairs to be carried out. In exceptional circumstances these checks and repairs may cost many millions of dollars. In many cases it is not known how severe the encounter has been until the checks have been undertaken. If the tell-tail signs of an encounter have been reported by the pilot and crew and advisories have indicated the possible presence of a volcanic cloud within the flight path, then thorough checks on the aircraft would seem warranted. However, not all encounters with volcanic clouds are necessarily encounters with volcanic ash. Recent research suggests that volcanic eruptions that produce ash and SO_2 may deposit these substances at different heights in the atmosphere. Vertical wind-shear will then cause transport of the ash and SO_2 clouds along different trajectories. This separation of the ash and gas appears to be common (see Bluth *et al*., 1994 for an example).

An encounter with an SO_2 cloud, as opposed to an ash cloud, will not cause engines to stall, will not cause abrasion of surfaces, and will not clog up pitot static tubes. While still to be avoided, encounters with SO_2 clouds are likely to lead to much less airframe damage and may call for a quite different overhaul procedure and repair. The costs of checks and repairs for an encounter with an SO_2 cloud are likely to be much less than those for an encounter with an ash cloud. These factors suggest that airlines need to know whether a volcanic cloud is predominantly SO_2 or predominantly ash. The current state of the science indicates that it is possible to detect both SO_2 and ash clouds from satellite-borne instruments simultaneously and monitor

their progress through the airways. This paper and a complementary paper by Schreiner *et al*. (2005) report a new observation of SO_2 clouds detected by the operational GOES sounder and suggest that use of the GOES sounder data will provide airlines with useful additional information on the composition of volcanic clouds.

The GOES Sounder

The Geostationary Orbiting Environmental Satellites (GOES) series provide frequent imagery and soundings for large parts of the globe. The current series are operationally known as GOES-8 through to GOES-12. The platform houses two instruments that view the earth – an imager and a sounder. Table 1 lists the band numbers and their respective central wavelengths for the GOES-12 platform.

GOES-12 Imager band	Central wavelength (μm)
1	0.65
2	3.9
3	6.48
4	10.7
5	13.3

GOES-12 Sounder band	Central wavelength (μm)
1	14.71
2	14.37
3	14.06
4	13.64
5	13.37
6	12.66
7	12.02
8	11.03
9	9.71
10	7.43
11	7.02
12	6.51
13	4.57
14	4.52
15	4.46
16	4.13
17	3.98
18	3.74

Table 1. Band numbers and central wavelengths for the GOES-12 imager and sounder. Note that the GOES sounder also has one broadband visible channel, not listed above.

The imager is used widely to provide frequent qualitative images for meteorological weather forecasting and analyses. The sounder is used for quantitative retrieval of atmospheric temperature and moisture profiles. This paper reports a new use for some of the sounder channels and the following discussion is restricted to the sounder. The spatial resolution of the sounder is ~10x10 km^2 and the temporal frequency is up to once per hour. Although the spatial scale is poorer than many of the polar orbiting satellites (e.g. AVHRR and MODIS), its temporal sampling is better.

SO_2 Retrieval

Sulphur dioxide has strong absorption bands in the infrared near to 4, 7.3 and 8.6 μm. The GOES sounder has bands at 3.98 and 7.43 μm (see Table 1). The band at 3.98 μm measures both reflected solar radiation and thermal emission, in approximately equal amounts under standard conditions. The band at 7.43 μm while not ideally situated for SO_2 detection does not include solar reflected radiation and covers the much stronger 7.3 μm SO_2 band. Sounder band 10 is also negligibly affected by volcanic ash, which can be detected independently by using the 11 and 12 μm bands (7 and 8) through the 'reverse' absorption effect (e.g., Prata, 1989).

A difficulty associated with retrieving SO_2 from band 10 arises because this band is responsive to mid-tropospheric water vapour. Indeed, the band is intended for studies of tropospheric water vapour. If the SO_2 cloud is high and concentrated however, then band 10 will respond to absorption due to SO_2. Typically for optimum detection, the SO_2 cloud should be situated near 200-300 kPa (5-8 km) and be relatively free of in-cloud water vapour. When such conditions are met then band 10 should register an anomalously low radiance (or brightness temperature). In practice, the height of the cloud is unknown and there is always likely to be some water vapour (or large amounts) in the volcanic cloud. To account for some absorption due to water vapour, a temperature difference image can be made. The difference removes some of the variations in radiance due to the heterogenous radiance field impinging onto the lower part of the SO_2/H_2O cloud. The heterogeneity may be due to variations in the radiation from the surface or atmospheric layers below the cloud, or may be due to horizontal variations in lower troposphere water vapour. We used several band differences to determine an optimum second band that maximised the SO_2 response. Ideally, three bands should be used:- two centred outside the 7.3 μm absorption feature and one band situated on the absorption feature. Bands 9, 11 and 10 seem obvious choices for the GOES-12 sounder. The approach taken for GOES SO_2 retrieval follows the method outlined by Prata *et al*. (2004). In this method a *synthetic* radiance

(or brightness temperature) is computed by linear interpolation of channels either side of band 10. The difference between the brightness temperature in band 10 and the synthetic value calculated for this band is a measure of the absorption due to SO_2. The reasoning behind this follows from the assumption that only SO_2 gas is causing the anomalous behaviour of band 10, and that water vapour effects have been removed through differencing with the synthetic estimate. The reader is referred to Prata *et a.l* (2004) for an in depth discussion of the veracity of these assumptions and for further information on the retrieval scheme, including the effects of water/ice clouds. Figure 1 shows the results of applying the retrieval scheme to four image frames of GOES-12 data for the July eruption of Soufriere Hills volcano on Montserrat.

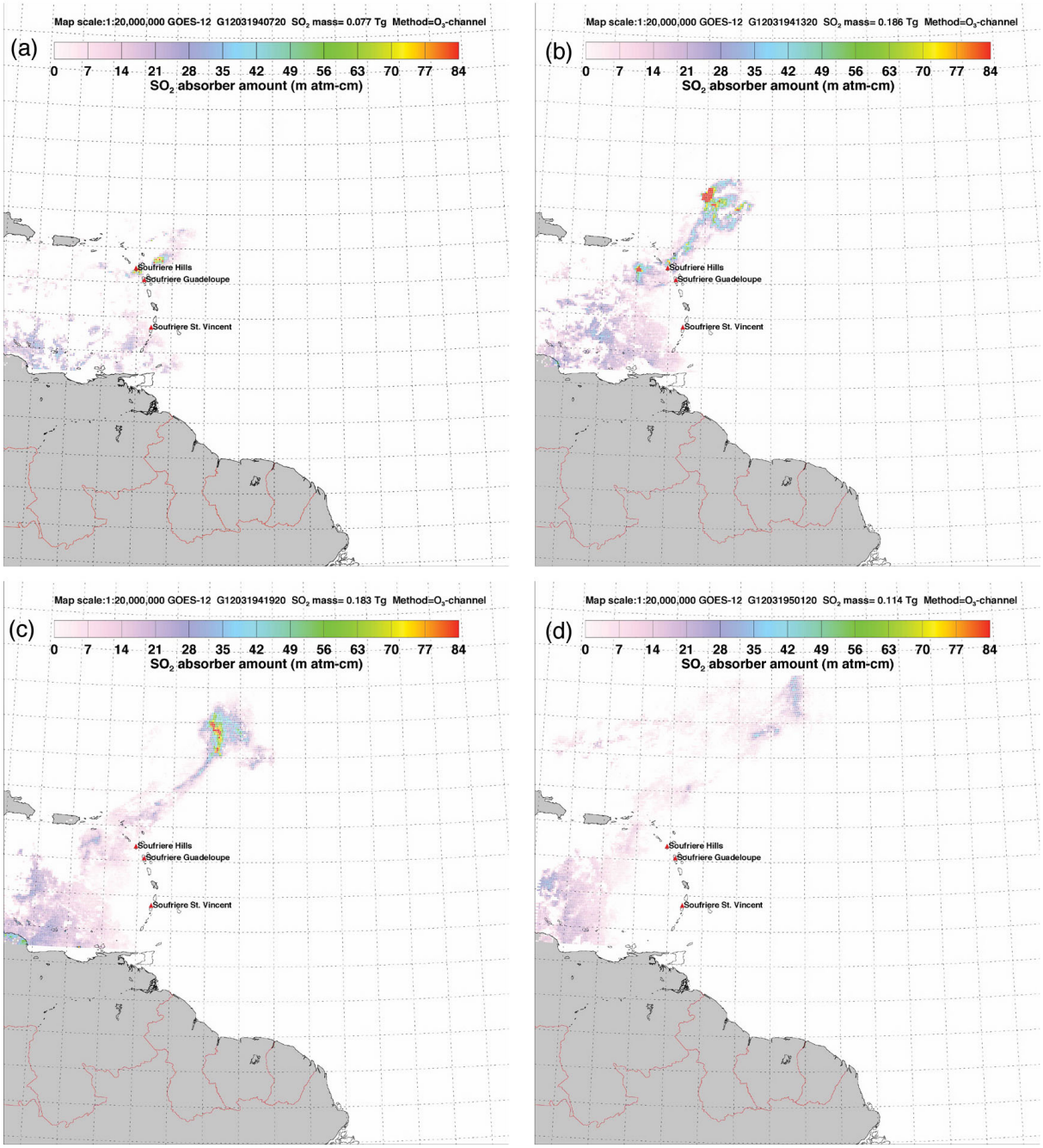

Figure 1. Sequence of GOES-12 SO_2 retrievals for the Soufriere Hills eruption, Montserrat. Each frame is separated by 6 hours in time (see the captions for day of year and time in UTC). SO_2 units are milli atm-cm.

The Soufriere Hills eruption is described in detail in the BGVN (2003). Analysis of the movement of the ash from this eruption suggests that it travelled predominantly to the west and west-northwest (Figure 2). By contrast the (higher) SO_2 cloud travelled northeast. This separation of the ash and SO_2 is a common feature of volcanic clouds that reach well into the upper troposphere (Bluth *et al*., 1994) and is a consequence of wind shear and the difference in densities of gases and particulates.

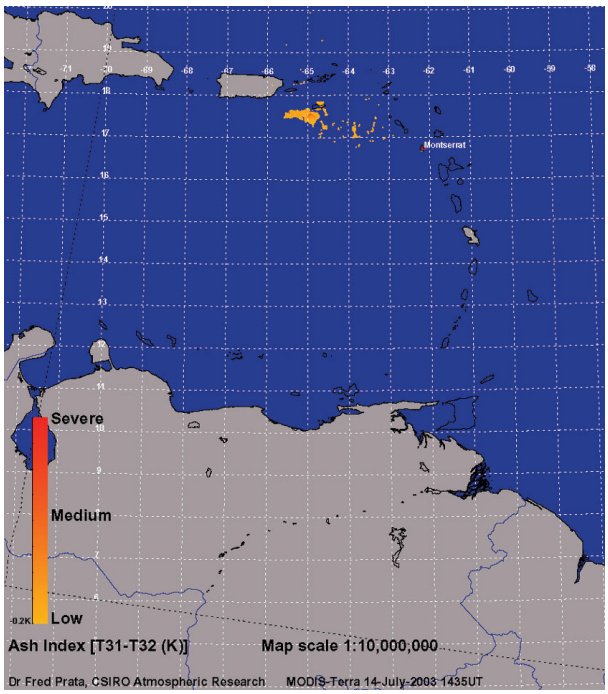

Figure 2. Volcanic ash from Soufriere Hills volcano. This MODIS image shows that the ash from Soufriere Hills moved westwards, whereas the SO_2 moved towards the northeast.

Validation

The Soufriere Hills eruption was monitored by several satellite instruments capable of measuring SO_2. These include, TOMS, MODIS and AIRS. Ground-based SO_2 flux measurements were also made during the eruption. The TOMS instrument estimated about 80 kT of SO_2 and the AIRS instrument retrieved values from 10 kT up to 290 kT, compared with the GOES retrievals of 77 kT up to 186 kT The errors in the SO_2 retrievals from these instruments are generally of the order 10-30%, and differences in timing, spatial coverage and footprint size preclude a comprehensive validation. However, the GOES retrievals are within the expected range of variation and compare quite favourably with AIRS and TOMS. We also note that the GOES band 10 is not optimum for quantitative SO_2 detection–the band centre is too far towards the long wavelength side of the SO_2 absorption and the band is a little broad.

For use by the aviation industry, quantitative SO_2 estimates may be of much less value than the certainty of identification; here the question of GOES sensitivity may be more important. Schreiner *et al*. (2005) show that GOES was able to track the SO_2 cloud for at least two more days at 6 hour time resolution.

Conclusion and implications for aviation safety

Work reported by Schreiner *et al* (2005) and in this paper, demonstrate that GOES may be useful in detecting volcanic SO_2 clouds that persist in the upper-troposphere/lower stratosphere and consequently may intersect airways. We have argued that clear identification of SO_2 from ash in volcanic clouds may be of economic benefit to the airline industry. Use of the 7.2-7.6 μm region for SO_2 detection looks promising as the effects of volcanic ash are much less; although water vapour absorption limits the detection to SO_2 residing at altitudes above 10,000 feet or so. It seems quite possible that a simple SO_2 index could be determined from GOES sounder data and transmitted to VAACs for dissemination to the airlines. Information in such images could be used in conjunction with trajectory models and other satellite data that detect volcanic ash, to allow airline operators to determine safe air routes. Furthermore, information gleaned from pilots and crew that believe they have encountered a volcanic cloud can be fused with the SO_2 and ash images to determine appropriate aircraft checks and maintenance procedures. An encounter with an SO_2 cloud is unlikely to warrant expensive aircraft repair, while it is known that an encounter with an ash cloud can lead to major engine damage.

References

Bluth, G.J.S., Casadevall, T.J., Schnetzler, C.C., Doiron, S.D., Walter, L.S., Kruger, A.J., and M. Badruddin, Evaluation of sulphur dioxide emissions from explosive volcanism: the 1982-1983 eruptions of Galunggung, Java, Indonesia, *J. Volcanol. Geotherm. Res.*, **63**, 243-256, 1994.

BVGN, *Bulletin of the Global Volcanism Network*, Vol. **28**, No. 7, 5-7, 2003.

Prata, A. J., Infrared radiative transfer calculations for volcanic ash clouds, *Geophysical research letters*, **16**, 1293-1296, 1989.

Prata, A. J., Rose, W. I., Self, S., and D. M., O'Brien, 2003, Global, long-term sulphur dioxide measurements from TOVS data: A new tool for studying explosive volcanism and climate, *Volcanism and the Earth's Atmosphere*, Geophys. Monograph **139**, AGU, 75–92.

Schreiner, A. J., Schmit, T. J., Ellrod, G., and Prata, A., Can upper-level SO2 be monitored using the GOES sounder?, Submitted to 85th Annual AMS meeting, 9-13 January, 2005, San Diego, CA. USA.

GROUND-BASED DETECTION OF VOLCANIC ASH AND SULPHUR DIOXIDE

Fred Prata and Cirilo Bernardo
CSIRO Atmospheric Research, Aspendale, Australia

Matthew Simmons and Bill Young
Tenix Investments, Sydney, Australia

Abstract

We present the first ground-based thermal infrared image data showing detection and discrimination of volcanic ash and sulphur dioxide gas emitted from erupting volcanoes. The images are acquired from a new multichannel uncooled thermal imaging camera suitable for deployment within ~10 km of an active volcano. Algorithms for ash and SO_2 detection are described. Images from the system, named G-bIRD (Ground-based InfraRed Detector) are acquired rapidly (within a few seconds), analysed and transmitted via satellite or landline to a computer with access to the Internet and utilising a standard web browser. Tests of the system have been undertaken at Etna and Stromboli, Italy, at Anatahan, Northern Mariana Islands and at Tavurvur, Rabaul, Papua New Guinea. G-bIRD offers a new means for monitoring hazardous volcanic substances from the ground and could provide complementary information for providing volcanic ash and SO_2 warnings to the aviation industry.

Introduction

Volcanic ash is a hazard to jet aircraft, causing engines to stall when ingested, scouring windows and the leading edges of the wings and causing instrument malfunctions (Casadevall, 1994 and references therein). Damage to aircraft can be counted in the millions of dollars. Most serious aircraft encounters with ash clouds have been at cruise altitudes (e.g. Tupper *et al*., 2004), but there is also a hazard to aircraft at airports affected by volcanic ash (Guffanti *et al.,* 2004 this volume). These airports are usually close to an active volcano (e.g. Anchorage and Kagoshima) but they can also be at some distance from the source of the eruption due to atmospheric transport that brings ash into the region. This paper addresses the problem of detecting volcanic ash in the vicinity of airports and suggests a practical design for an infrared device that can monitor the sky overhead. The cost of ash hazards to airport operations is not known, but must be significant if the costs include those due to delays to landings and take-offs as well as re-routing costs incurred by airline operators (Cantor, 1998). Other environmental hazards consist of the toxic gases emitted by volcanoes. Of particular importance and abundance is sulphur dioxide gas. This gas is colourless, but has a characteristic pungent odour. Eye irritation and inflammation of the respiratory tract occurs at relatively low concentrations. Amounts of 6-12 ppm will cause immediate irritation of the nose and throat. Long term exposure can exacerbate asthma and can be dangerous to persons with pre-existing cardiopulminary diseases. Thus monitoring near strong sources of SO_2 (e.g. from industrial sources and at volcanoes) is important, as is longer term monitoring at some distance from the source. Currently there are no regulatory requirements for airport operators to provide warnings of ash hazards. Warnings are issued based on information from volcano observatories, meteorological advisories and, in some cases, radar observations of eruption columns. Radar information is generally only reliable at the start of an eruption when the ash cloud is thick and usually such information is only available at airports in close proximity to an erupting volcano. For airports distant from the source of ash there are few direct observations available. Some observations come from satellite systems and other sources of information come from trajectory forecasts based on wind data and cloud height information. Much of this information is sporadic and untimely and there is a need for better coordinated information systems and better observational systems. A detector placed on the ground at an airport affected by volcanic ash would provide a useful adjunct to existing information sources. The device would be capable of viewing the sky overhead at horizontal distances of several kilometers in all directions. Given that ash clouds and gases travel at the mean speed of the winds the system would provide crucial advance warning. For example, a cloud moving at 10 ms^{-1} (36 km hr^{-1} at an altitude of 3 km (~10,000 feet) would be observed by the detector ~16 minutes before it appeared overhead. At 30 ms^{-1} (108 km hr^{-1}) the warning time shortens to ~5 minutes. The G-bIRD system detects ash clouds by their unique signature in the infrared window between 8–12 μm (see Prata and

Barton, 1993 for details). SO_2 is detected by exploiting the absorption caused by the gas near 8.6 μm.

Wind-blown dust from desert regions or semiarid lands can be a hazard to aircraft, reduces visibility significantly and can cause eye and throat irritation to humans. Large parts of the habitable earth are prone to dust storms, including northern Africa, the Mediterranean islands, southern Italy, Spain and France, southwestern USA, central and southern Australia, western parts of South America, central China, Japan and south and north Korea and the central deserts of Asia. The wind blown dust can also be transported long distances–dust from China has been detected in north America. The dust can consist of nearly spherical particles of SiO_2 in concentrations that will limit visibility to a few 10's of metres. Fine (1-10 μm diameter) particulates of SiO_2-bearing minerals have characteristic absorption features (Restrahlen effects) in the region 8-9 μm and can be detected by G-bIRD.

Principle of operation.

The Ground-based InfraRed Detector–G-bIRD (Prata and Bernardo, 2004; Prata, 2004) is a new passive thermal infrared imaging camera based on uncooled microbolometer technology and is a natural extension of earlier precision radiometers developed by Prata and Barton (1993) and Prata *et al.* (1991). The device operates by comparing infrared signals from the sky above, at up to 5 pre-defined wavelengths (the central wavelengths and wavelength intervals are given in Table 1). The infrared radiation measured by the detector is linearly proportional to the resistance change in the detector, which is recorded and logged by a signal processing unit. The instrument concept is made possible by the recent commercial availability of relatively cheap uncooled focal plane detector arrays (FPAs). An uncooled microbolometer staring array sensitive to radiation in the 6-14 μm wavelength interval is used to detect filtered radiation by use of a filter wheel (or similar mechanism). The radiation from the sky is focussed onto the array by means of focussing optics (a Ge lens or mirror) and the field-of-view is a cone of up to 90 degrees. The use of a filter-wheel mounted with circular interference filters is an option.

The G-bIRD camera

The prototype G-bIRD camera consists of an uncooled focal plane infrared array of dimensions 320x240 pixels, with F0.86 optics and a custom built filter wheel holding up to five narrow band (<1 μm width) interference filters. The detector has a nominal noise temperature of no less than ~50 mK in the broadband channel. To achieve sufficient temperature sensitivity in the narrow band channels, frame averaging is employed. Table 1 shows the theoretical noise equivalent temperatures (NEΔT's) expected for various frame averaging values in 5 narrow bands or channels and one broadband channel.

Band (λ)	High (λ)	Low (λ)	No of frames (NEΔT, mK)			
			4	16	32	64
7.3	7.05	7.55	1346	476	337	238
8.6	8.35	8.85	890	315	223	157
10.1	9.85	10.35	643	227	161	114
11.0	10.75	11.25	657	232	164	116
12.0	11.75	12.25	900	318	225	159
8-14	8	14	65	23	16	11

Table 1. Noise equivalent temperatures (NEΔT, mK) for different amounts of frame averaging.

Calibration

The G-bIRD camera provides raw digital counts as output from the FPA; the output has some corrections applied. These counts can be related to the scene temperature through a linear calibration process. A two point blackbody calibration procedure was developed which uses the output from the FPA corresponding to two cooled and heated blackbody cavities placed in front of the lens. The combined effect of the filters and detector response is considered in the calibration procedure. No account has been taken of the effects of off-axis viewing through the filters and the filter responses are single measurements of the response of the central portion of the filter (50 mm diameter). To convert from the calibrated radiances to scene temperature, the calibration equation must be inverted. This is a nonlinear problem that requires a minimisation procedure. The approach adopted is to generate a series of look-up tables that give radiances equivalent to pre-specified temperatures. The procedure is accurate to 10 mK over the range of observable temperatures 220 K to 330 K. The calibration procedure is repeated several times and average look-up tables are generated. In actual use the calibration is performed in the laboratory and not done in the field. This is possible because once a calibration file has been derived under idealised conditions this can be used in all future measurements to convert the raw signals into temperatures. However, in practice the optics (particularly the lens) may heat up or cool down and thus produce a different temperature to its value when calibrated in the laboratory. This causes an off-set in the measured signals. To overcome this problem we have devised an innovative field calibration procedure that makes use of a single shutter

measurement. The shutter fills or slightly overfills the field-of-view of the instrument and provides a uniform radiation source to the detector. The temperature of the side of the shutter facing the lens is continuously monitored using a contact temperature probe. The shutter side facing the lens is blackened so that its infrared emissivity is high (exceeding 0.96) and uniform across the region 6-14 μm. In the field, the calibration is performed by making a single measurement of the shutter, followed by a measurement of the scene and then application of the calibration equations and shutter measurement that accounts for the off-set generated by any change in temperature of the lens. Fig. 1 shows a photograph of the camera in use in the field.

Field Testing

The G-bIRD camera has been field tested at several active volcanoes and sites where ash and SO_2 emissions are observed. The complete field program, testing and analyses cannot be reported here and only a summary of the main results is given.

Figure 1. The G-bIRD camera on site at Etna.

The field program was divided into three parts: (A) testing of the camera hardware, processing system, communications and real-time image delivery, (B) testing the camera in elevated SO_2 conditions, and (C) testing the camera in elevated volcanic ash conditions. To achieve the goals of the field program the following sites were visited:

(1) Kilauea, Hawaii - system testing,
(2) Anatahan, NMI - system testing and measurement site for goals (A, B, C),
(3) Port Pirie, South Australia–SO_2 measurements goal (B)
(4) Etna and Stromboli, Italy–SO_2 measurements and system test goals (A, B),
(5) Tavurvur, Rabaul, PNG–ash measurements goal (C).

To give an indication of the results of the trials we present data for field tests (4) and (5), which clearly show the usefulness of the system for volcanic SO_2 and ash monitoring.

Mt Etna and Stromboli, Sicily, Italy. Mt Etna (3300 m ASL) has been active since starting an eruptive phase in November 2002. The G-bIRD camera was deployed about 15 km from the active crater in the town of Nicolosi (1015 m ASL) on the south-western flank of the volcano. When measurements were made during September 2003, the emissions from Etna were predominantly SO_2 with a few minor ash eruptions, never attaining significant height and rarely visible beyond a few 100 m's away. The viewing elevation angle of the camera was varied from 10 to about 30 degrees above the horizon. The G-bIRD camera was tested for monitoring SO_2 and for communications trials. At Stromboli, the emissions were also SO_2 and the activity there provides a more or less continuous gaseous plume. Intermittent explosions of ash were observed, but these also rarely attained heights of more than a few 10's m above the summit and the ash did not get transported any significant distance in the air. G-bIRD was mounted ~3 km from the active crater on Stromboli. Results are provided in Figures 2 and 3.

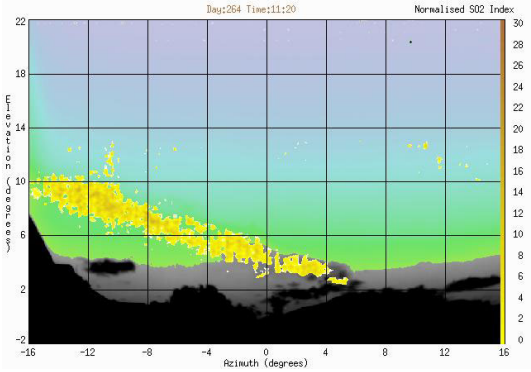

Figure 2. SO_2 plume observed over Mt Etna. The SO_2 index is a qualitative measure of the SO_2 concentrations in the plume.

Each of the Figures shows a single frame of data identifying the plume as SO_2-laden. Consecutive

frames of data can be looped to form a movie-style animation of the plume.

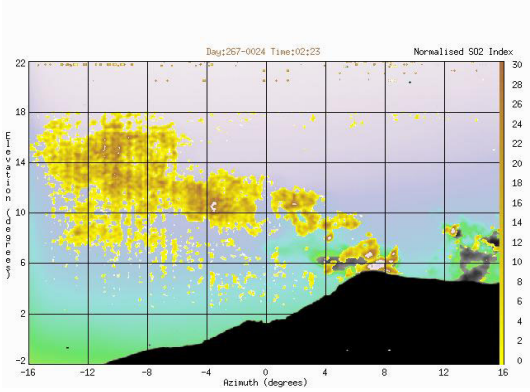

Figure 3. SO_2 plume from Stromboli.

These movies reveal typical plume dynamical features such as: thinning, turbulent eddies, puffs, fumigation and vertical and horizontal mixing. On many occasions G-bIRD detected large changes in the apparent concentrations of SO_2; most notable were instances where the SO_2 concentrations would dip below the detection level of G-bIRD and the plume appeared to be predominantly water vapour. A whole sequence of data was collected where a white-looking water-laden plume from Etna was indistinguishable to the naked eye (or a web-cam) from an SO_2-laden plume. The G-bIRD imagery made a distinct discrimination between these two plumes.

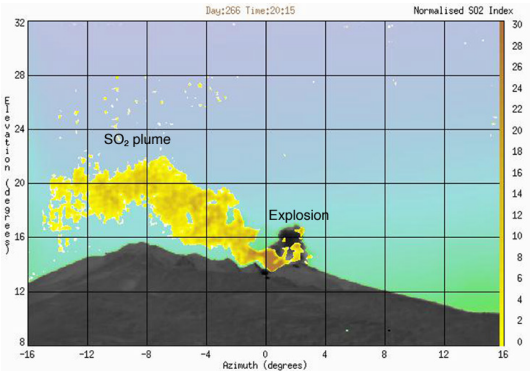

Figure 4. G-bIRD camera viewing a plume of SO_2 and an explosion (coloured grey to black) from Stromboli.

The results for Stromboli (Fig. 4) were similarly striking and unambiguous, although much less water vapour was apparent in the Stromboli plume and the strength of the SO_2 signal was greater due to the closer proximity of the camera deployment there. That there is water vapour in both plumes is undeniable and obvious through observation of the white-coloured plumes from both volcanoes. Less obvious is the detection of separate regions of SO_2 above the craters, where no plume is visible at all to the naked eye (or web-cam). Measurements were also made during the night at both volcanoes. If anything, the data are clearer during the night than during the day–the reason, perhaps, being due to less evaporation and subsequent lower water vapour loadings in the plumes at night compared to during the day. The G-bIRD camera was also able to capture discrete explosions from Stromboli. In the case of the explosion, the pyroclastic material is mostly hot rocks, cinders and ash and reveals itself as grey to black colours when the SO_2 algorithm is used. In contrast when the ash algorithm is used, that is, by taking temperature differences using only two channels, the resulting image appears as shown in Figure 5.

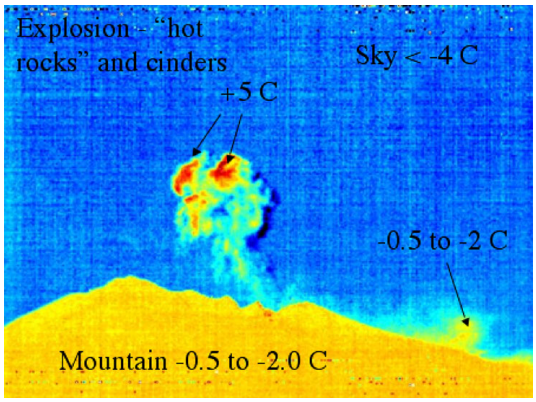

Figure 5. Ash algorithm used on an image with an explosion obtained at Stromboli.

In this case the algorithm identifies the hot rocks and cinders as positive differences (high ash content), and resuspended ash as slightly negative (similar to the material on the surface of the mountain slopes). The sky has markedly negative differences. The interference effects of water vapour at these low elevation viewing angles has not been accounted for.

There is a nonlinear relation between the temperature differences and the SO_2 amount measured in atm-cm or other suitable units. This relation is of the form:

$$u = \ln [\alpha \Delta T + \beta],$$

where α and β are parameters that depend on the absorption coefficient of SO_2 around 8.6 μm and on instrumental characteristics. ΔT is a temperature difference formed between two channels and u is the absorber amount in suitable units. The parameters α and β are determined from modelling studies and from calibration data for the instrument, including the response functions of each filter. An SO_2 index has been derived to account for the minor nonlinearity and provide a fast, non-quantitative measure of the SO_2 content in a G-bIRD image. Quantitative estimates of the SO_2 loadings from the G-bIRD camera, while

possible, were not attempted at Etna or Stromboli, principally because no independent validation data were acquired and the lack of a meteorological station close to the camera precludes accurate modelling of the interfering effects of water vapour.

Tavurvur, PNG. The Tavurvur crater at Rabaul has been in near-continuous activity since the catastrophic and near simultaneous eruptions from Tavurvur and Vulcan on opposite sides of Rabaul harbour in September 1996. Tavurvur activity is characterised by ash-rich explosions occurring at intervals of between 10-30 minutes. G-bIRD measurements at Tavurvur were conducted during 4 days in November 2003 from locations with line-of-sight of the crater and from distances of 1-10 km. A good example of ash identification is shown in Figure 6; Fig 7. Shows the corresponding visible camera image

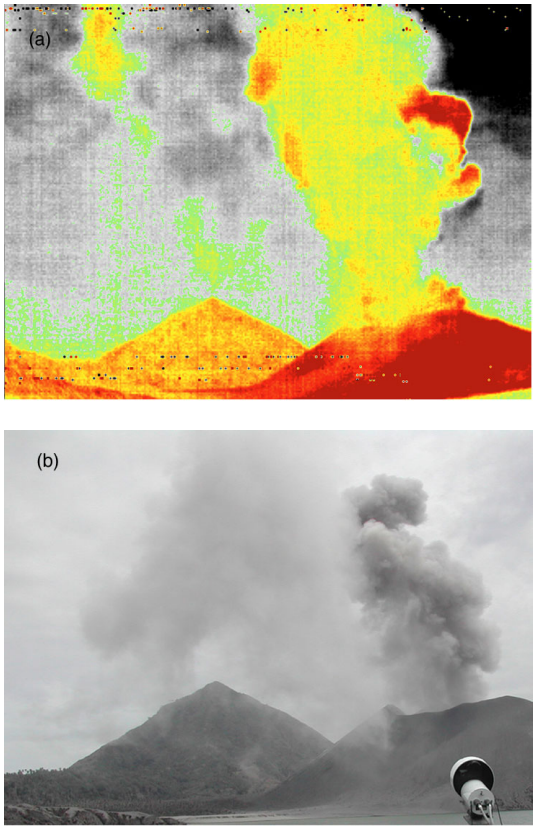

Figure 6. (a) Ash discrimination by G-bIRD for the Tavurvur plume (*upper panel*). (b) Visible camera image of the ash plume from Tavurvur, taken at almost the same time as the G-bIRD image (*lower panel*).

Although present, SO_2 was not detected by G-bIRD at Tavurvur. The reasons for this are thought to be due to the excessively high water vapour loadings, the interference from ash effects within the SO_2 channel (~8.6 μm), and possibly the much lower SO_2 concentrations (in comparison to H_2O). Excellent results were acquired at the "hot springs" within 2 km of the crater and from Rabaul observatory, some 6 km distant. Beyond 10 km or so, identification became increasingly difficult due to obscuration by water vapour over such long path lengths.

Variation with elevation

In clear and cloudy skies when there is no ash or SO_2 present, water vapour causes differential absorption of radiation in the atmospheric window between 6–14 μm. Theoretical calculations and modelling studies indicate that this difference will be negative when the camera views the sky above the horizon. The exact value of the difference depends on the amount of water vapour, but also on the path length that the radiation traverses through the atmosphere. Figure 7(a) shows the variation of the temperature difference (11–12 μm) with elevation for a cloudless atmosphere containing about 3 cm of precipitable water. At low elevation angles the temperature difference is slightly negative, but gets progressively more negative until at around 60 degrees elevation when the difference decreases slowly. A consequence of this behaviour is that it is not possible to set a constant threshold for deciding whether G-bIRD images contain ash-affected pixels

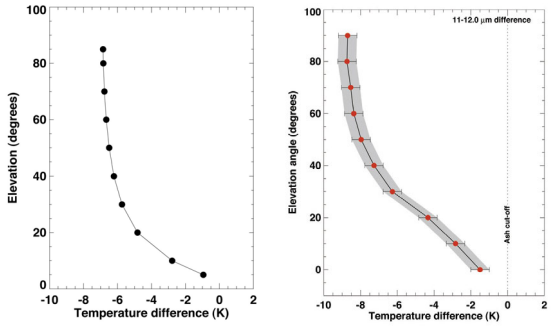

Figure 7. (a) Variation of elevation angle with temperature difference (11-12 μm) for clear skies determined from radiative transfer modelling, and (b) the difference as determined from measurements made at Saipan.

Figure 7(b) shows results using a series of G-bIRD images taken on Saipan island in clear skies. The variation with elevation angle mimics the theoretical behaviour. The same effect with elevation can be seen for 8.6–12 μm temperature differences, except that after 60 degrees the difference starts to increase rather than decrease. This is not seen in the modelling results, and more data are required to determine the cause of this effect. These data show more variation than the theoretical studies because the scene also contains clouds and unmodelled water vapour variations. Nevertheless, the temperature difference decreases with

elevation angle in all cases studied and agrees with the theoretical behaviour.

Conclusions

G-bIRD is a new thermal imaging passive infrared camera capable of detecting SO_2 and volcanic ash. The prototype camera has been successfully field tested at several active volcanoes and it has been demonstrated that SO_2 and ash can be discriminated from meteorological clouds. Rapid imaging, remote, autonomous operation and secure communications have also been successfully achieved. The camera works well up to distances of ~10 km from the volcano. It provides information 24 hours a day in clear conditions, but can also work well in slightly cloudy conditions. During rain or snowfall or heavily overcast skies, G-bIRD suffers the same limitations as other passive devices and may not provide reliable detection under these adverse circumstances.

There remains some work to be done in assessing the quantitative value of the G-bIRD imagery, particularly with respect to SO_2 concentrations. To this end, it would be most valuable to conduct field validations against established SO_2 monitors (e.g. COSPEC or mini-DOAS devices). Laboratory and field investigations aimed at quantifying the minimum ash concentrations detectable by G-bIRD would also be of great value. Regardless of the ability of G-bIRD to quantify SO_2 and ash, a rapid-imaging, thermal infrared camera for use at volcano observatories, ash-affected airports, and at the sites of active volcanoes seems warranted if timely hazard warnings of airborne volcanic emissions are required.

References

Cantor, R., Complete avoidance of volcanic ash is only procedure that guarantees flight safety, ICAO Journal, **53**(7), 18, 1998.

Casedevall, T. J., Proceedings of the *First International Symposium on Volcanic Ash and Aviation Safety*, USGS Bull. **2047**, U.S. Geological Survey, Washington, DC, 450p, 1994.

Guffanti, M., Casadevall, T., and Mayberry, G., Reducing Encounters of Aircraft with Volcanic Ash Clouds, *This Volume*.

Prata, A. J. and I. J. Barton, Detection system for use in an aircraft, *Australian Patent* **No PJ9518**, *European Patent* **No. 91907594.5**, *U.S. Patent* **No. 5,602,543**, 1993.

Prata, A. J., Barton, I.J., Johnson, W., Kingwell, J., and Kamo, K., Hazard from volcanic ash, *Nature*, **354**, 25, 1991.

Prata, A. J., Sulphur dioxide detection method. *Australian Provisional Patent* **No. 2004900213**, 2003.

Prata, A. J. and C. Bernardo, An infrared detection apparatus. *Australian Provisional Patent* **No. 2004900214**, 2003.

Tupper, A, Carn. S., Davey, J., Kamada, Y., Potts, R., Prata, A., and Tokuno, M., An evaluation of volcanic cloud detection techniques during recent significant eruptions in the western 'Ring of Fire', *Remote Sensing Environ*, **91**, 27–46, 2004.

Acknowledgements. This work was supported by Tenix Investments and Tenix Electronics Systems Division. We thank Nigel Basheer and Simon Langsford for their help with system design and field testing. Georgina Sawyer and Mike Burton provided generous assistance for the Etna field tests.

UW-MADISON ADVANCED SATELLITE AVIATION-WEATHER PRODUCTS MODIS/AVHRR/GLI SATELLITE VOLCANIC ASH DETECTION

Steven A. Ackerman*, Wayne F. Feltz*, Michael S. Richards*, Timothy J. Schmit[@], Anthony J. Schriener*, John Murray[#], and David Johnson[%]

* Cooperative Institute for Meteorological Satellite Studies (CIMSS), University of Wisconsin-Madison, Madison, WI
[@] NOAA/NESDIS, Office of Research and Applications, Madison, WI
[#] NASA LaRC, Langley, VA
[%] NCAR, Boulder, CO

1. Introduction

Geostationary satellite instrumentation offers relatively good temporal resolution for the monitoring of airborne ash resulting from volcanic eruptions. While geostationary platforms provide better temporal resolution, their large fields of view and limited global coverage over volcanically active regions act as disadvantages for the tracking of volcanic ash in the atmosphere. In contrast, polar orbiting satellites provide high spatial resolution and better global coverage but, in general, poor temporal sampling. At any given time there are several polar orbiting satellites, each capable of detecting volcanic ash with fairly frequent time intervals at upper latitudes. This ongoing study focuses on determining how best to optimize satellite platform and infrared channel selection from different IR instruments aboard satellites in both polar and geostationary orbits in an effort to better monitor volcanic ash in the atmosphere.

This paper provides results obtained by Schreiner et al. during their investigation of upper-level SO_2 monitoring by the current GOES sounder. A separate investigation of volcanic ash monitoring by the MODIS, NOAA AVHRR and the Japanese Global Imager (GLI) instruments is also presented. Both investigations focus on volcanic eruptions of Soufriere Hills on the island of Montserrat, located in the eastern Caribbean, during the period 13-15 July 2003.

Corresponding author address:
Steven A. Ackerman, CIMSS/SSEC,
1225 West Dayton Street Room 251,
Madison, WI, 53706
stevea@ssec.wisc.edu

2. Methodology

The methodology used in this research to detect the presence of volcanic ash plumes consisted of utilizing measurements from instruments onboard several polar orbiting satellites. These instruments include MODIS (Terra), AVHRR (NOAA 15, 16 and 17) and GLI (ADEOS-II). The ash detection method used is based on knowledge of spectral signatures resulting from the presence of suspended particulates. These particulates produce spectral signatures caused by differential scattering, absorption and/or emission of infrared radiation by the plume constituents. The spectral signatures from the ash cloud are driven by the microphysical properties and index of refraction of the aerosols. Spectral measurements near 11 and 12 μm have been successful at detecting these volcanic ash aerosols.

Detection of SO_2 can also be useful in monitoring ash clouds when SO_2 is released along with ash during a volcanic eruption. While both SO_2 and ash do not always follow the same post-eruption trajectories (Seftor et al. 1997), monitoring SO_2 clouds does provide insight for locating possible regions of volcanic ash. Considering the aforementioned spectral signature methodology, spectral measurements at 7.3 and 8.5 μm have been successful at detecting volcanic plumes containing SO_2. Both SO_2 and volcanic ash detection examples from the Soufriere Hills volcanic eruption follows.

3. Using the GOES Sounder to detect SO_2

The first major eruption of Soufriere Hills occurred around 0230 UTC on 13 July. This eruption was triggered by a major collapse of the Soufriere Hills lava dome with the resulting ash cloud reaching a level of approximately 16 kilometers[1]. A calculation of SO_2 concentration (Dobson Units) based on AIRS radiance information (**Figure 1**) from 13 July at 1653 UTC shows that SO_2 concentrations from the volcanic plume approached 300 milli atm-cm and extended towards the northeast from Monsterrat Island. Using a trajectory model (NOAA HYSPLIT Model), forward trajectories were calculated (**Figure 2**). Utilizing bands 10 (7.4 μm) and 5 (13.3 μm) on the GOES sounder, a series of "band differenced" images (BT_{10}-BT_5) were derived (**Figures 3-6**). The derived images were obtained in order to subtract out the background temperature difference, since these two bands are "sensing" the same layer of the atmosphere. The resulting difference band shows the "SO_2 plume" (dark areas) over an eighteen-hour period following the eruption.

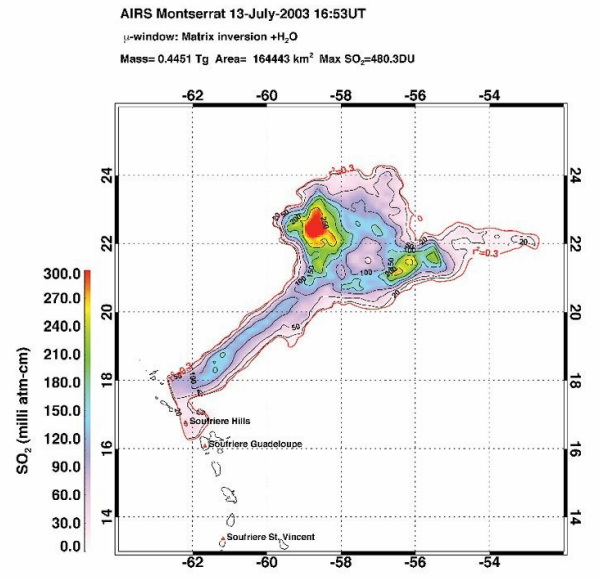

Figure 1: ***Calculation of SO_2 concentration (Dobson Units) based on AIRS radiance information from 13 July at 1653 UTC. Figure provided by Dr. Fred Prata CSIRO.***

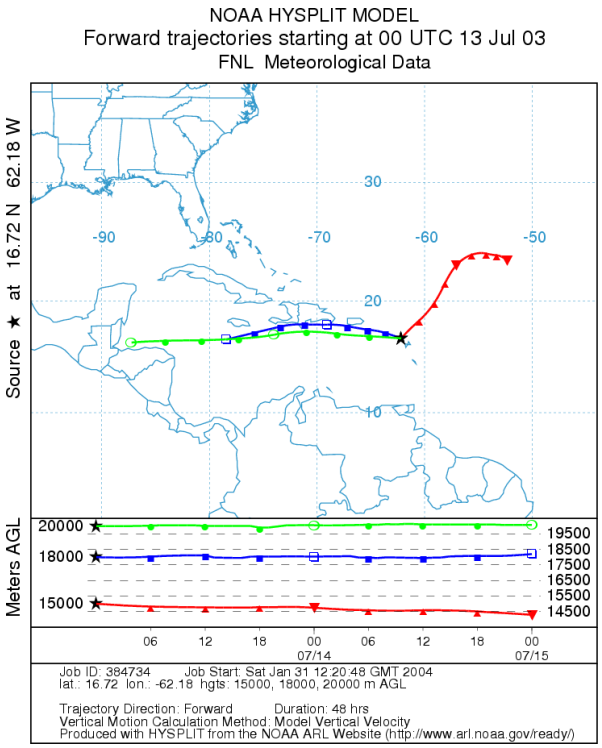

Figure 2: ***NOAA HYSPLIT 24 hour trajectory model beginning 00 UTC 13 July 2003. Figure provided by Dr. Fred Prata CSIRO.***

4. Using MODIS, AVHRR and GLI to Detect Volcanic Ash and SO_2

Between the dates of 13-15 July 2003, numerous explosive events occurred at the Soufriere Hills volcano on Montserrat. During this period, ash was observed to have reached altitudes greater than 10 kilometers on more than one occasion[2]. Instruments aboard polar orbiting satellites Terra, NOAA 15, NOAA 16, NOAA 17 and ADEOS-II were able to scan the Caribbean in the hours immediately following Soufriere Hills's explosive volcanic activity.

Presented here are images derived from the MODIS, AVHRR and GLI instruments. All instruments have channels near 11 and 12 μm, and the MODIS and GLI yield spectral measurements sensitive to SO_2, near 8.6 and 7.4 μm. The following derived images show the polar orbiting

[1] based on estimates from the Volcanic Ash Advisory Center in Washington, D.C.

[2] Smithsonian Institute – Global Volcanism Project

13 July 2003 0720 UTC (figure 3)

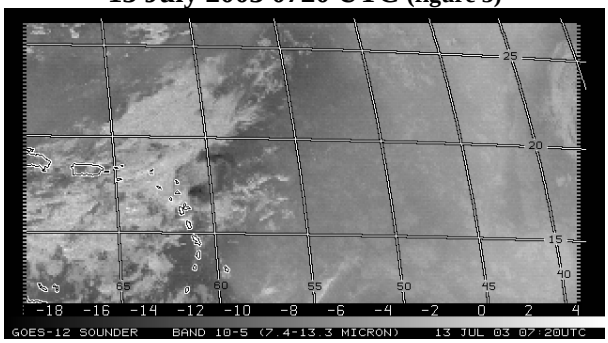

13 July 2003 1320 UTC (figure 4)

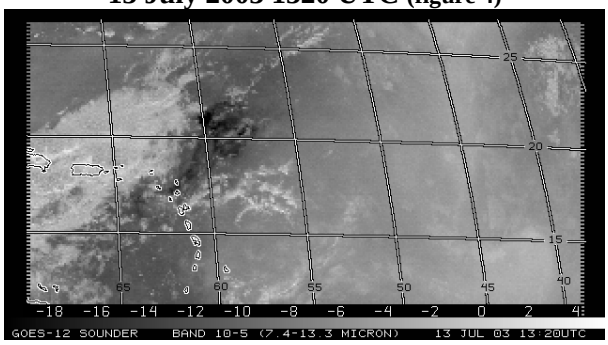

13 July 2003 1920 UTC (figure 5)

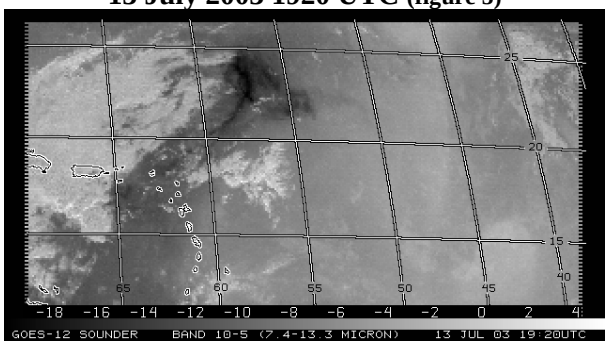

14 July 2003 0120 UTC (figure 6)

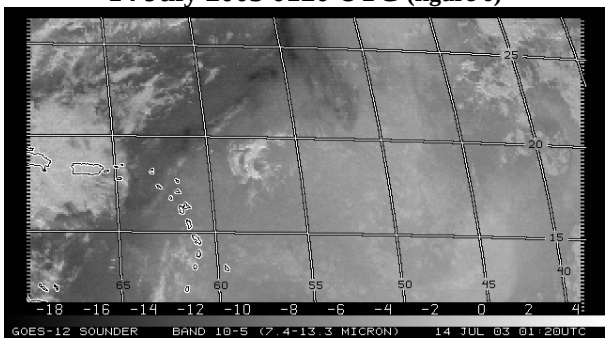

Figures 3-6: ***GOES sounder images from 13-14 July 2003 Images are sounder band*** *10 (~7.4 μm) minus sounder band 5 (~13.3 μm).*

satellites' perspective of the Soufriere Hills' eruptions from several different instruments and viewing angles. The series of MODIS (**Figures 7-8**), AVHRR (**Figures 9-11**) and GLI (**Figures 12-13**) images are band differenced (11-12μm) brightness temperatures. These so-called "split-window" channels are used to "observe and quantify silicate ash" (Elrod and Im 2003, Watson et al. 2004). Corresponding band subtractions for MODIS, AVHRR and GLI are 31-32, 4-5 and 35-36, respectively. Negative differences in the band differenced images show likely locations for airborne volcanic ash. It should be noted that the changing satellite viewing geometries and instrument spectral response functions lead to instrument differences.

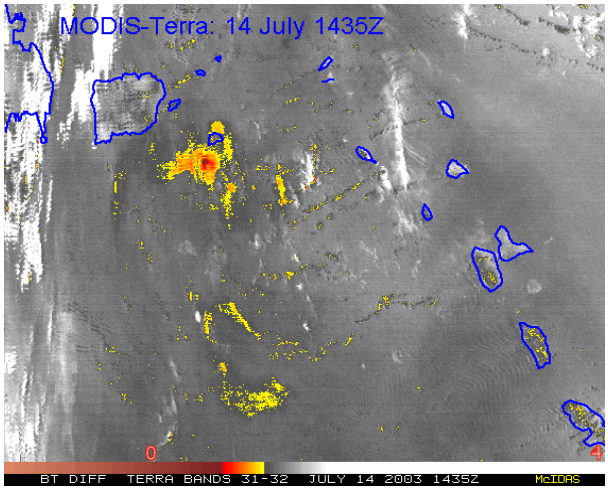

Figure 7: *MODIS (Terra) image from 1435 UTC 14* ***July 2003. Images are band*** *31 (~11 μm) minus band 32 (~12 μm).*

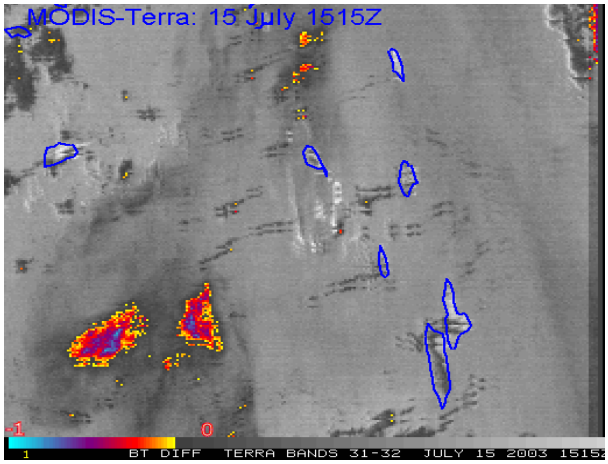

Figure 8: *MODIS(Terra) image from 1515 UTC 15* ***July 2003. Images are band*** *31 (~11 μm) minus band 32 (~12 μm).*

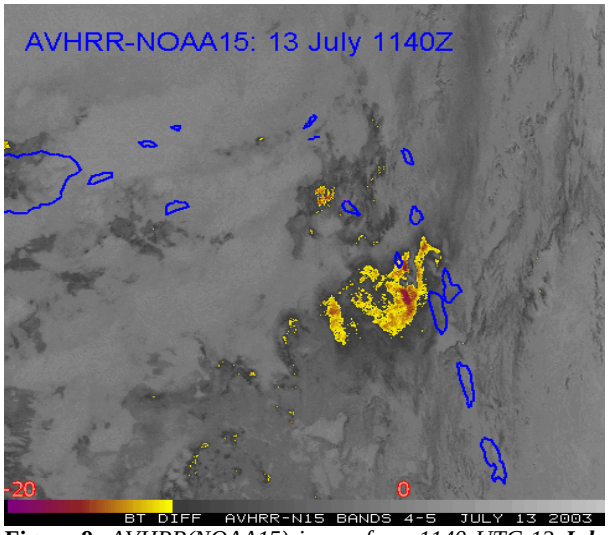

Figure 9: *AVHRR(NOAA15) image from 1140 UTC 13* ***July 2003. Images are band*** *4 (~11 μm) minus band 5 (~12 μm).*

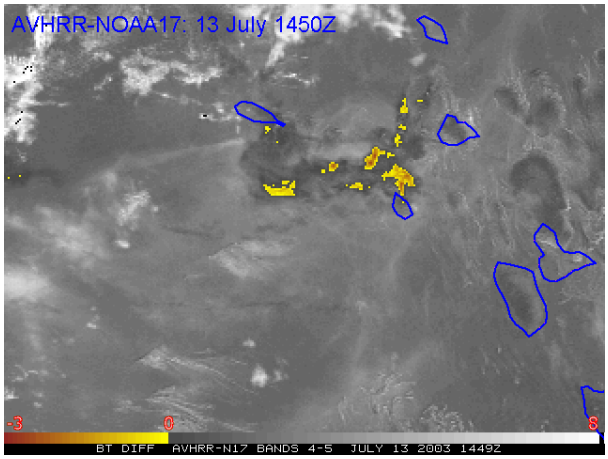

Figure 10: *AVHRR(NOAA17) image from 1450 UTC 13* ***July 2003. Images are band*** *4 (~11 μm) minus band 5 (~12 μm).*

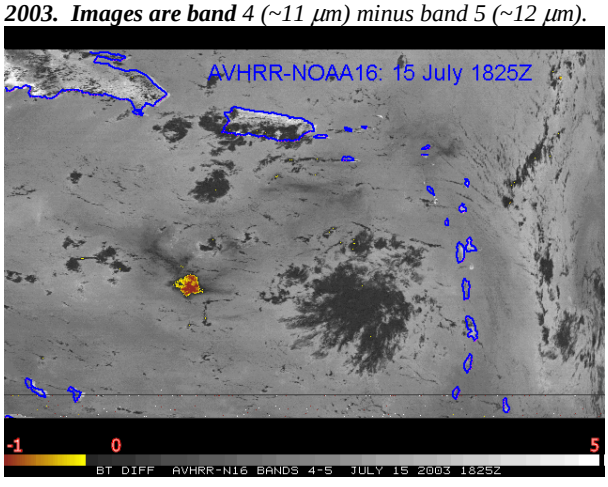

Figure 11: *AVHRR(NOAA16) image from 1825 UTC 15* ***July 2003. Images are band*** *4 (~11 μm) minus band 5 (~12 μm).*

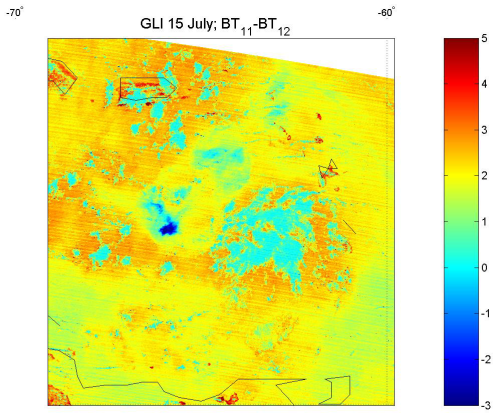

Figure 12: *GLI(ADEOS-II) image from 15* ***July 2003. Images are band*** *35 (~11 μm) minus band 36 (12 μm).*

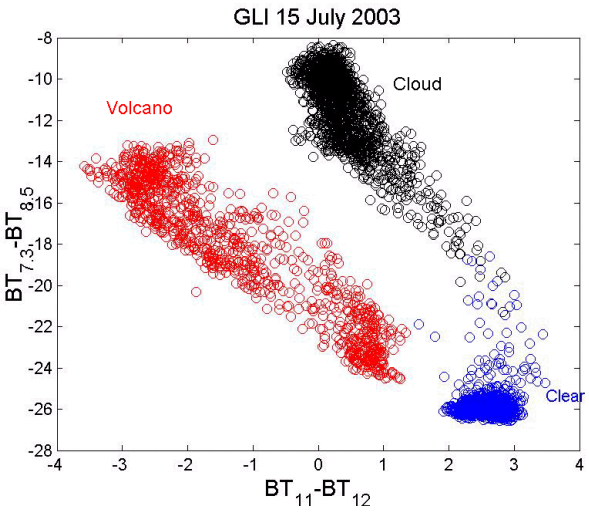

Figure 13: *GLI(ADEOS-II) from 15* ***July 2003.***

The advantage of GLI and MODIS measurements is that both instruments have channels at the 7.3 and 8.5 μm region. This provides the ability to distinguish volcanic ash, clear, and cloudy scenes from one another as presented in figure 13.

5. Conclusions and Future Work

Instruments in both geostationary and polar orbits provide unique methods for the detection and tracking of volcanic ash in the atmosphere. Results by Schreiner et al. presented here reveal that the current GOES Sounder is able to detect upper-level SO_2 over areas of normally low

probabilities of volcanic eruption. In this case the sounder scan sector only provided a six hour temporal resolution. Optimally a high spatial and temporal resolution with spectral coverage in volcanically sensitive IR regions is desired. Trajectories illustrated in **Figure 2** indicate the SO_2 detected by the GOES sounder, a plume of relatively negative band differences (7.4-13.3μm) to the northeast of the island **(Figures 3-6)**, might have existed at a height of approximately 15 kilometers a.s.l. While AVHRR imagery (**Figure 9**) does indicate the likely presence of a volcanic ash plume (relatively negative 11-12μm band difference) to the northeast of the island, the highest concentrations of airborne ash exist to the immediate south and west of the island (**Figures 9-10**). As illustrated here, the polar orbiting platform provides a necessary compliment to geostationary instruments such as the GOES sounder when monitoring volcanic ash in the atmosphere.

Future work includes optimizing the operational Geostationary and Polar infrared instrument (GOES and AVHRR) volcanic eruption detection algorithms to sense SO_2, volcanic ash, and plume height. In fact, good estimates of volcanic ash altitude are not routinely available via satellite remote sensing systems and is a major concern to the aviation community.

In addition, polar research satellites (MODIS, GLI, and AIRS) will be used to provide insight for improvement of volcanic ash tracking and dissipation rates for high latitude volcanic eruptions with emphasis places on determining the altitude of the volcanic ash cloud.

The next generation geostationary infrared weather instruments (ABI, GIFTS and HES) will have spectral coverage similar to existing instruments on polar orbiting satellites. This investigation, therefore, provides an opportunity to lay the ground work for future "volcanic ash detection" algorithms.

6. References

Elrod, G. P. and J. Im, 2003: Development of Volcanic Ash Image Products Using MODIS Multi-spectral Data. Preprints, 12th Conference of Satellite Meteorology and Oceanography, 9-13 February 2003. Boston, MA, American Meteorological Society,

Schreiner A. J., T. J. Schmit, J. Li, G. P. Ellrod, M. Gunshor, and K. Karnauskas, 2004: Using GOES-R to Help Monitor SO_2. Presented at the GOES-R Users Conference. 10-13 May, 2004. Broomfield, CO.

Seftor, C. J., N. C. Hsu, J. R. Herman, P. K. Bhartia, O. Torres, W. I. Rose, D. J. Schneider and N. Krotkov, 1997: Detection of volcanic ash clouds from Nimbus-7/TOMS, *J. Geophys. Res., 102: 16749-16760.*

Watson, I. M., V. J. Realmuto, W. I. Rose, A. J. Prata, G. J. S. Bluth, Y. Gu, C. E. Bader and T. Yu, 2004: Thermal infrared remote sensing of volcanic emissions using the moderate resolution imaging spectroradiometer, *J. Volcanol Geoth Res 135: 75-89*

REMOVAL PROCESSES OF VOLCANIC ASH PARTICLES FROM THE ATMOSPHERE

Gregg J.S. Bluth and William I. Rose, Michigan Technological University

INTRODUCTION

The use of satellite techniques provides valuable information for mapping ash hazards, as well as the means to study and predict the fates of volcanic clouds. We have used ultraviolet (TOMS – *Total Ozone Mapping Spectrometer*) and infrared (e.g., AVHRR – *Advanced Very High Resolution Radiometer*; HIRS2 – *High Resolution Infrared Radiation Sounder/2*; GOES – *Geostationary Operational Environmental Satellite*; MODIS – *Moderate Resolution Imaging Spectroradiometer*) satellite sensors to examine the solid, liquid and gas species in numerous volcanic clouds over the past 25 years. Each sensor provides a somewhat different perspective of volcanic clouds, depending on their spatial, spectral and temporal resolutions. Thus, when combined these techniques provide important constraints on the interactions and fates of species within the clouds. Quantitative infrared techniques can provide information on how the size, size distribution, and total mass of fine ash particles evolve as a cloud mixes with the atmosphere. Here we present a review of past relevant observations and research, and the results of ongoing satellite studies.

VOLCANIC CLOUD PARTICULATES

Volcanic clouds are typically composed of a variety of particulates, derived from:

-volcanogenic sources (silicate particles, erupted gases and liquids)

-the atmosphere (water/ice, dust, sea salt, gases)

-products from volcano-atmosphere reactions (aerosols, coatings, adsorbed species on existing particles)

(1) Particle compositions

-silicates: glassy pyroclasts and minerals, which represent the crystalline fraction of the magma. Their shapes are highly angular, and in fact can be composed of shards, bubble fragments, as well as microcrystals. The silicate particles reflect the magmatic origins, ranging from rhyolitic (high silica) to basaltic (low silica).

-non-silicates: the most common type is sulfate aerosols. Many other minor and rare phases have been observed (Rose et al., 1982).

(2) Shapes and Sizes:

A thorough examination of particle size, geometry, and composition by Riley et al. (2003) revealed:

-extremely high surface areas relative to volume, due to roughness and vesicularity (up to 2 orders of magnitude greater areas than calculated using shape alone).

-aspect ratios of 1.5 – 2.6 (long-to-short 2D dimensions, compared to 1 for a perfect sphere). See Figure 1.

Erupted materials are composed of a full spectrum of particle sizes, which quickly becomes differentiated through gravitational settling and physical interactions in the clouds. Based on satellite studies, about 1-2% of the total ash mass erupted is 1-12 microns (μm) in radius (Rose et al., 2001), which is the fraction which can be most easily tracked by satellite.

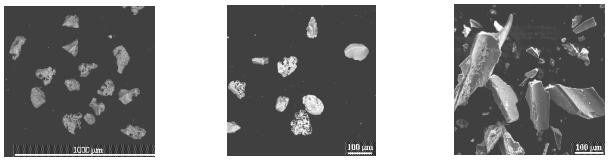

Figure 1. SEM photos of (l-r) Fuego, Guatemala basaltic ash; Mt. Spurr, Alaska andesitic ash; bubble wall shards from the rhyolitic ash of the Ash Hollow Member, Nebraska (Riley et al., 2003). Scale bars are 1000μm for Fuego, 100μm for Mt. Spurr and Ash Hollow Member.

THREE STAGES OF VOLCANIC CLOUD EVOLUTION

Rose et al. (2001) developed three general stages based on satellite observation of evolving clouds from the Mt. Spurr (Alaska) eruptions in 1992:

(1) High energy and growth

During the eruption and for the first few hours afterward, the clouds resemble thunderstorms, and are often opaque to IR sensors. Most of the coarse (>50 microns diameter) material falls out near the vent source (Figure 2).

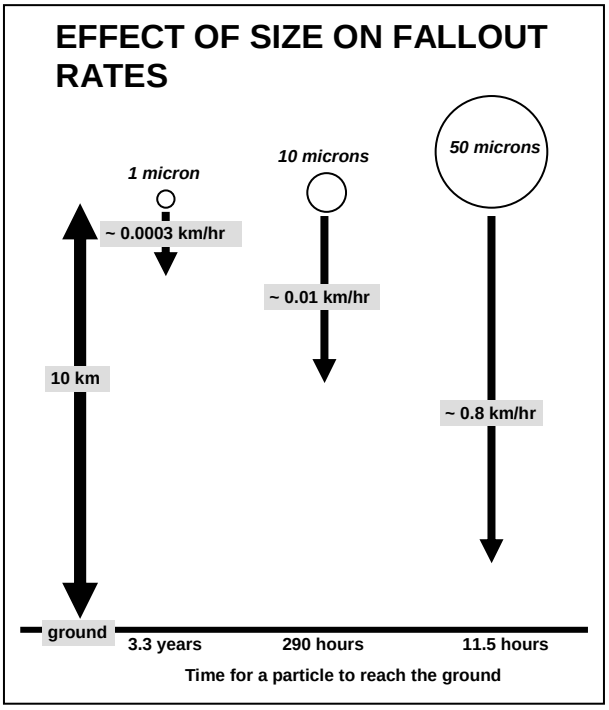

Figure 2. This simple calculation (after Bonadonna et al., 1998) shows that most large (>50 micron diameter) particles will fall out of a volcanic plume within the first day at rates of around 0.8 km/hr; on the other hand, very small particles (<1 micron) could persist in the atmosphere for years. "Particles" may be composed of a single fragment; aggregates of various sizes; particles with coating of water or ice; particle with adsorbed gas or liquid. Clearly, the shape and density of a particle or group of particles will affect how it falls (laminar or turbulent), and how fast it will fall, but this calculation gives a rough estimate, assuming laminar flow and high latitude atmospheric conditions.

(2) Rapid physical and chemical changes

Lasting approximately one day, the cloud expands in areal extent, but the optical depth and fine-particle size concentrations decrease rapidly (by 1 or more orders of magnitude). Fine ash is rapidly removed from the cloud, most likely by aggregation or as icy ash balls (see next section).

(3) Drifting aircraft hazard

This stage lasts 3-5 days, during which the cloud can move thousands of kilometers. Ash concentrations and optical depths decrease very slowly, and ash masses slowly decrease to below sensor detection limits.

PARTICLE REMOVAL RATES

Table 1 compares the removal rates of ice and ash for several different eruptions. The measurement periods vary owing to instrument

Table 1. Ash and ice removal rates measured by satellite

Volcano	Meas. Period (hrs after eruption)	Particle type	Mean Removal Rate (kt/hr)	E-folding (hrs)	Sensor	Ref
El Chichón, Mexico (1982a)	5 – 68	ash	34	13	AVHRR	a
El Chichón, Mexico (1982b)	7 – 70	ash	99	15	AVHRR	a
Pinatubo, Philippines (1991)	5 - 111	ash	482	24	HIRS/2	b
Pinatubo, Philippines (1991)	5 - 111	ice	819	30	HIRS/2	b
Pinatubo, Phillipines (1991)	6 - 104	ash	363	27	AVHRR	b
Pinatubo, Philippines (1991)	6 - 104	ice	648	27	AVHRR	b
Hudson, Chile (1991)	2 – 132	ash	21.8	30	AVHRR	c
Spurr, USA (Jun 1992)	13 – 152	ash	2.3	143	AVHRR	d
Spurr, USA (Aug 1992)	14 – 84	ash	3.7	43	AVHRR	d
Spurr, USA (Sept 1992)	8 – 70	ash	4.9	52	AVHRR	d
Hekla, Iceland (2000)	6 – 24	ice	48	8	AVHRR	d
Cleveland, USA (2001)	6 – 20	ash	1.6	10	GOES + MODIS	e

a) Schneider et al., 1999; b) Guo et al., 2004b; c) Constantine et al., 2000; d) Rose et al., 2001; e) Gu, 2004.

temporal resolution, and the period reflects the time between when ash decrease is measured to the end of sensor detection. While this represents only a small portion of volcanic eruptions, it appears that the large events (El Chichón, Pinatubo, Hudson) exhibit fast removal rates of ice or ash and consequently much shorter residence times than the smaller events (Spurr, Hekla). However, note the exception from the Cleveland event, which was small, yet underwent rapid removal. In contrast to ash cloud decrease (e-folding, which is the time for the cloud to reduce to 1/e of its original mass), sulfur dioxide gas e-folding rates are on the order of 2 – 25 *days*, rather than hours (e.g., Figure 3).

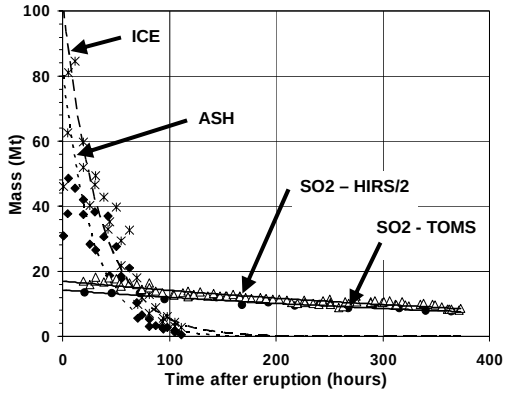

Figure 3. Mass removal patterns of ash, ice and sulfur dioxide in the 1991 Pinatubo volcanic cloud (Guo et al., 2004a; 2004b).

REMOVAL PROCESSES

(1) Ash/ice hydrometeors

Satellite studies find that the radii of suspended particles can *increase* over the first 36 hours after eruption, which we interpret as indicative of ice formation on ash particles (Rose et al., 2000). Modeling studies suggest that these aggregates may be over 80% ash by weight (e.g., Herzog et al., 1998; Textor, 1999).

(2) Particle aggregation (sticking)

The rate of fine ash removal during the first 1-2 days shows a rapid decrease (Figure 3), which cannot be explained through discrete particle settling rates (Figure 2). These fine particles must be removed by either adsorption onto larger particles or aggregation as a result of particle collisions.

REMOVAL RATES OF DIFFERENT CLOUD SPECIES

Note that in Figure 3 the ice and ash have similar removal rates, which are much faster than gas removal. Sulfur dioxide removal is largely a function of its chemical conversion rates to sulfate aerosol, rather than any kind of gravitational process. The resulting formation of sulfate aerosol is essentially the inverse of the gas decay. Other eruption clouds have shown similar patterns where fine ash removal is much faster than the sulfur dioxide gas (Table 1). The similarity of ice and ash removal rates, together with slow fallout calculated for discrete particles of this size, strongly suggest that both of these species undergo aggregation which drives their relatively rapid removal from the atmosphere.

DOES ASH IN LARGE ERUPTIONS FALL OUT FASTER?

For Pinatubo, about 90% of the 1-15 micron sized ash fell out within the first 4 days of eruption (Figure 3). Approximately 99% of the fine ash was removed within 6 days. We have observed that several large eruptions have a significantly faster removal rate than smaller eruptions. How might this occur?

(1) The more intense eruption columns typically involve greater upward velocities. These stronger events are therefore more efficient at re-entraining particles in the rising ash and gas plumes than low-intensity eruption columns (Ernst et al., 1996).

(2) More intense eruptions have higher eruption rates (volume emitted per time), so that the emitted volume of fragmented ash is higher.

(3) More fragmentation, and a higher ash volume, results in more electric charge generated in the volcanic plume, producing more electrostatic "sticking" of particles.

(4) Higher columns entrain more moist air and experience higher temperature gradients leading to the formation of hydrometeors, resulting in further charge generation by processes similar to electric charge formation in thunderstorms.

(5) The combination of processes magnified by the more intense eruption columns produce more efficient particle removal by ash aggregation, ice coating and rapid removal as icy pyroclasts.

CONCLUSIONS

Satellite sensors have the ability to detect and quantify the 1-12 micron radius size fraction of drifting volcanic ash clouds. Studies of removal rates and processes for a range of volcanic eruptions reveal that ash and ice particles fall out at much faster rates than do the co-emitted sulfur dioxide gas. The rapid fallout of fine particulates is best explained by aggregation processes, and in some cases, the formation of ice on ash particles.

ACKNOWLEDGEMENTS

Our satellite-based studies over the past several years have been supported by NASA's Solid Earth and Natural Hazards program, NASA Headquarters, and the TOMS Science Team; and the National Science Foundation's Petrology and Geochemistry program.

REFERENCES

Bonadonna, C., G.G.J. Ernst, and R.S.J. Sparks (1998) Thickness variations and volume estimates of tephra fall deposits: the importance of particle Reynolds number. J. Volc. Geotherm. Res., 81, 173-187.

Constantine, E.K., G.J.S. Bluth, and W.I. Rose (2000) TOMS and AVHRR observations of drifting volcanic clouds from the August 1991 eruptions of Cerro Hudson. AGU Geophys. Mon. 116, 45-64.

Ernst, G.G.J., M.I. Bursik, S.N. Carey and R.S.J. Sparks (1996) Sedimentation from turbulent jets and plumes. J. Geophys. Res., 101, 5575-5589.

Gu, Y. (2004) Particle Retrieval Using Satellite Remote Sensing. Ph.D. thesis, Michigan Technological University.

Guo, S., G.J.S. Bluth, W.I. Rose, I.M. Watson, and A.J. Prata (2004a) Re-evaluation of SO2 release of the 15 June 1991 Pinatubo eruption using ultraviolet and infrared satellite sensors. Geochem. Geophys. Geosys., 5, Q04001, doi:10.1029/2003GC000654.

Guo, S., W.I. Rose, G.J.S. Bluth, and I.M Watson (2004b) Particles in the great Pinatubo cloud of June 1991: The role of ice. Geochem. Geophys. Geosys., 5, Q05003, doi:10.1029/2003GC000655.

Herzog, M.,H.-F. Graf, C. Textor, and J.M. Oberhuber (1998) The effect of phase changes of water on the development of volcanic plumes. J. Volc. Geotherm. Res., 87, 55-84.

Riley, C.M., W.I. Rose and G.J.S. Bluth (2003) Quantitative shape measurements of distal volcanic ash. J. Geophys. Res., 108, n. B10, 2504.

Rose, W.I., R. Chuan, and D.C. Woods (1982) Small particles in plumes of Mount St. Helens. J. Geophys. Res., 87, 4956-4962.

Rose, W.I., G.J.S. Bluth and G.G.J. Ernst (2000) Integrating retrievals of volcanic cloud characteristics from satellite remote sensors: a summary. Phil. Trans. Roy. Soc. London A, 358, 1585-1606.

Rose, W.I., G.J.S. Bluth, D.J. Schneider, G.G.J. Ernst, C.M. Riley, L.J. Henderson, and R.G. McGimsey (2001) Observations of volcanic clouds in their first few days of atmospheric residence: The 1992 eruptions of Crater Peak, Mount Spurr Volcano, Alaska. J. Geology, 109, 677-694.

Schneider, D.J. et al. (1999) Early evolution of a stratospheric volcanic eruption cloud as observed with TOMS and AVHRR. J. Geophys. Res., 104, 4037-4050.

Textor, C. (1999) Numerical simulation of scavenging processes in explosive eruption clouds. Ph.D. thesis, Max Planck Institute for Meteorology, Hamburg, Germany.

SOUNDING OF VOLCANIC CLOUDS WITH BALLOON-BORNE INSTRUMENTS: IMPROVING ALGORITHMS FOR ASH AND SO_2 IN REMOTE SENSING IMAGERY

John Chadwick, Idaho State University, Pocatello, ID, USA
Zach Lifton, Idaho State University, Pocatello, ID, USA
Ken Dean, University of Alaska, Fairbanks, AK, USA
Jim Chadwick, Mitre Corporation, Mclean, VA, USA

The Volcanic Ash Sulfur Dioxide Balloon Experiment (VASDBE) is a set of sampling instruments designed for rapid balloon-borne deployment into a volcanic cloud 24 – 96 hours after a large volcanic eruption. High precision instruments for measuring ash and sulfur dioxide concentrations, as well as meteorological parameters, will be used to characterize the atmospheric column from the surface to 32,000 m. The 4-6 balloon sensor platforms to be built will be tracked using GPS, and recovered after a parachute descent for data collection. For launch planning, volcanic clouds will be tracked using near real-time GOES imagery and meteorological prediction models such as Puff. The results of this study will be used to refine the calibration of algorithms for the measurement of ash and SO_2 from remote sensing imagery, and will thus improve remote sensing based ash warnings for aircraft. GOES imagery is acquired every half-hour, and balloon launches can be synchronized with image collection with little temporal offset to allow for direct comparisons between imagery and sounding data. However, repeat cycles for polar-orbiting MODIS, TOMS, and ASTER platforms will render it more difficult to time balloon data collection to coincide with image acquisition. It is anticipated that this study will help to better constrain the viewing depths into volcanic clouds by various types of satellite imagery, and soundings near the periphery of the cloud will allow for the assessment of the minimum ash and SO_2 concentrations that are detectable using remote sensing.

FALL3D: A NUMERICAL MODEL FOR VOLCANIC ASH DISPERSION IN THE ATMOSPHERE

A. Costa, and G. Macedonio, Osservatorio Vesuviano - Istituto Nazionale di Geofisica e Vulcanologia, Napoli, Italy

Aircrafts may unexpectedly encounter volcanic ash clouds during their flight that often cause engines failure. In order to mitigate the risk related to this accident it is of vital importance for public safety, the knowledge of the temporal evolution of the ash cloud dispersal. For these reasons reliable computational model are needed. Here, we propose a new Eulerian model, called FALL3D, for the simulation of dispersion and deposition of volcanic ashes. The model is based on the solution of an advection-diffusion-settling equation, coupled with a Limited Area Model (LAM) for the wind field, and a parameterization of the turbulent diffusivity tensor based on the K-theory. The equations are solved using a fully explicit third-order upwind scheme in a terrain-following coordinate system. The wind and temperature fields given by the LAM are assimilated to the finer scales using the meteorological processor CALMET. The procedure can be used for forecasting ash concentration from volcanic plumes in the atmosphere and ash loading on the ground. The input to the model are the topography, the meteorological field data as given by the LAM, the mass eruption rate and the settling velocity distribution of volcanic ashes in the source. A test application to the Etna 2001 volcanic eruption is presented.

USE OF DISPERSION MODELS TO TRACK ERUPTION CLOUDS

Ken G. Dean, Rorik A. Peterson, Ken Papp and Jonathan Dehn
Geophysical Institute, University of Alaska Fairbanks, Koyukuk Dr., P.O.Box 757320,
Fairbanks, Alaska 99775-7320, USA

An overview of ash-tracking (dispersion) models will be presented, highlighting their strengths, weaknesses, and usefulness. The models are a tool for rapid response to predict the location, structure and movement of eruption clouds. Three models used in North America are Canerm (Montreal VAAC), Hysplit (Washington VAAC), and Puff (NWS Anchorage, AVO, U.S. Air Force Weather Agency, and universities). All three are similar in that they require gridded wind fields and specification of the initial eruption column size and shape. Wind fields are available with various spatial resolutions, time steps and geographical coverage. For operational eruption response, current wind fields are required. Dispersion models are initiated by releasing hypothetical particles above a volcano that are subsequently transported by advection, diffusion, and gravitational settling. The models diverge in their implementations of these transport mechanisms. Models must be fast, efficient, and easily configurable for diverse conditions, and they must approximate transport physics without becoming cumbersome. Model predictions are validated using satellite images, and are often "tuned" to match clouds observed on images. However, recent observations from the Mt. Cleveland eruption suggest that model predictions may be accurate when satellite images do not detect airborne volcanic material. In general, tracking models have been accurate for moderate altitude plumes (5 km to 16 km), and have had limited success with low and high altitude plumes (<5 km, and > 16km) and in situations with complex ground-relief. Some causes of these limitations are difficulties in accurately modeling diffusion in the near-surface boundary layer and lack of wind data in stratospheric regions. The accuracy of the models depends upon the accuracy of the wind fields, which can be variable between climate models. Furthermore, their course space and time resolution of many wind fields creates difficulties for short-term and nearby hazard forecasts for local communities in the immediate vicinity of a volcano.

LABORATORY MEASUREMENTS OF HETEROGENEOUS ICE NUCLEATION BY VOLCANIC ASH: IMPORTANCE FOR DETECTING AND MODELING VOLCANIC CLOUDS

Adam J. Durant, Department of Geological Engineering and Sciences, Michigan Technological University, Houghton, Michigan, USA, [ajdurant@mtu.edu]
Raymond A. Shaw, Department of Physics, Michigan Technological University, Houghton, Michigan, USA
Youshi Mi, Department of Physics, Michigan Technological University, Houghton, Michigan, USA
William I. Rose, Department of Geological Engineering and Sciences, Michigan Technological University, Houghton, Michigan, USA

Analysis of brightness temperature difference images from thermal infrared measurements on meteorological satellites is a primary method that VAACs around the globe use for detecting volcanic ash clouds and mitigating hazards to aviation. A significant proportion of volcanic cloud particles are ice, and ice may conceal the characteristic spectral absorbance features of ash, making detection challenging. Cloud processes (e.g., lifetime, radiative properties) are sensitive to the competing effects of heterogeneous and homogeneous ice nucleation. We have designed a laboratory experiment that investigates heterogeneous ice nucleation, concentrating on ice formation on volcanogenic particles. The statistical nature of heterogeneous ice nucleation can provide insight into the physical mechanisms responsible for ice formation. In our experiments, we measure the freezing temperature for a single ice nucleus (IN) in a water drop hundreds of times to obtain detailed estimates of the probability density functions (PDFs) for freezing time (or temperature). The PDFs can be compared to the idealized inhomogeneous Poisson process based on the classical model of heterogeneous ice nucleation. We frequently observed a variation in freezing temperature of an IN between two 'modes', representing surface versus immersion freezing: the freezing temperature for the surface mode is ~5 K higher than the immersion mode. The distribution of freezing temperatures is nearly identical in both instances, suggesting the physical mechanisms for ice nucleation are not fundamentally different. Our data support the hypothesis that distinct interfacial and bulk nucleation rates exist for water. We speculate that the total nucleation rate is the sum of a nucleation rate corresponding to the interaction of bulk water with the IN, and a nucleation rate corresponding to the interaction of water at the surface of the drop (i.e., interfacial water) with the IN. Our measurements may have application in the representation of ice formation in models of volcanic plume dynamics.

P3.7

VOLCANIC ASH DETECTION AND CLOUD TOP HEIGHT ESTIMATION FROM THE GOES-12 IMAGER: COPING WITHOUT A 12μm INFRARED BAND

Gary P. Ellrod[1], Anthony J. Schreiner[2], and Alonzo M. Brown[3]

[1] Office of Research and Applications (NOAA/NESDIS), Camp Springs, MD
[2] Cooperative Institute for Meteorological Satellite Studies (CIMSS), University of Wisconsin, Madison,
[3] Washington Volcanic Ash Advisory Center (NOAA/NESDIS), Camp Springs, MD

1. INTRODUCTION

On 1 April 2003, Geostationary Operational Environmental Satellite (GOES)-12 replaced GOES-8 as the primary spacecraft to monitor weather and environmental hazards over North and South America. Hillger et al 2003 describe the GOES-12 data and products and assess their quality. A major change to the GOES-12 Imager was the replacement of a 4 km resolution 12μm Infrared (IR) band with a lower resolution (8 km) IR band centered near 13.3μm (see Table 1). The 12μm band will not be restored until about 2013 when the GOES-R spacecraft becomes operational. There has been a concern that the loss of the 12μm band will negatively affect volcanic ash detection and aviation safety for the next ten years, since that channel has been effectively used in a two-band "split window" technique (Prata 1989) for over a decade. An impact study (Ellrod 2004) has indicated that there will likely be some degradation of volcanic ash detection, leading to both under-detection of thin ash, and an increase in the area of "false" ash, resulting in possible over-warning for aviation advisories.

	GOES 8-11		GOES M-P	
Band	Wave-length (m)	Res. (km)	Wave-length (m)	Res. (km)
1	0.6	1	0.6	1
2	3.9	4	3.9	4
3	6.7	8	**6.5**	**4**
4	10.7	4	10.7	4
5	12.0	4	-	-
6	-	-	**13.3**	**8**

Table 1. *Summary of GOES Imager spectral bands showing changes in the new series (M-P) in bold, compared with previous spacecraft (GOES 8-11).*

The first significant opportunity to evaluate GOES-12 volcanic ash detection capabilities occurred with several moderate eruptions of Soufriere Hills Volcano on the island of Montserrat in the Eastern Caribbean from 12-15 July 2003. The eruptions were triggered by a major lava dome collapse, followed by pyroclastic flows (Montserrat Volcano Observatory 2003). Ash was dispersed throughout the troposphere across the region, with maximum ash top heights estimated to range from 8-16 km (Washington Volcanic Ash Advisory Center (W-VAAC)). The VAACs were established during the mid 1990's as part of the International Airways Volcano Watch (IAVW) to provide current advisories on existing volcanic ash clouds. Regional Meteorological Watch Offices then issue warnings (known as SIGMETs) to en route aircraft that are based on the VAAC advisories. The W-VAAC has responsibility for the Caribbean region, as well as large portions of North and South America, and the Central and Western Pacific (International Civil Aviation Organization, 2000).

2. VOLCANIC ASH DETECTION METHODS

Traditional methods for detection of volcanic ash often employ a bi-spectral technique based on the brightness temperature difference (BTD) of two Infrared (IR) bands centered near 11.0 and 12.0 μm (Prata 1989; Holasek and Rose 1991). These two IR bands have been available at 1 km resolution from the Advanced Very High Resolution Radiometer (AVHRR) on the polar orbiting National Oceanic and Atmospheric Administration (NOAA) satellite series since the early 1980's. By the mid 1990s, similar spectral bands also became available on the GOES. Although the spatial resolution of GOES IR sensors is only 4 to 8 km, their advantage is frequent coverage (nominally 30 min) over most volcanically active regions of North and South America, as opposed to four times daily from the AVHRR.

The two-band difference method (hereafter referred to as the Two-Band Split Window (TBSW)) sometimes fares poorly however, due to: (1) the excessive thickness of the eruption cloud, which often contains copious amounts of water and large ejected particles within a few hours after the eruption, (2) a lack of temperature contrast between the airborne ash and underlying surface, and (3) ambient atmospheric moisture that can mask low level ash clouds (e.g. Simpson et al 2000). Despite these shortcomings, the TBSW technique has become an international benchmark for volcanic ash detection. The loss of this channel on GOES-12 created the urgent need for a different approach.

The altitude of the ash cloud is also important to aviation, and estimates of the top of the ash layer are provided in the VAAC messages. At the W-VAAC, the ash cloud heights are determined by matching the trajectory of different portions of the ash cloud with upper level wind profiles obtained from adjacent radiosondes or numerical prediction models. In this paper, we will describe new techniques for detecting volcanic ash clouds and estimating their maximum heights using the new spectral band combination available from the GOES-12 Imager.

3. GOES-12 IMAGER ASH DETECTION ALGORITHM

A new technique has been developed to detect ash from GOES-12 Imager Infrared (IR) brightness temperature (BT) data, using an arithmetic combination of Bands 2 (3.9μm), 4 (11μm) and 6 (13.3μm). Bands 6 and 4 can help discriminate volcanic ash from ice-laden cirrus cloud layers due to emissivity differences at those wavelengths (Ellrod 2004). Thermal differences between Bands 2 and 4 have been used in a three-band method (Ellrod et al 2003) which exploits reflectivity and absorption effects near 3.9 μm. The GOES-12 algorithm was empirically determined using NASA MODerate resolution Imaging Spectroradiometer (MODIS) data (Ellrod and Im 2003) and GOES Sounder data. The new algorithm is:

$$B = 5\,(T_2 - 1.5T_4 + 1.5T_6) - 230 \qquad (1)$$

Where B is output brightness count, T_2 is the BT observed in Band 2 (3.9μm), T_4 is BT in Band 4 (10.7μm) and T_6 in BT in Band 6 (13.3μm). Volcanic ash is relatively bright (large values of B) compared to surrounding clouds and terrain volcanic ash. Thresholds for volcanic ash detection using this new approach have not yet been established due to the diurnal variation of T_2. Even in bright daytime scenes, the ash clouds stand out against the background if they are sufficiently dense (see Figure 2). The plot in Figure 1 shows brightness count (B) from Equation (1) obtained on 14 July 2003 at 0915 UTC (0515 Caribbean Standard Time (CST)) for several different types of features. The volcanic ash (solid circles) is clearly distinguishable from the cirrus (open triangles), mid-level clouds (stars), and ocean (diamonds) at this time. Note that if only thermal IR data are used, the ash would be virtually indistinguishable from other cloud types in the region due to similar brightness temperatures.

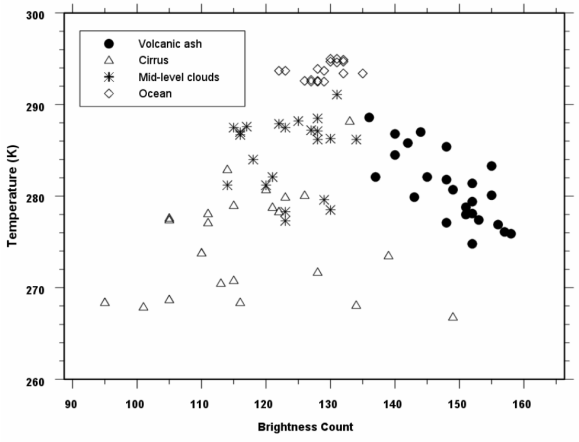

Figure 1. *Scatter plot of brightness count from Equation 1 versus IR band 4 from GOES-12 on 14 July 2003 at 0915 UTC for volcanic ash, ocean surface, cirrus clouds, and mid-level clouds.*

The three-band technique was evaluated for three of the four Soufriere Hills eruptions. For validation and comparison, graphical ash analyses from W-VAAC were available, as well as imagery and derived products from the GOES Sounder. The Sounder is an independent instrument that employs a different scanning strategy, with the goal of producing temperature and humidity profiles (retrievals), as well as image products such as cloud top pressures (CTP), total precipitable water (TPW), and Lifted Index (Menzel et al 1998). The GOES Sounder has nineteen spectral bands, with a resolution of 10 km at nadir compared with 4-8 km for the Imager. For the Eastern Caribbean, Sounder data were only available at 0120 UTC, 0720 UTC, 1320 UTC and 1920 UTC. The GOES-12 Sounder includes the same spectral bands as the Imager (except for the water vapor channel), but they are slightly narrower spectrally.

4. CASE I: 12-13 JULY 2003 EVENT

Triggered by a major collapse of the Soufriere Hills lava dome, first eruption occurred late on the evening of 12 July 2003 (around 0230 UTC, 13 July 2003). The resulting ash cloud reached 15.7 km based on an IR estimate by the Washington VAAC. The development, expansion, and northeastward drift of cold cloud tops associated with the eruption column could easily be seen in GOES-12 Band 4 thermal IR images. However, the three-band IR product described in Section 2 was not effective, probably due to extensive water in the eruption cloud, and because high level non-volcanic clouds in the area obscured most of the dissipating ash. This is a common weakness of IR detection techniques (see Section 2). Minimum cloud top temperatures were around 200K for several hours following the eruption. Later confirmation of a volcanic ash cloud came from the Total Ozone Mapping Spectrometer (TOMS) at around 1530 UTC that day (not shown), which indicated that there were large concentrations of high altitude SO_2 gas to the northeast of the Leeward Islands (image available from the NASA TOMS archive: http://skye.gfsc.nasa.gov/archives.html).

5. CASE II: 14 JULY 2003 EVENT

Shortly after Midnight on 14 July 2003, another release of ash occurred, with maximum cloud top heights estimated by the VAAC to be 11.3 km. Minimum T_4 cloud top temperatures for this event were about 238K at 0615 UTC, but quickly became warmer as the cloud thinned out. For this case, there was less cloud cover in the region, allowing an evaluation of multi-spectral ash detection techniques. An hourly sequence of the three-band IR images depicted the mid-upper level ash cloud as it drifted toward the west and northwest. Lower level ash was more difficult to distinguish against the ocean background.

6. CASE III: 15 JULY 2003 EVENT

On 15 July 2003 at approximately 0530 UTC, the fourth eruption in this series sent ash to as high as 47,000 ft (14.7 km) as reported by the Washington VAAC. The minimum cloud top temperature (T_4) was 224K at 0645 UTC. Figure 2 provides a two-hour interval sequence of three-band IR images showing the spread of the eruption clouds from 0745 UTC to 1345 UTC. The ash cloud, the background ocean, and

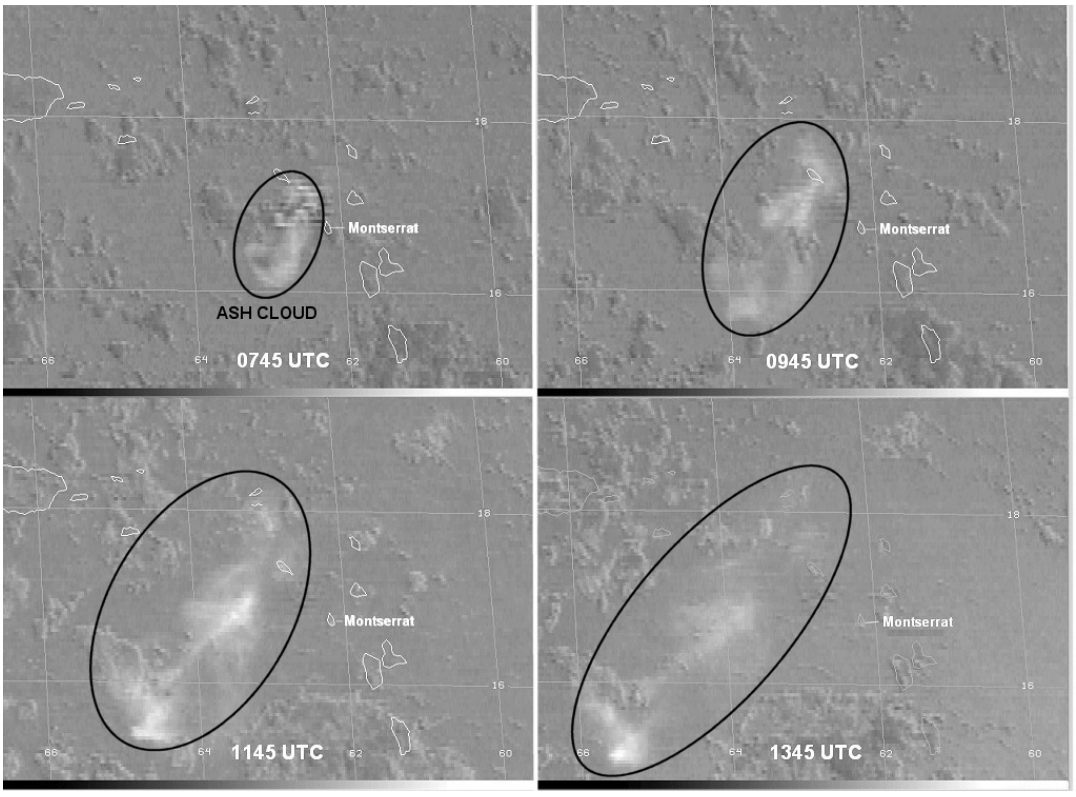

Figure 2. *Two- hourly interval GOES-12 three-band IR volcanic ash product images showing evolution of ash on 15 July 2003 from 0745 UTC to 1345 UTC.*

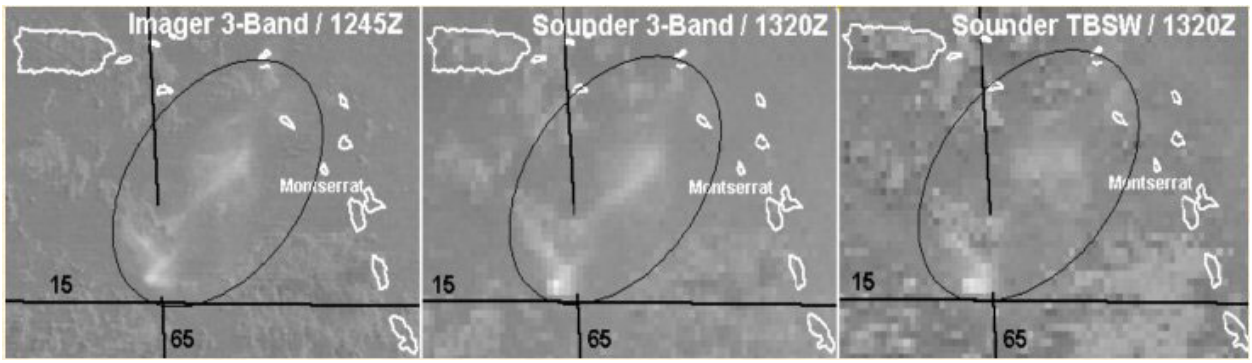

Figure 3. *Volcanic ash product (based on the 3.9, 10.7 and 13.3 μm bands) from the GOES-12 Imager (left) at 1245 UTC compared with the same product from the Sounder at 1320 UTC (center), versus a two-band difference based on the 12.0 and 11.0 μm channels from the Sounder, also at 1320 UTC (right).*

meteorological clouds all brighten around 1145 UTC due to solar reflectance in the 3.9 μm IR band.

7. CLOUD TOP HEIGHT ESTIMATION

The availability of the 13.3 μm IR band from the Imager on GOES-12 and its successors provides the capability of estimating volcanic ash cloud top heights with a CO_2 Absorption Technique (COAT) (Schreiner and Schmit 2001; Schreiner et al 2002). Cloud Top Pressure (CTP), Effective Cloud Amount (ECA), and other derived products have been available hourly from the GOES Sounder for a number of regions since the mid-1990's (Menzel et al 1998). The COAT is a physical relationship based on a special version of the Radiative Transfer Equation. The main assumptions are (1) cloud is opaque but infinitesimally thin (thus allowing application for semi-transparent clouds), and (2) emissivity is the same in both spectral ranges. The latter assumption, when applied to the 13.3 μm and 10.7 μm bands, is only valid when a volcanic cloud is at least partially composed of ice.

A comparison of a GOES cloud height analysis from 14 July 2003 at 0545 UTC with the VAAC graphical height analysis is shown in Figure 4. Based on subjective, textural evaluation of IR data, the high level ash was nearly opaque, while the low-mid level ash was semi-transparent. Cloud top heights from the GOES-12 product ranged from 7.6 km (24 kft) for the mid-level ash, to about 11.1 km (35 kft) for the high level ash, in good agreement with the VAAC analysis (based on an independent technique described in section 2).

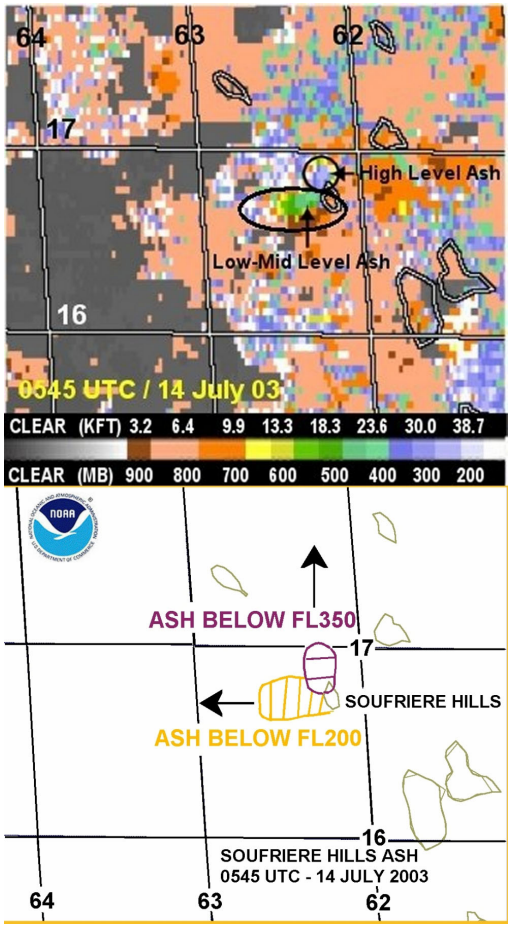

Figure 4. *Cloud top height product based on the GOES-12 Imager CO_2 Analysis Technique (COAT) (top) compared with the VAAC analysis both valid 0545 UTC, 14 July 2003.*

8. SUMMARY AND CONCLUSIONS

The first significant volcanic eruptions observed by the new GOES-12 satellite occurred from 12-15 July 2003 following a lava dome collapse at the Soufriere Hills Volcano, Montserrat. A new IR technique that used the 3.9, 10.7 and 13.3 μm channels (Bands 2, 4, and 6) was able to observe the ash clouds effectively for two of the events during the period, while the strongest event could be monitored by a sequence of Band 4 IR images. Ash cloud heights based on the CO_2 Absorption Technique for the 14 July 2003 case were consistent with those from the VAAC analysis, which employs an independent wind trajectory matching technique. The uniformly warm ocean background, which provided excellent thermal contrast with the airborne ash clouds, was an advantage for observing these events which will not be present for some Continental volcanoes. The presumption that there would be under-detection and increased false alarms for ash detection using GOES-12 was not observed for this particular event. While the loss of the 12 μm IR band is likely to degrade the overall volcanic ash detection capability somewhat, this episode shows that imagery from GOES-12 and its successors will still be an effective means of warning pilots of hazardous ash clouds in many situations.

9. REFERENCES

Ellrod, G. P., (2004): Loss of the 12μm "Split Window" Band on GOES-M: Impacts on volcanic ash detection. *J. Volc. Geothermal Res.*, Elsevier, Inc., Vol. 135/1-2, pp 91-103.

_____, B. H. Connell, and D. W. Hillger, (2003): Improved detection of airborne volcanic ash using multispectral infrared satellite data. *J. Geophys. Res.*, *108*(D12), 4356.

_____, and J-S. Im, (2003): Development of volcanic ash image products using MODIS multi-spectral data. 12th AMS Conference on Satellite Meteorology and Oceanography, 9-13 Feb 2003, Long Beach, California

Hillger, D. W., T. S. Schmit and J. Daniels, (2003): Imager and Sounder Radiance and Product Validations for the GOES-12 Science Test, NOAA Technical Report 115, U.S. Department of Commerce, Washington, DC, URL: http://www.cira.colostate.edu/ramm/goesm/GOES-12_Science_Test_Report.htm

Holasek, R. E., and W. I. Rose, (1991): Anatomy of 1986 Augustine eruptions as revealed by digital AVHRR satellite imagery. *Bull. Volcanol., 53*, 420-435.

International Civil Aviation Organization (ICAO), (2000): Handbook on the International Airways Volcano Watch (IAVW): Operational Procedures and Contacts List, First Edition ICAO Doc. 9766-AN/968.

Menzel, W. P., F. Holt, T. Schmit, R. Aune, A. Schreiner, G. Wade, and D. Gray, (1998): Application of GOES-8/9 soundings to weather forecasting and nowcasting. *Bull. Amer. Meteor. Soc.*, *79*(10), 2059-2077.

Montserrat Volcano Observatory, (2003): Summary of the 12-15 July 2003 dome collapse and explosive activity at the SoufriPre Hills Volcano, Montserrat. URL: http://www.mvo.ms/

Prata, A. J., (1989): Observations of volcanic ash clouds in the 10-12 micrometer window using AVHRR/2 data. *Int. J. Remote Sens.*, *10*, 751-761.

Schreiner, A.J., T.J. Schmit, and R.M. Aune, (2002): Maritime inversions and the GOES Sounder cloud product, *National Weather Digest*, *26*, 27-38.

_____ and T.J. Schmit, (2001): Derived Cloud Products from the GOES-M Imager, Preprints, 11th Conference on Satellite Meteorology and Oceanography, Madison, Wisconsin, Amer. Meteor.Soc., 420-423.

Simpson, J. J., G. Hufford, D. Pieri, and J. Berg, (2000): Failures in detecting volcanic ash from a satellite-based technique. *Remote Sens. Environ.*, *72*, 191-217.

Washington Volcanic Ash Advisory Center, (2003) Operational Volcanic Ash Advisories (VAA) for 2003 are available from: http://www.ssd.noaa.gov/VAAC/ARCH03/archive.html

RESUSPENSION OF RELIC VOLCANIC ASH AND DUST FROM KATMAI: STILL AN AVIATION HAZARD

David Hadley, NWS Alaska Aviation Weather Unit, Anchorage AK, USA
Gary L. Hufford, NWS Alaska Region Headquarters, Anchorage AK, USA
James J. Simpson, Scripps Institution of Oceanography, University of California, San Diego
La Jolla, CA, USA

Northwest winds were strong enough to continuously resuspend relic volcanic ash from the Katmai Volcano Cluster and the Valley of Ten Thousand Smokes on 20-21 September 2003. The ash cloud reached over 1600 m and extended over 230 km into the Gulf of Alaska. Several factors influenced the resuspension of the ash: (1) the atmosphere and land surface were very dry prior to the event, further enabling the resuspension and subsequent atmospheric transport of the relic volcanic ash; (2) production of winds strong enough to entrain and lift the ash over 1600 m into the atmosphere; (3) complex terrain with numerous mountains interspersed with valleys, channels and gaps; (4) super adiabatic lapse rate for the troposphere below 850 mb; and (5) the presence of a strong subsidence inversion around 1400-1600 m. We propose that the strong winds are due to accelerations in a super adiabatic atmosphere below 850 mb that is buoyant to both upward and downward perturbations resulting in a hydraulic flow that exposes the lee side of the mountains to sweeping, high speed turbulent winds near the base of the lee slope. Some unique features of the ash cloud are also examined, including its hazardous nature to aviation. Finally, this presentation provides the forecaster with the ability to: (1) recognize the conditions needed for relic volcanic ash resuspension; and (2) respond immediately to such an event.

OBSERVING POPOCATEPETL'S VOLCANIC ASH CLOUDS USING MODIS INFRARED DATA

M. Alexandra Matiella, Department of Geological Engineering and Sciences, Michigan Technological University, Houghton, MI, USA [mamatiel@mtu.edu]
Hugo Delgado-Granados, Instituto de Geofisica, Universidad Nacional Autonoma de Mexico (UNAM), Mexico
William I. Rose, Department of Geological Engineering and Sciences, Michigan Technological University, Houghton, MI, USA
I. Matthew Watson, Department of Geological Engineering and Sciences, Michigan Technological University, Houghton, MI, USA

Popocatepetl Volcano, Mexico, is a tropical volcano with significant and persistent emissions of SO_2 and ash that pose significant hazards to the large population in close proximity to the volcano. The country's main international airport, located approximately 55 km northwest of Popocatepetl in Mexico City, services about 800 flights a day and 20 million passengers a year. A large eruption of volcanic ash from Popocatepetl could devastate the city of 8 million inhabitants and shut down Mexico City's international airport. Moderate Resolution Imaging Spectroradiometer (MODIS) satellite imagery provides us with a synoptic perspective of volcanic emissions and atmospheric interactions, information unavailable from ground-based or aircraft studies, which can be useful for hazard mitigation. Ash masses are retrieved using silicate absorption features at 11 μm and 12 μm. A suite of MODIS images was collected for a period of increased activity during December 2000 – January 2001. One particular image collected January 23rd, 2001, at 0450 UT, shows four large eruptions that have dispersed volcanic clouds over an extensive area of Mexico. Using upper air data and monitoring records, the movements of the 4 ash clouds are fit with eruption times and winds, and using retrieval data for ash we can derive a time based fine ash emission record. The results of these retrievals complement ground-based measurements which cannot measure large scale ash eruptions into the atmosphere and provide a possible scenario for the amount of time it would take a large ash cloud to reach Mexico City.

COMPARISON OF ASH DETECTION TECHNIQUES USING TOMS, MODIS, AVHRR, AND GMS: A CASE STUDY OF THE AUGUST 18 AND 28 ERUPTION CLOUDS OF MIYAKEJIMA VOLCANO, JAPAN

Emily McCarthy, Gregg Bluth, I. Matthew Watson, Michigan Technological University
Andrew Tupper, Darwin Volcanic Ash Advisory Center
Yasuhiro Kamada, Tokyo Volcanic Ash Advisory Center

Introduction

Volcanic eruptions can eject ash, sulfur dioxide, and other gases into the atmosphere. Ash eruptions have been recognized as a serious aviation hazard, including engine failure, electronic failures, and poor visibility. Remote sensing techniques allow long-term tracking of volcanic clouds, analysis of eruptions in isolated areas, and measurements of an entire eruption cloud. Both ultraviolet (TOMS) and infrared (MODIS, AVHRR, and GMS) satellite sensors are capable of detecting volcanic ash. However, IR sensors are susceptible to interference of water vapor. Since each sensor uses different wavelengths their ability to detect volcanic clouds varies. For example, ash clouds may be seen using one IR sensor for several days and only one day using another. Therefore, this project also aims to understand and explain the limitations of each satellite sensor in detecting volcanic ash. The moist atmosphere of Miyakejima presents an opportunity to examine their sensitivity to atmospheric water vapor. Ash mass retrievals without a water vapor correction are compared to those run after the effects of water vapor are removed from the system. The mass, extent, and height of the cloud are important factors when considering the mitigation of aviation hazards. In this case study of Miyakejima Volcano, Japan, data from four different satellite sensors are compared and used to produce constraints on the masses and distributions of ash released by the August 18 and 28, 2000 eruptions.

Miyakejima Background

Miyakejima, a basaltic andesite stratovolcano, rises to an elevation of 813 m. Part of the Izu-Bonin volcanic island chain, Miyakejima is located about 200 km south of Tokyo (Figure 1). The summit consists of two calderas, Kuwakidaria and Hatchodaria, and a central cone. Mount Oyama (Geshi et al., 2002). Recent activity began in June of 2000 with small submarine eruptions and continues today with high emissions (average of 11,000 tons/day) of sulfur dioxide (Kinoshita et al., 2002). Several large eruptions occurred on August 18 and 28, 2000. In September 2000, the island was completely evacuated and remains uninhabited. Monitoring responsibilities are shared between the Japan Meteorological Agency (JMA) and the Tokyo Volcanic Ash Advisory Center (VAAC). All observations are made remotely through the use of satellites and video monitoring. SO_2 measurements are taken monthly with the COSPEC.

The 18 August eruption at 08:02 UTC emitted an ash and SO_2 cloud with a height of approximately 15 km, moving south. The 28 August eruption (19:35 UTC) was smaller with the ash and SO_2 cloud reaching 9 km and moving northeast.

Figure 1. A map of the major volcanoes of Japan. Miyakejima is located about 200 km south of Tokyo in the Izu-Bonin volcanic island chain.

Methods

The Volcanic Ash Retrieval. The infrared channels 4 (11μm) and 5 (12μm) of AVHRR and channels 31 (11μm) and 32 (12μm) of MODIS are used to discriminate volcanic clouds from meteorological clouds. Volcanic clouds generally have a negative brightness temperature difference (BTD) when the 12 μm channel is subtracted from the 11 μm channel, while meteorological clouds generally have a positive BTD (Wen and Rose, 1994). The ash retrieval is based upon a radiative transfer model that allows the estimation of the mass and size of particles in the volcanic cloud. This model assumes that the particles are spherical, the particle size distribution within a pixel is consistent, and the cloud is continuous (Wen and Rose, 1994). User inputs include the temperature of the underlying surface and the top of the cloud, which can be gathered from the satellite image or radiosonde data.

Atmospheric Corrections. A forward model, developed by Watson et al. (2003), was used to correct for atmospheric water vapor. In this model, an atmospheric profile is run through MODTRAN to determine the brightness temperature values of the system. The model was run with different relative humidities, ranging from 0%-100%. Due to the noisiness of the data, the values from 8-12 μm and the sensor response functions for the respective channels were convolved to generate a weighted average and, hence a more accurate brightness temperature. Using the pressure, dry bulb, and wet bulb temperatures of the atmospheric profile, the relative humidity (RH). This new RH was input into the atmospheric profile and run through the forward model again to calculate true values for the brightness temperatures at 11 and 12 μm. A brightness temperature difference (11-12 μm) was calculated and subtracted from the 12 μm channel of the original data used in the ash retrieval.

Results

Volcanic ash retrievals were conducted using original BTDs and corrected BTDs for one MODIS and three AVHRR images. GMS images show ash clouds for both eruptions, however, we are unable to quantify the mass at this time and the images are hence used for locating purposes only. A comparison of the two eruptions, indicates that the 18 August eruption is much more ash-rich than the 28 August eruption.

On 18 August an ash cloud was detected by AVHRR, containing 511,301 metric tons of ash, at 19:48 UTC (Figure 2). Unfortunately, the TERRA/MODIS instrument was not operational, so no cloud comparisons could be made. The TOMS image available for that day, at least 6 hours prior to the eruption, shows no evidence of ash. GMS was able to track the eruption cloud for the entire day following the eruption. Figure 3 shows the infrared image taken approximately 10 minutes prior to the AVHRR image.

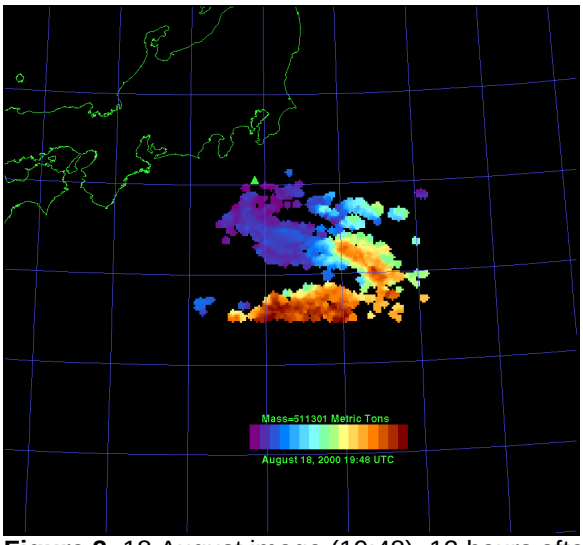

Figure 2. 18 August image (19:48), 12 hours after the eruption, contains 511300 metric tons of ash

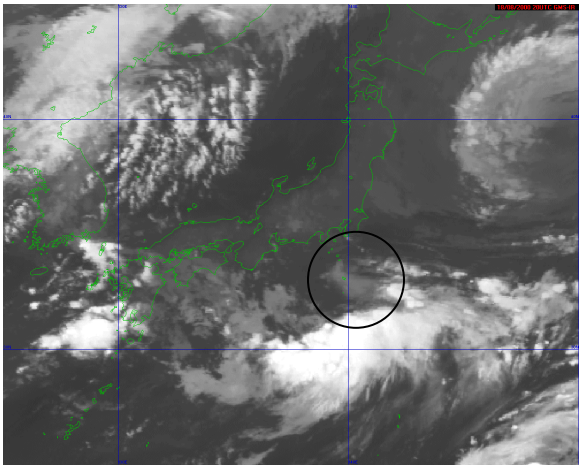

Figure 3. 18 August GMS infrared image (19:38) taken approximately 10 minutes prior to the AVHRR image.

The ash cloud is also detected on 19 August by both MODIS (Figure 4) and AVHRR (Figures 5). Both images, though only 6 hours apart, show drastically different results: MODIS (01:05 UTC) =

20,015 metric tons and AVHRR 07:12 UTC) = 148,939 metric tons. A TOMS Aerosol Index (AI) dataset (00:40 UTC) shows a substantial ash cloud, collocated with the other two sensor clouds (Figure 6). GMS images at near coincident times with the MODIS, AVHRR, and TOMS images are presented in figures 7-9 respectively.

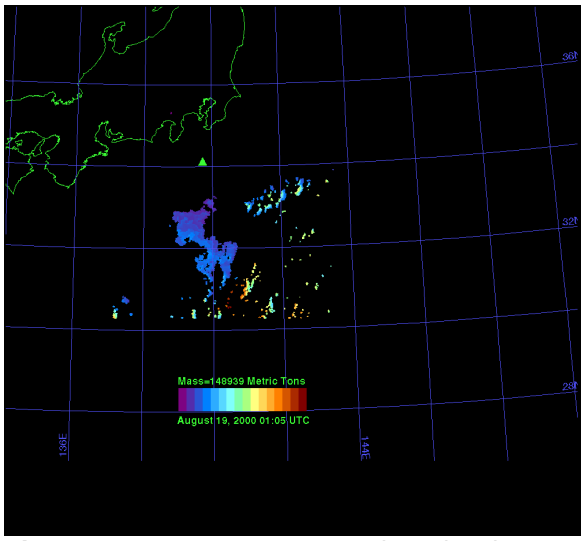

Figure 4. 19 August MODIS ash retrieval (01:05), 17 hours after the eruption. At this time the cloud contained about 150,000 metric tons of ash.

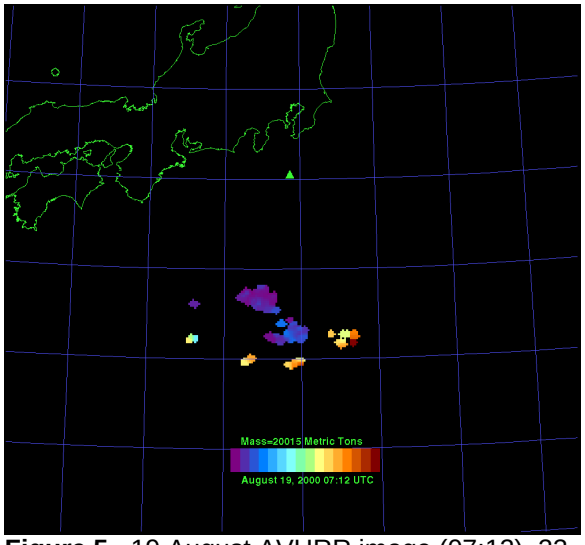

Figure 5. 19 August AVHRR image (07:12), 23 hours after eruption, contains approximately 20000 metric tons of ash.

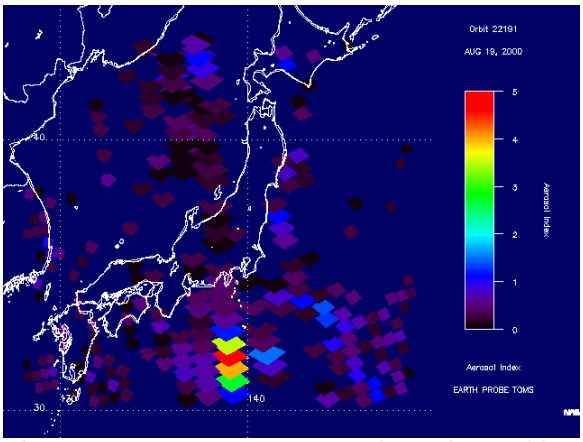

Figure 6. 19 August TOMS AI (00:40). Positive values indicate the presence of volcanic ash.

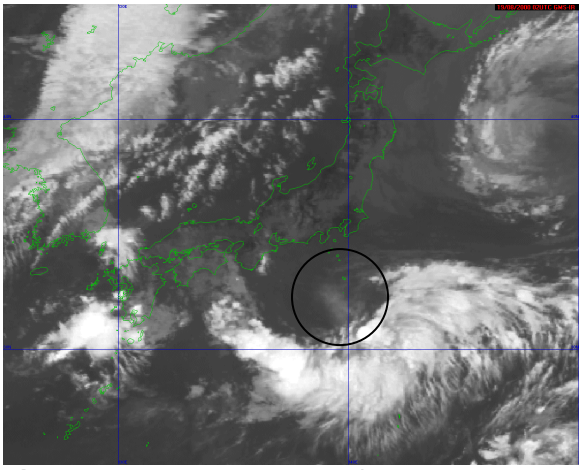

Figure 7. 19 August GMS IR image at 01:38 UTC.

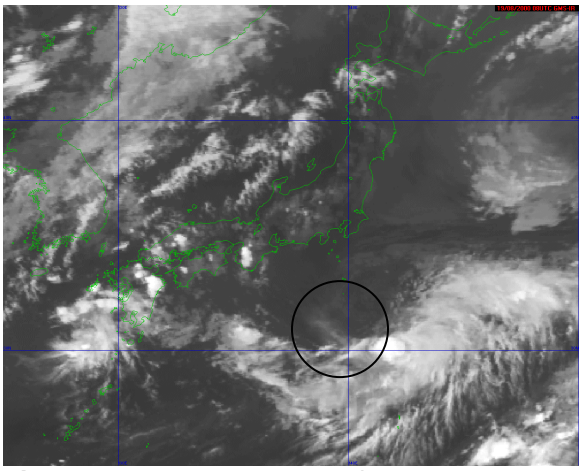

Figure 8. 19 August GMS IR image at 07:38 UTC.

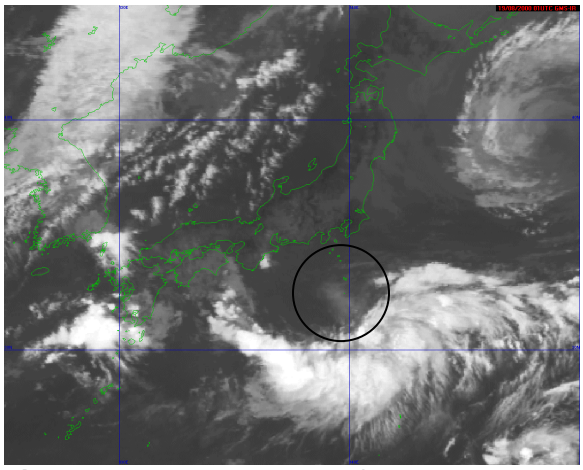

Figure 9. 19 August GMS IR image at 00:40 UTC.

The 28 August ash cloud is significantly smaller than the 18 August cloud. An AVHRR image taken approximately one hour after the eruption shows only 211 metric tons of ash (Figures 10). Four minutes after the AVHRR image, GMS was also able to detect the ash cloud (Figure 11). TOMS was unable to detect this small injection of ash into the atmosphere when the image was taken several hours later.

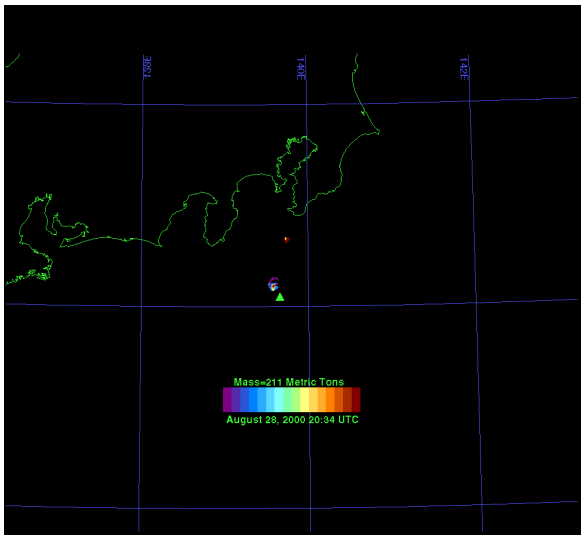

Figure 10. 28 August image (20:34), 1 hour following eruption, contains 211 metric tons of ash.

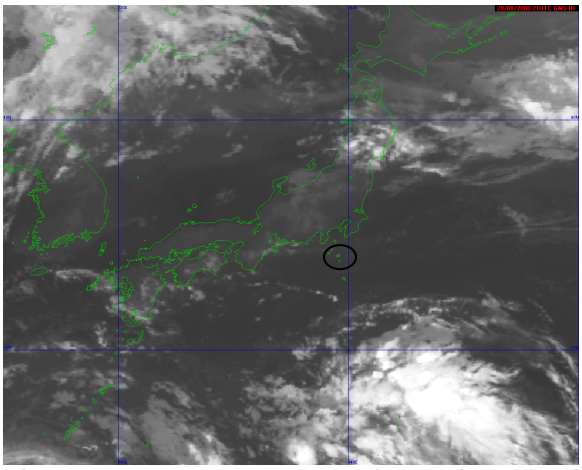

Figure 11. 28 August GMS IR image (20:38), within four minutes of the AVHRR image.

Discussion

Since Miyakejima is located in a moist, marine environment, atmospheric water vapor is a concern when attempting to quantify ash. Table 1 compares the difference seen in the mass, mean effective radius (MER) of the particles, and optical depth of the cloud. In all cases, the three variables increased as water vapor was removed from the system. Mass was the most changed in all four cases, with corrected values ranging from 2.5 to almost 29 times larger than the original result. In an attempt to better understand how the correction works, a plot of corrected mass divided by the original mass versus the change in brightness temperature (which was calculated from the removal of water vapor) was created (Figure 12). While the graph indicates a high R^2 value (0.9137), it is important to note a few points: 1) the highest point represents the large difference between the two retrieved masses and appears anomalously large, 2) only four images detected ash, while typically any sort of convincing correlation should contain a larger dataset, and 3) two of the brightness temperature differences are the same because the images are on the same day. Generally, the trend shown is what one would expect, the ash cloud mass decreases with time and the smaller the brightness temperature difference, the smaller the difference between the two masses. In order to insure the accuracy of such a correction technique, an eruption with a persistent, detectable ash cloud should be used.

Date, Time	Mass (tons)	MER (μm)	Optical Depth
8/18, 19:48	17954	8.41	0.97
	511301	*9.27*	*1.31*
8/19, 01:05	22680	7.27	0.39
	148939	*8.84*	*0.75*
8/19, 07:12	8152	6.35	0.43
	20015	*6.36*	*0.49*
8/28, 20:34	74	6.65	0.31
	211	*6.91*	*0.34*

Table 1. Comparison of original and atmospherically corrected ash retrievals. Corrected retrieval results are in italics.

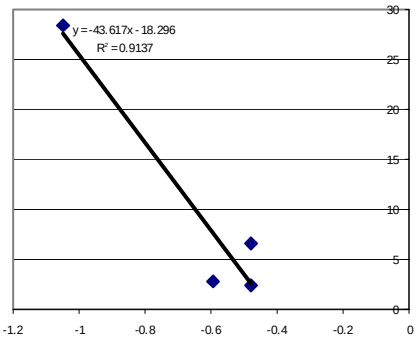

Figure 12. Plot of brightness temperature difference versus the mass from the corrected and original data.

Conclusions

Ash was best detected by and can be quantified using infrared sensors. Geostationary satellites seem to be the best option for tracking ash clouds and therefore for use by VAACs. AVHRR and MODIS are both aboard polar orbiting satellites, which cover the same area earth approximately twice per day. At this time, these are the only satellites available in the Japan area to use for quantification of mass and particle size. GMS will be of use for quantification in the future, however, creating a retrieval method was out of the scope of this study.

Acknowledgments

Financial support for this project was received from the Michigan Space Grant Consortium Graduate Fellowship Program, Sigma Xi Grants-in-aid of Research, and a NASA grant: Validation of TOMS Volcanic Aerosol and SO_2 Products Using MODIS and AVHRR. GMS data is courtesy the Japan Meteorological Satellite Center. We would also like to thank the Japan Meteorological Agency and the Volcanic Clouds Group at Kagoshima for sharing Miyakejima information.

References

Geshi, N., T. Shimano, T. Chiba, S. Nakada, Caldera collapse during the 2000 eruption of Miyakejima Volcano, Japan, Bull. Volcanol, 64, 55-68, 2002.

Kinoshita, K, C. Kanagaki, N. Iino, M. Koyamada, A. Terada, A. Tupper, Volcanic plumes at Miyakejima observed from satellites and from the ground, Remote Sensing of the Atmosphere, Ocean, Environment, and Space, Hangzhou, China, October, 2002.

Wen, S. and W. I. Rose. Retrieval of sizes and total masses of particles in volcanic clouds using AVHRR band 4 and 5, J. Geophys. Res., 99, 5421-5431, 1994.

Watson, I.M., Realmuto, V.J., Rose, W.I., Bluth G.J.S., Forward modeling of volcanic aerosols transmissions at different latitudes; quantifying the effects of varying water vapor on ash detection, Abstract, AGU Meeting, Fall 2003.

PREDICTING REGIONS SUSCEPTIBLE TO HIGH CONCENTRATIONS OF AIRBORNE VOLCANIC ASH IN THE NORTH PACIFIC REGION

Kenneth Papp, Ken Dean, and Jonathan Dehn, Geophysical Institute, University of Alaska, Fairbanks, AK, USA

Airborne ash probability distribution (AAPD) maps have been generated to show the distribution of airborne volcanic ash in the North Pacific (NOPAC) region by simulating volcanic eruption clouds from 22 of the 100 most historically active volcanoes in the region. The PUFF ash-dispersion model was run daily using archived wind field data between 1994–1995 and 1997–2001 for low and high aircraft flight levels. Subsequent statistics are generated representing the distribution of simulated airborne ash at 6 and 24 hr intervals, defining the regions most likely to contain airborne ash and the direction and distance a volcanic ash cloud may propagate from a given volcano. The AAPD maps suggest eruptions originating from the Kamchatkan Peninsula would travel due east into the NOPAC air-traffic routes during summer. During the winter, wind directions over the Kamchatkan Peninsula are more variable, often resulting in a bimodal airborne ash distribution. In contrast, AAPD maps show that eruptions originating from the Aleutians and Alaskan Peninsula are more likely to travel in southeast directions during the summer and E-NE during winter. The results indicate that the paths of many NOPAC air traffic routes coincide with airborne ash distribution probability maxima. The upper atmospheric region most likely to contain airborne ash is located off the eastern coast of the Kamchatkan Peninsula, and is generally centered over the heavy air traffic flight corridor of the NOPAC.

REANALYSIS OF ERUPTION CLOUDS FROM THE NORTH PACIFIC AND THEIR IMPACT ON AIRCRAFT ROUTES

Rorik Peterson, Ken Dean, Jonathan Dehn, Laura Bickmeier,
and Joanne Groves
Geophysical Institute, Univ. of Alaska, Fairbanks

Introduction

The Alaska Volcano Observatory has been monitoring volcanoes in the North Pacific (NOPAC) Region for approximately 15 years using satellite data and dispersion models. Over this period nearly a hundred plumes and eruption clouds have been detected. During this time, detection and monitoring capabilities have evolved and improved significantly, and the growing data archives have been organized and consolidated.

The relatively recent 2001 eruption of Mt. Cleveland, Alaska, was reanalyzed by AVO's University of Alaska, Fairbanks (UAF) site with regard to potential aircraft exposure to airborne volcanic ash. The combination of satellite data, dispersion model forecasts, and flight route data provides an insightful perspective on the impact the ash cloud had on air traffic in the region.

Background

Analysis of aircraft flight-paths during and after the eruption of Mt. Cleveland suggests that some aircraft may have flown through the drifting ash cloud 18-24 hours after the start of the eruption. However, no mechanical problems were reported. To assess these potential encounters, we have compared the flight paths of the aircraft to satellite observations of the ash cloud and to Puff dispersion model predictions. Also, we have developed a relative ash exposure rating for aircraft that may have flown through the ash cloud.

The 19 February eruption of Mt. Cleveland produced a volcanic cloud that formed an arc over 1,000 km long, and drifted to the NE across Alaska (Dean et al., 2004, Dean et al. 2002). The cloud was detected and its movement tracked using data from multiple satellite sensors, including GOES, AVHRR and MODIS for approximately 50 hours. The translucent cloud was detected on the GOES data at half-hour intervals after the start of the eruption, approximately 1430 UTC. These data were processed using the brightness temperature difference (BTD) technique (Prata, 1989). The altitude of the cloud increased over time from 7.5 km a few hours after the start of the eruption to 12 km eight hour later (Dean et al., 2002).

The Anchorage Volcanic Ash Advisory Center (VAAC), working with the Alaska Volcano Observatory (AVO), issued alerts (SIGMET) warning aircraft of the presence of the cloud and its position. The first SIGMET was issued Feb. 19 at 1847 UTC warning of a "possible eruption at Cleveland Volcano", a short time later an18-hour forecast was issued based on dispersion model simulations. A portion of the cloud was reported at "FL200-FL400" (approximately 20-40 thousand feet). Several pilots reported observing the cloud and gave height estimates, and others reported ash and a sulfur odor in the cockpit (Simpson, et. al, 2002).

Method

Real-time and archived air traffic control data are publicly available from several vendors. These data include the latitude, longitude, altitude and speed of aircraft with a one-minute time resolution. Using archived data obtained from Flight Explorer®, we compared air traffic flight paths in the North Pacific (NOPAC) Region to satellite data and dispersion model simulations for the 48 hour period after the start of the eruption.

For the most part, aircraft avoided the general area of the ash cloud during the first 16 hours (1430 to 0630 the following day), although there is a four-hour gap in the air-traffic data from 0100-0400 on Feb. 20. For the subsequent 18 hour period, some aircraft flew through a vertical plane that included the ash cloud. Figure 1 shows the BTD-processed satellite image at 1345 UTC superimposed with air-traffic routes from 1315 – 1415 UTC. Circles indicate the last recorded location of each flight during this time period. The altitude of aircraft is known and the altitude of the ash cloud-top is estimated using cloud-atmosphere temperature correlations, pilot reports

and dispersion models at various times. However, the lower extent of the cloud is nearly impossible to ascertain. Thus, we are able to predict/estimate if a plane flew above the cloud (missing) or near the height of the cloud (possibly an encounter) but it is impossible to determine if the aircraft encountered ash at altitudes lower than the top of the cloud.

To determine the three-dimensional extent of the ash cloud, the Puff volcanic ash dispersion model was used to simulate this event using NCEP reanalysis windfield data. Puff is a Lagrangian model that uses tracer particles, and calculates advection, diffusion, and sedimentation rates for individual tracer particles using a first-order Euler method (http://puff.images.alaska.edu).. Relative concentration information is possible and absolute concentration may be calculated if the eruptive mass rate can be approximated. Simulation results of the two-dimensional lateral extent agree with the BTD data (compare Figures 1 and 2).

A Puff simulation using a 10-minute time resolution was performed in order to analyze the flight paths of some selected flights nearby the ash cloud. A one-hour sequence of forecasts superimposed with flight trajectories are shown in Figure 3. Comparing flight paths to the 4-dimensional (space and time) Puff simulations indicate that some aircraft flew through regions with predictions of elevated ash concentration. Estimating the total tephra volume at $1x10^8$ m^3, the absolute concentration was calculated for the regions through which the planes flew. A total *potential exposure* was then calculated as $E = c \cdot t$, where c is the ash concentration in mg/m^3, and t is time in minutes. The potential exposure for all flights in the vicinity was calculated during the 48-hour period following the event, and the ten highest exposure values are shown in Figure 4. Letters correspond to the flights labeled in Figure 3. Three flights (A, B, and K) traveled through the northern tip of the simulated cloud between 0800-1000 UTC on Feb. 20. Six other flights traveled though the center of the predicted cloud between 1330-1530 UTC of the same day, and one flight (C) through the southern tip.

Dispersion model forecasts also contain particle size and distribution information in addition to concentration. More complicated exposure calculations involving particle size are possible. Although there is limited data concerning the effect of different particle sizes on jet engines, it is reasonable to assume that the smallest fraction, that less than 1 micron, would have negligible effect on jet engines. Since particle fall velocity is proportional to the cube of the particle size (in laminar flow), only the smallest fraction remains airborne at longer times. However, until more precise information about the actual particle-size cutoff for damage is available, a conservative estimate that does not depend on size is presented.

Discussion

The meaning of these results deserves careful scrutiny for three major reasons: (1) model simulations are extremely difficult to validate; (2) absolute ash concentration is based on some potentially tenuous assumptions about effusive rate and initial ash column dynamics; and (3) the concentration of volcanic ash that damages jet engines is unknown. However, further investigation of calculating *potential exposure* has several merits. First, low-level exposure to volcanic ash may be difficult to detect during routine aircraft maintenance. If aircraft that potentially encountered ash are identified, a more thorough inspection can be performed, possibly mitigating a future dangerous situation. Second, potential exposure can be calculated ahead of time for an existing air route during an on-going volcanic event as a tool to determine the degree of avoidance and caution necessary. This may be particularly beneficial in later stages when ash concentrations have dropped to levels that are difficult or impossible to detect with remote sensing techniques.

The exposure rating project is in its early stage of development and our initial analysis of these data is presented here. AVO and UAF will be refining the modeling techniques, and will attempt to validate the exposure rating system based on reports of aircraft-ash encounters in order to further assess possible uses of this information.

References

Dean, K. G., J. Dehn, K. R. Papp, S. Smith, P. Izbekov, R. Peterson, C. Kearney, and A. Steffke, 2004. Integrated satellite observations of the 2001 eruption of Mt. Cleveland, Alaska, Jour. Volc. Geophy. Res., 135, doi10.1016/j.jvolgeores.2003.12.013

Dean, K.G., Dehn, J., McNutt, S., Neal, C., Moore, R. Schneider, D. 2002. Satellite Imagery Proves Essential for Monitoring Erupting Aleutian Volcano. EOS Trans. Am. Geophys. Union, 83, 241, 246-247.

Prata, A. J., 1989. Infrared radiative transfer calculations for volcanic ash clouds. Geophys. Res. Lett., 16, 1293-1296.

Simpson, J. J., Hufford, G. L., Pieri, D., Servranckx, R., Berg, J. S., Bauer, C., 2002. The February 2001 Eruption of Mount Cleveland, Alaska: Case Study of an Aviation Hazard. Am. Met. Soc.V. 17, 691–704.

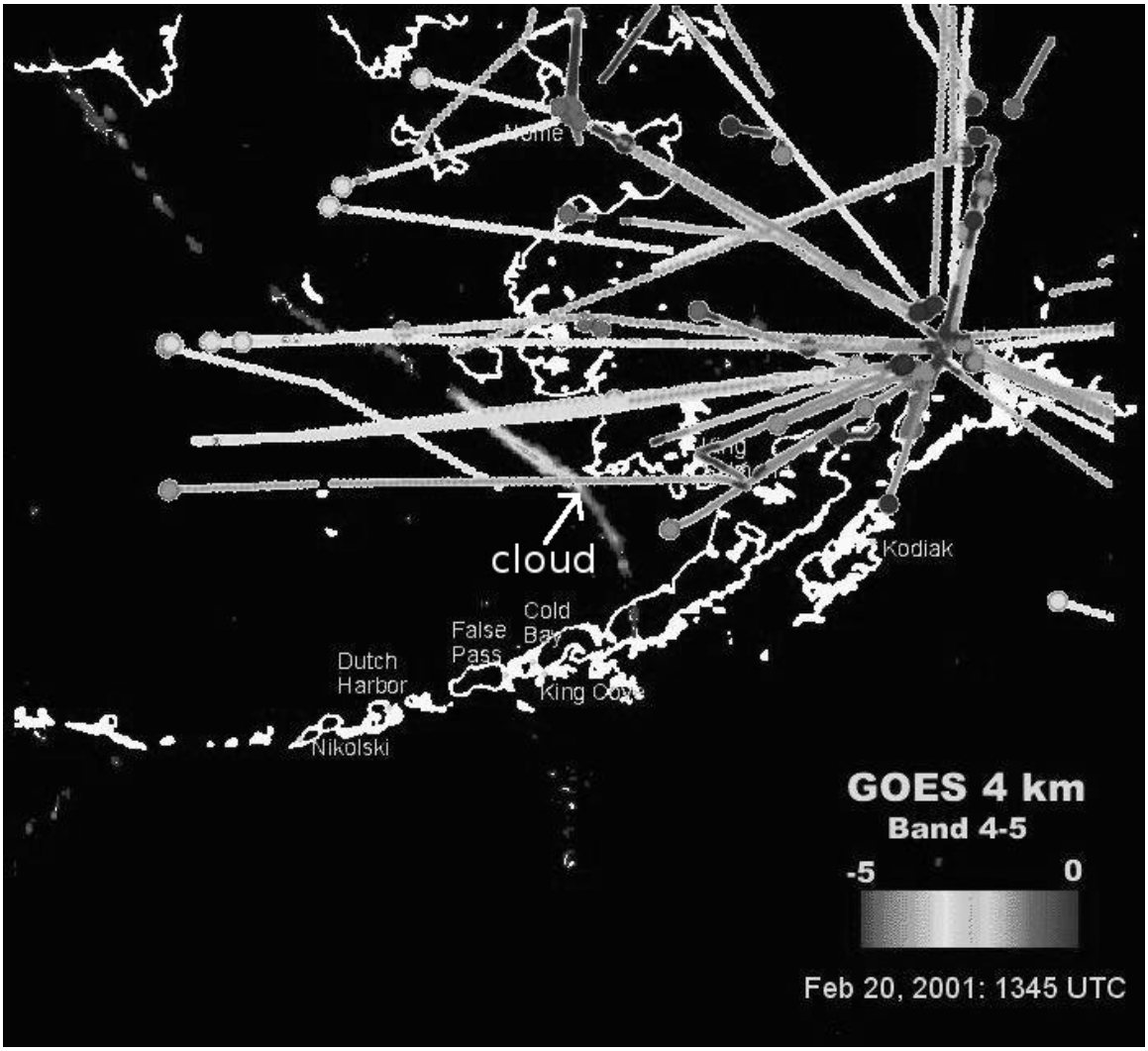

Figure 1 – Composite GOES brightness temperature difference (BTD) image at 1345 UTC on February 20, 2001 overlaid with all flight routes at 1345 ±30 minutes. The last recorded position of each flight is shown with a filled circle. Most all flights are entering or leaving Anchorage Int'l Airport. The ash cloud as detected using BTD is shown just slightly off of the west coast.

Figure 2 – Puff dispersion model forecast for 1345 UTC on February 20, 2001 overlaid with all flight routes at 1345 ±30 minutes. The last recorded position of each flight is shown with a filled circle. Ash forecasts are color-coded by height and correspond with the color-coding of the flight routes.

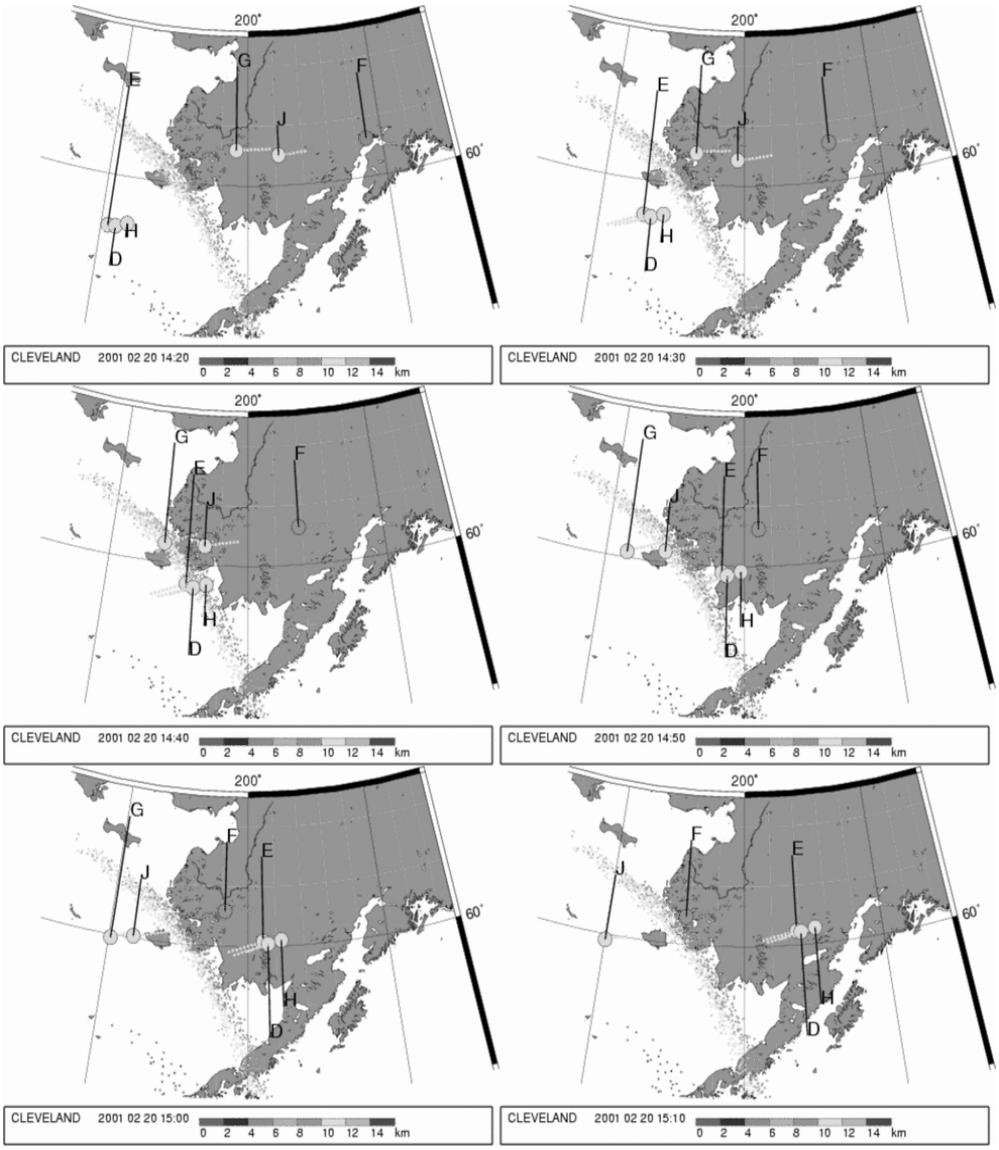

Figure 3 – One hour time-series of Puff dispersion model forecasts superimposed with selected flight routes. Ash forecasts are color-coded by height and correspond with the color-coding of the flight routes. Potential ash exposure calculations recorded the highest values for the flights shown.

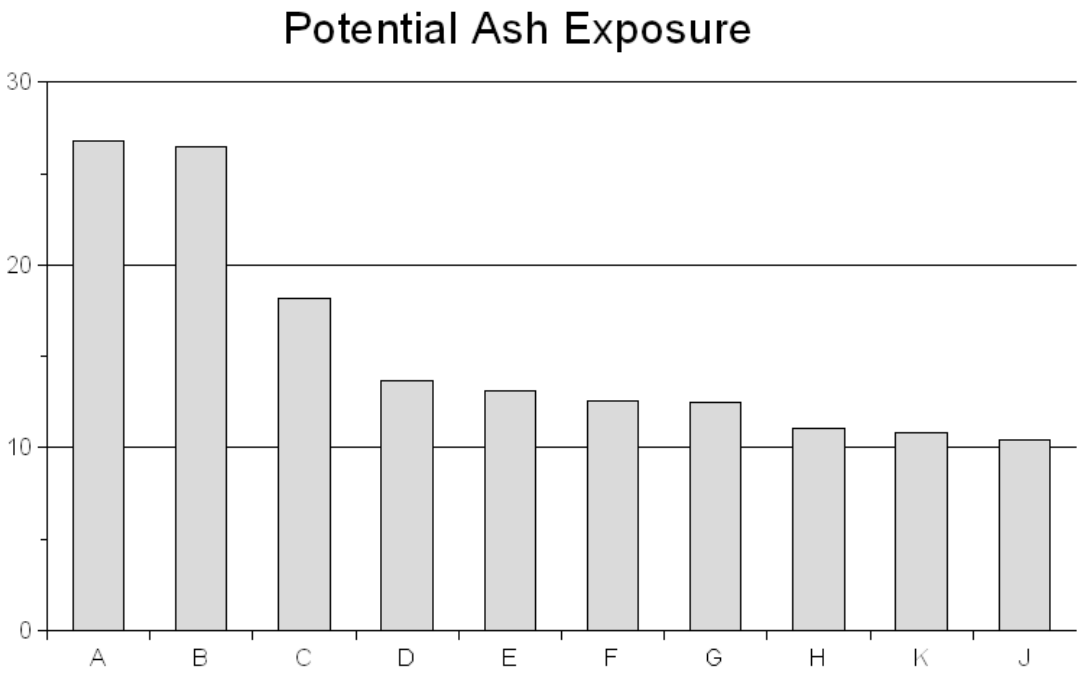

Figure 4 – Potential ash exposure [mg·min/m^3] for the 10 flights with highest values calculated during the 48 hours following the eruption. Letters correspond to flight trajectories shown on Figure 3.

QUANTITATIVE SULPHUR DIOXIDE RETRIEVALS FROM AIRS, MODIS AND HIRS

Fred Prata, CSIRO Atmospheric Research, Aspendale, Australia
Cirilo Bernardo, CSIRO Atmospheric Research, Aspendale, Australia

A new suite of algorithms is proposed for retrieving upper troposphere/lower stratosphere sulphur dioxide from the infrared channels of the AIRS, MODIS and HIRS satellite instruments. The retrieval schemes are tailored to the strengths of each instrument, but all utilise the same principle of detecting the strength of absorption by the anti-symmetric stretch of the SO_2 molecule centred around 1360 cm^{-1} (7.34 μm). The AIRS instrument covers this region of the infrared spectrum with more than 130 channels and is capable of accurate total column amount retrievals with a spatial scale of ~15x15 km^2. We also explore the possibility of using micro-windows and the 8.6 μm and 4.0 μm regions to infer SO_2 height information. The MODIS instrument provides a broadband measure of the 7.34 μm SO_2 absorption feature, but offers unprecedented ~1x1 km^2 spatial resolution and up to 4 measurements per day from two satellites. The retrievals are less accurate than those from AIRS. The HIRS family of instruments also provide broadband measurements and are of lower spatial resolution (~18 x18 km^2 at nadir) than MODIS, but these data span nearly 25 years and are complemented by simultaneous measurements of atmospheric temperature, moisture, clouds, radiative parameters and ozone. Consequently these data are of great value for studies of the effects of volcanic emissions on climate and on the chemical balance of the atmosphere. These new infrared measurements of SO_2 are compared and contrasted to established measurements from TOMS and GOME.

Sakura – AN AIRBORNE INFRARED IMAGING CAMERA FOR THE DETECTION OF VOLCANIC ASH AND SULPHUR DIOXIDE GAS

Fred Prata, CSIRO Atmospheric Research, Aspendale, Australia

Since the early 1990's CSIRO Atmospheric Research have been investigating the use of infrared radiometers for the detection and discrimination of volcanic ash from airborne platforms. The intention has been to develop a forward looking infrared camera system that could be deployed on commercial jet aircraft. Simulations studies and airborne trials at Sakurajima volcano in Japan suggest that infrared radiometry can be used to detect volcanic ash. More recent ground-based trials of an uncooled imaging infrared camera have indicated that sulphur dioxide gas can also be detected and the system is now being improved to provide an indication of other atmospheric hazards, such as clear-air turbulence, low level wind shear, severe weather and desert dust outbreaks. We describe the basic operation of the proposed infrared airborne camera ("Sakura") and demonstrate the overall system performance, "look and feel" and suggest likely operating modes. Results from the airborne trials in Japan will be presented and the operation of the technology from the ground, from an airborne platform and from a satellite platform will be compared and contrasted. Testing of an uncooled infrared imaging camera on board a commercial jet aircraft remains a major goal of this project.

TESTING REAL-TIME REMOTE SENSING FOR MONITORING VOLCANIC ACTIVITY IN CENTRAL AMERICA

Armando Saballos, INETER, Managua, Nicaragua
Peter Webley and Martin Wooster, Department of Geography, King's College, London, UK

We describe the implementation and results of a project to design, install and operate a remote sensing-based monitoring system for Central American volcanoes, locally based in Managua, Nicaragua but capable of monitoring all of Central America. The system is based on AVHRR data capture, and up to eight satellite passes a day are received and processed automatically to provide information on volcanic hotspots, and in future ash clouds, with minimal human intervention. The project aims to assess whether this type of technology is able to significantly improve the capability to locally monitor volcanoes in regions such as Central America. Validation is being conduced against other remote sensing and geophysical datasets, and a social science component is assessing the onward dissemination of the data and its use in hazard assessment.

ADVANCES IN ULTRAVIOLET DETECTION OF VOLCANIC ERUPTION CLOUDS

Stephen J. Schaefer, Joint Center for Earth Systems Technology UMBC, Baltimore MD, USA
Arlin J. Krueger, Joint Center for Earth Systems Technology UMBC, Baltimore MD, USA
Simon A. Carn, Joint Center for Earth Systems Technology UMBC, Baltimore MD, USA

Sulfur dioxide is the most readily quantified material in volcanic eruption clouds due to low background amounts in the atmosphere and strong absorption bands in near ultraviolet wavelengths, which are sampled by polar orbiting Total Ozone Mapping Spectrometers (TOMS). The new hyperspectral Ozone Monitoring Instrument (OMI) has an increased sensitivity and a smaller pixel size (13 x 25 km) than the Nimbus 7 TOMS (50 x 50 km) or the current Earth Probe TOMS (39 x 39 km). The OMI will have a greater than 10^2 improvement in detection limit of SO_2 in eruption clouds relative to the Nimbus 7 TOMS. Pre-eruptive, passive degassing of SO_2 on the order of $10^2 – 10^3$ tons/day should be detectable by OMI and will aid in eruption forecasting. Characterization of aerosol particles by type (e.g. ash, sulfate or ice) and size is expected utilizing the OMI data and will further refine the risk posed to aircraft by different clouds. Current IR instruments have high spatial resolution but may fail to detect volcanic clouds at low altitudes or above high clouds due to water vapor interference or poor thermal contrast. The UV instruments allow for an unambiguous detection of all volcanic clouds, which produces a very low false alarm rate. OMI is on the Aura platform to be launched in June 2004. The data are expected to be processed orbit-by-orbit in near real-time for use in volcanic hazard detection.

REAL-TIME MONITORING OF THE VOLCANIC ASH FALLOUT WILL IMPROVE AIRPORT SAFETY

Simona Scollo, INGV, Catania, Italy
Mauro Coltelli, INGV, Catania, Italy
Marco Folegani, Nubila, Bologna, Italy
Stefano Natali, Nubila, Bologna, Italy
Franco Prodi, ISAC, Bologna, Italy

PLUDIX instrument was tested to measure terminal settling velocity of volcanic particles during the pyroclastic fallout of 2002 Etna's eruption. The instrument is a new generation radar rain-gauge disdrometer, based on the Doppler shift induced by falling particles on the transmitted electromagnetic signal, usually used to investigate the space and the time variability of rainfall, together the total mass of rain accumulated in the ground. The measuring campaign was performed on 18 and 19 December, when explosive activity of Mt. Etna produced a long-lived volcanic plumes high 4000 m a.s.l. During the experiment PLUDIX instrument detected coherently volcanic ash fallout. Data processing permitted to estimated their fall-velocities, using a simple Doppler shift formula. Measured fall velocities have been compared with that obtained from Wilson and Huang experiment for particles with density, dimension and shape similar to Etna's ashes. Both data sets are fully comparable demonstrating that PLUDIX is not only able to detect volcanic ashes but also to characterize in real-time their falling velocities and then the sedimentation rate during the ash fallout. In the next step PLUDIX detection method will be modified reducing the maximum detectable Doppler shift to improve spectral resolution. Moreover a conversion algorithm to estimate in real time the grain size distribution of ash will be implemented. This category of instruments could be very useful for real-time monitoring of the volcanic ash fall rate in the airports close to the active volcanoes in which operations are often disrupted by explosive eruptions like at Catania International Airport during the 2001 and 2002 Etna's eruptions.

P3.18

DEVELOPMENT OF VOLCANIC ASH IMAGE PRODUCTS USING MODIS MULTI-SPECTRAL DATA

George Stephens, NOAA/NESDIS Office of Satellite Data Processing and Distribution, Camp Springs MD
Gary P. Ellrod, NOAA/NESDIS Office of Research and Applications, Camp Springs, MD
Jung-Sun Im, IM Systems Group, Inc, Camp Springs, MD

1. INTRODUCTION

The Moderate Resolution Imaging Spectroradiometer (MODIS) on National Aeronautics and Space Administration's (NASA) Aqua and Terra polar-orbiting spacecraft provides a total of thirty-six spectral bands: twenty 1 km resolution Infrared (IR) bands, and sixteen higher resolution (250-500m) visible and near-IR bands available for daytime applications. Based on studies with data from aircraft or other satellite sensors, several of the spectral bands available from MODIS have been shown to be useful for the detection of airborne volcanic ash clouds that pose hazards to aircraft (Miller and Casadevall 2000). For example, the brightness temperature difference (BTD) of MODIS Band 31 (11 □m) and Band 32 (12 □m) is able to distinguish silicate volcanic ash from meteorological clouds (Prata 1989) due to differential absorption. Another longwave IR channel (Band 29 - 8.6 □m) exhibits strong absorption in the presence of volcanic ash as well as sulfur dioxide (SO_2) gas emitted by volcanoes (Realmuto et al 1997).

Due to some degradation in the volcanic ash detection capability of the Geostationary Operational Environmental Satellite (GOES) Imager series beginning with GOES-12 (2002) through GOES-Q (late 2008 launch), there is a need for polar orbiting satellite image products to augment GOES in support of the operational aviation volcanic ash warning system. The reduced capability of GOES is due to the temporary removal of a 12 □m IR band that has a proven capability for volcanic ash detection (Prata 1989; Schneider and Rose 1994). The global aviation warning system consists of Volcanic Ash Advisory Centers (VAACs) established in 1997 by the World Meteorological Organization to provide timely alerts of active volcanic hazards and predictions of ash cloud locations to Meteorological Watch Offices (MWOs) (Miller and Casadevall 2000). Each VAAC has multi-spectral satellite data and derived products at its disposal to help detect and monitor airborne ash clouds.

Work has begun within NOAA/NESDIS to develop prototype volcanic ash image products from MODIS to support the VAACs, as well as to prepare for advanced satellite systems such as the National Polar Orbiting Environmental Satellite System (NPOESS) scheduled for a prototype launch in 2006, and the GOES Advanced Baseline Imager (2012) that will have multi-spectral capabilities and resolutions similar to the MODIS.

2. DATA ANALYSIS

Initial analysis of MODIS data has been completed for two volcanic eruptions: (1) Cleveland volcano in the Aleutian Islands on 19-20 February 2001, and (2) Popocatepetl volcano near Mexico City on 19-20 December 2000. Two data sets were analyzed for each of the first two cases (one daytime, one nighttime) using Man-computer Interactive Data Access System (McIDAS) image processing software on PC workstations. The emphasis in this work was to develop an optimum IR volcanic ash product that could be used twenty-four hours a day, regardless of location. However, visible and near-IR bands were also evaluated for daytime applications.

Various combinations of MODIS IR bands have been evaluated. Some initial tests involved producing multi-spectral ash products used operationally at VAACs such as the Two-Band Split Window (TBSW) based on the BTD of Bands 32 (12.0 □m) and 31 (11 □m) described earlier in this paper, the Three-band Volcanic Ash Product (TVAP) that is based on the TBSW plus Band 22 (3.9 □m) (Ellrod et al 2002) and a four-channel algorithm (Mosher 2000) that also incorporates visible channel information. Other combinations were evaluated that utilized Band 30 (9.7 □m), Band 29 (8.6 □m), Band 28 (7.3 □m), and Band 25 (4.5 □m).

The best results for ash cloud discrimination were obtained from a three-channel combination of Band 32 (12.0 □m), Band 31 (11.0 □m) and Band 29 (8.6 □m) (hereafter referred to as the Longwave Volcanic Ash Product (LVAP)). The most useful shortwave IR channel was determined to be Band 25 (4.5 □m), which supports the results of Hillger and Clark (2002). An advantage of Band 25 is that it exhibits considerably less solar reflectance than the other shortwave bands, which provides more consistent results for both day and night. By examining scatter plots of the BTD's for each of the channels, appropriate BTD ranges were empirically selected to highlight the likely ash cloud, and minimize the meteorological clouds and surface features.

3. CASES ANALYZED

3.1 *Popocatepetl, 18-20 December 2000*

On the evening of 18 December 2000, Popocatepetl Volcano near Mexico City began an eruption of ash that was not explosive, but persisted until the afternoon of the 20th. It was considered to be the largest eruption of the

volcano in 75 years**.** Ash spewed southward from the volcano across southern Mexico, reaching the Pacific coast on the south, and the Gulf of Mexico on the east after Midnight, 20 December 2000. Maximum height of the ash was estimated to be about 10.6 km (35,000 ft) (Washington VAAC advisory).

MODIS observed the ash clouds over southern Mexico at 0505 UTC on 20 December 2000. The three-band LVAP (Figure 1) provided depiction of the ash cloud extent that was in good agreement with concurrent GOES imagery, shown in an analysis by the Washington VAAC (Figure 2). Comparison with the TBSW image in Figure 1 indicates that the addition of Band 29 has resulted in a slightly larger area of ash compared with the TBSW alone. The LVAP detects more of the thin ash over southern Mexico, but may also be observing some surface features, possibly due to the presence of underlying silicate soils.

Scatter plots of Band 32 - 31 and Bands 32 - 29 versus Band 31 IR temperature (Figure 3) reveal that the TBSW alone provides the best discrimination, but Band 32 - 29 contains some additional information on the presence of ash.

3.2 *Cleveland, 19 February 2001*

On the afternoon of 19 February 2001, Cleveland Volcano in the Aleutian Islands of Alaska erupted, sending ash as high as 9.1 km (30,000 ft) (Alaska Volcano Observatory (AVO) Web site). The ash cloud bifurcated as it drifted eastward, with the highest portion of the cloud stretching northward across the Bering Sea, and the portion below about 6.1 km moving southeast into the Gulf of Alaska.

A MODIS LVAP image was produced at 2310 UTC, 19 February 2001 (A - Figure 4). The majority of the ash cloud is shown being elongated north and northwest of the Aleutian chain, with a thinner component to the southeast. Comparison with a simple TBSW product (B) indicates that the addition of Band 29 data adds significant value to the analysis by detecting the thinner ash to the east and southeast of the main ash cloud. The ash cloud coverage from MODIS compares favorably with the 2315 UTC analysis based on 30-minute interval GOES TBSW images from the Alaska Volcano Observatory (Figure 5).

A scatter plot of the BTD's for Bands 32 – 31 and Bands 32 – 29 versus Band 31 IR temperature (Figure 6) shows that both allow good discrimination of ash from meteorological water and ice clouds, but the latter provides the best result in this case.

4. ADDITIONAL EXPERIMENTS

Tests were conducted of techniques for detection of sulfur dioxide (SO_2). The SO_2 test involved the use of a multi-channel, stepwise threshold test developed by Crisp (1995). The Crisp technique employs Bands 27, 28, 31, and 36. The tests were negative for all cases, presumably because the technique is only able to detect SO_2 at altitudes between 6 km and 25 km. The eruption cases studied in this paper were relatively weak eruptions that did not emit ash and SO_2 into the Stratosphere.

Experiments with Red-Green-Blue (RGB) color composite techniques were also conducted to produce images that provide optimum colorized depiction of the ash cloud, meteorological cloud types, and surface conditions to aid in interpretation of the event. One result of the tests is a daytime image product that combines information from the three-band IR volcanic ash image with visible Band 1 (0.6 □m) and near-Infrared Band 6 (1.6 □m) data. The latter two channels help distinguish ice versus water clouds due to the lower solar reflectance of ice cloud particles and snow cover in Band 6 than in Band 1. An example of this RGB image for the Cleveland eruption derived using the McIDAS software is shown in Figure 7. Volcanic ash appears red, water droplet clouds as a greenish hue, and ice clouds and snow as blue.

5. ANALYSIS OF REAL-TIME MODIS DATA

Procedures were developed to analyze near real-time "Level 1b" MODIS data downloaded from the NASA DAAC via a file transfer protocol (ftp) site at Federal Building 4 in Suitland, Maryland. Once the data were downloaded, a program written in McIDAS was run to generate LVAP images in an effort to evaluate the MODIS data for "null" events in which no known volcanic activity was occurring. In these images it was discovered that there are some regions over land areas where "false alarms" for ash clouds were observed. These are believed to be due to the radiation characteristics of sandy soils consisting of silicate minerals. In order to avoid this, a sequential test can be used, requiring that a Band 32 – Band 31 threshold be satisfied before information from the Band 32 – Band 29 can be incorporated into the final image product.

6. DATA PROCESSING AND DISTRIBUTION

NESDIS' Satellite Services Division is implementing the product operationally for use in issuance of Volcanic Ash Advisories by the Washington Volcanic Ash Advisory Center (W-VAAC). Level 1b MODIS data are pulled from NOAA computers located at the NASA Goddard Space Flight Center for use in various products, including the Ash Product. LVAP and RGB composites are processed over geographic areas of responsibility of the W-VAAC and the Alaska VAAC in Anchorage AK, and will be made available on a Geospatial Information System compatible web site. (Figure 8.)

7. RECENT EXAMPLES FROM THE W-VAAC

A continuing series of eruptions at Tungurahua Volcano in Ecuador in August, 2003 provided several opportunities to validate the MODIS Volcanic Ash Product, as implemented in the W-VAAC. A comparison, below, of MODIS (Figure 9.), Advanced Very High Resolution Radiometer (AVHRR) (Figure 10.) and Geostationary

Environmental Operational Satellite (GOES) Imager derived graphical analysis (Figure 11.) demonstrates excellent agreement, with the MODIS product providing enhanced detection of thin ash to the west of the volcano.

8. SUMMARY AND CONCLUSIONS

Experimental volcanic ash products have been derived and evaluated using MODIS data from the Terra spacecraft for two volcanic eruptions: Popocatepetl, Mexico (20 December 2000) and Cleveland, Alaska (19 February 2001). The best results, based on subjective comparisons with frequent interval GOES imagery, were obtained from a tri-spectral combination of Bands 29 (8.6 □m), 31 (11.0 □m) and 32 (12.0 □m). Volcanic ash detection using a simple two-band split window (TBSW) derived from Band 32 - Band 31 was only slightly less effective. Optimum color composite images have been developed to provide information on ash cloud location, as well as cloud phase and surface characteristics, to aid in interpretation both day and night. Additional work will attempt to reduce false alarms from silicate soils in Band 29, and develop procedures for real-time production of operational products for use in VAACs.

9. ACKNOWLEDGMENTS

The authors would like to thank Dr. Donald Hillger of the NESDIS Regional and Mesoscale Meteorology Team, Ft. Collins, Colorado, and Drs. Matthew Watson and William Rose, Michigan Technological University, Houghton, Michigan, for providing the MODIS data described in this paper.

10. REFERENCES

Crisp, J., 1995: Volcanic SO2 Alert. EOS IDS Volcanology Team Data Product Document #3288, Jet Propulsion Laboratory, California Inst. of Technology, 13 pp.

Ellrod, G. P., B. Connell and D. W. Hillger, 2002: Improved detection of airborne volcanic ash using multi-spectral infrared satellite data. *J. Geophys. Res.*, In review.

Hillger, D. W., and J. D. Clark, 2002: Principal component image analysis of MODIS for volcanic ash, Part-1: Most important bands and implications for future GOES Imagers. *J. Appl. Meteor*., In press.

Miller, T. P., and T. J. Casadevall, 2000: Volcanic ash hazards to aviation. In: *Encyclopedia of Volcanoes*, H. Sigurdsson, Ed., Academic Press, San Diego, California, pp 915-930.

Mosher, F. R., 2000: Four channel volcanic ash detection algorithm. Preprint Volume, 10th Conf. on Satellite Meteor. and Oceanography, 9-14 January 2000, Long Beach, California, 457-460.

Prata, A. J., Observations of volcanic ash clouds in the 10-12 micrometer window using AVHRR/2 data. *Int. J. Remote Sens.*, **10**, 751-761, 1989.

Realmuto, V. J., A. J. Sutton, and T. Elias, 1997: Multispectral imaging of sulfur dioxide plumes from the East Rift Zone of Kilauea volcano, Hawaii. *J. Geophys. Res.*, **102**, 15057-15072.

Schneider, D. J., and Rose, W. I., Observations of the 1989-1990 Redoubt volcano eruption clouds using AVHRR satellite imagery. In: Volcanic ash and aviation safety: Proceedings of the First International Symposium on Volcanic Ash and Aviation Safety. *U. S. Geological Survey Bulletin 2047*, 405-418, 1994.

Wright, R., L. Flynn, H. Garbeil, A. Harris, and E. Pilger: 2002: Automated volcanic eruption detection using MODIS. *Remote Sensing of Environment*, **82**, 135-155.

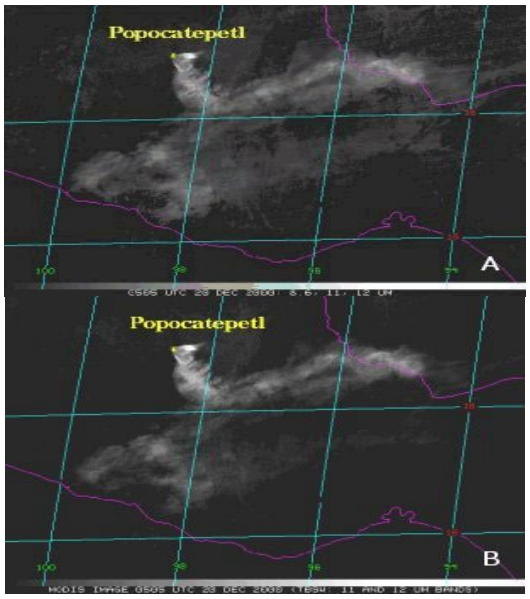

Figure 1. *Comparison of MODIS LVAP (A), and TBSW (B) images at 0505 UTC, 20 December 2000.*

Figure 2. *VAAC analysis near the time of MODIS image in Figure 1, based on GOES imagery.*

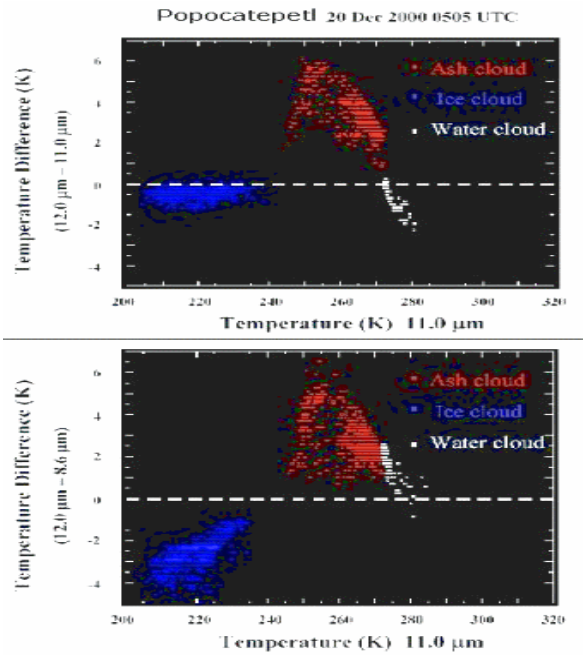

Figure 3. *Scatter plots showing BTDs for Bands 32-31 (top) and Bands 32 – 29 (bottom) at 0505 UTC, 20 December 2000.*

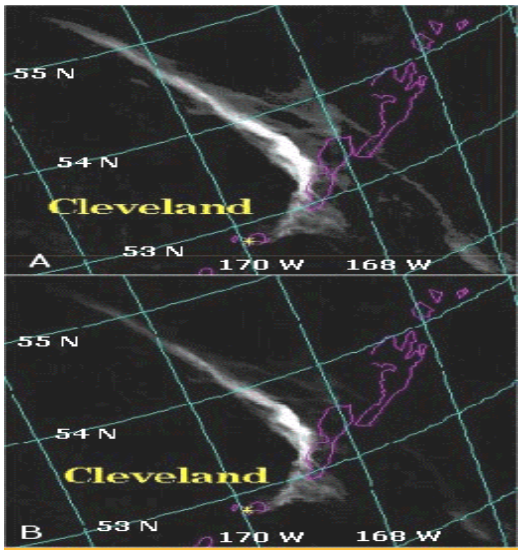

Figure 4. *Comparison of MODIS LVAP (A) With TBSW (B) at 2310 UTC, 19 February 2001.*

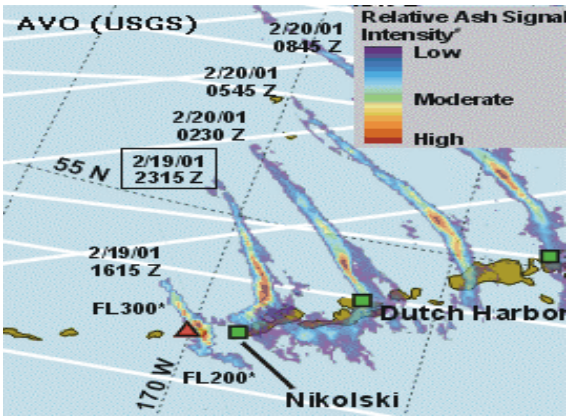

Figure 5. *Spreading of ash cloud from Cleveland Eruption on 19 February 2001 based on GOES TBSW animation. Time closest to MODIS data is outlined. (Alaska Volcano Observatory)*

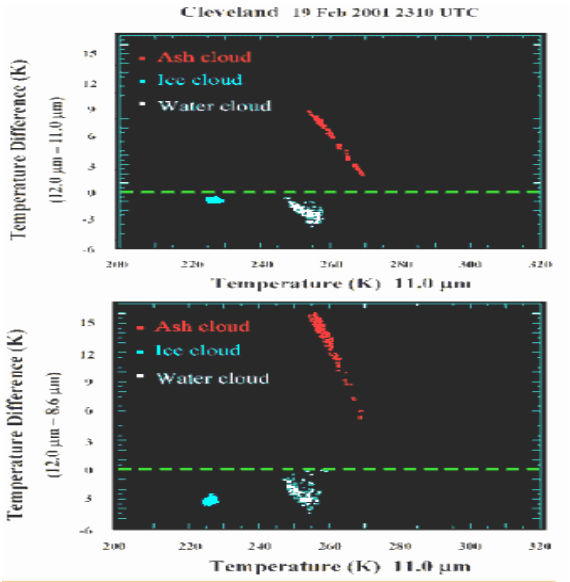

Figure 6. *Scatter plots of Bands 32 – 31 (top) and Bands 32 – 29 (lower) versus Band 31 temperature for Cleveland case at 2310 UTC, 19 February 2001.*

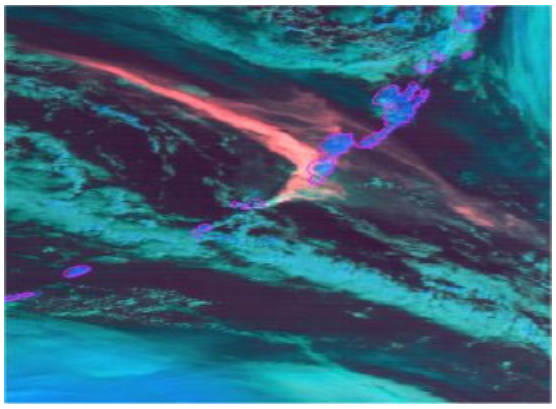

Figure 7. *Red-Green-Blue composite showing ash coverage from MODIS LVAP as red, Band 6 (1.6 □m) as green, and Band 1 (0.6 □m visible) as blue.*

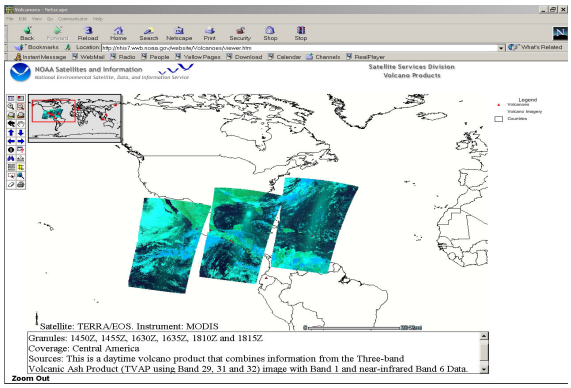

Figure 8. *Geospatial web site display of LVAP RGB composite imagery covering Central American region, delineated above.*

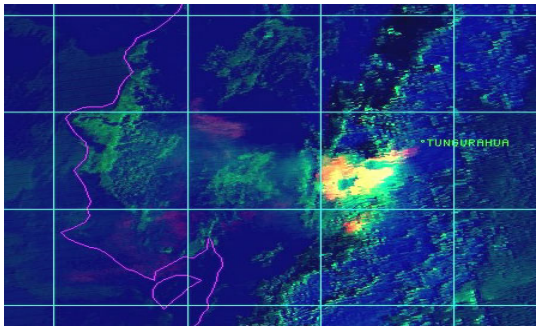

Figure 9*. MODIS AQUA LVAP RGB composite Aug. 31, 2003 1910 UTC.*

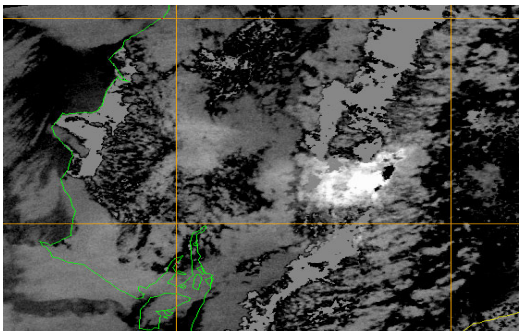

Figure 10. *AVHRR "split window", ch.4 – ch.5 Aug. 31, 2003*
1926 UTC

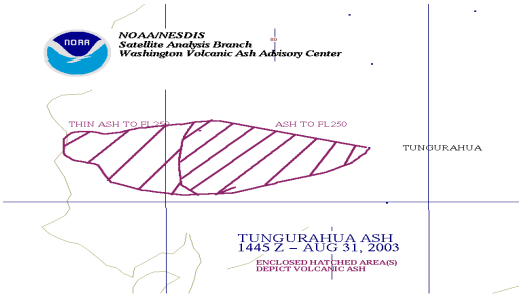

Figure 11. *W-VAAC graphical analysis from GOES imagery Aug. 31, 2003 1445 UTC*

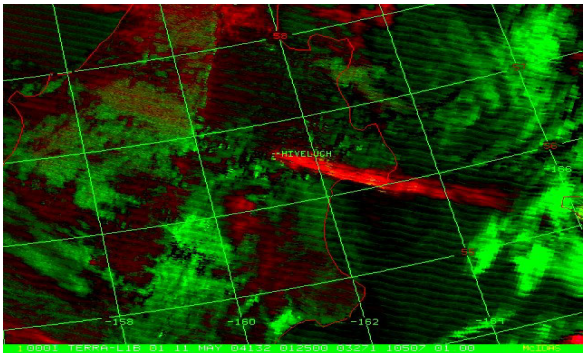

Figure 12. *LVAP detected an eruption of Sheveluch Volcano on Siberia's Kamchatka Pen-insula, May 10, 2004*

VOLCANIC ASH DISPERSION MODELING RESEARCH AT NOAA AIR RESOURCES LABORATORY

Barbara J.B. Stunder[1] and Jerome L. Heffter
NOAA Air Resources Laboratory, Silver Spring, MD, USA

ABSTRACT

The National Oceanic and Atmospheric Administration (NOAA) Air Resources Laboratory (ARL) is conducting research, using the HYSPLIT model, to improve volcanic ash forecast guidance. In one project, preliminary results suggest an archive of trajectory forecasts and dispersion forecast patterns from hypothetical eruptions and corresponding (hypothetical) analysis dispersion patterns can be used to predict the reliability of subsequent forecasts. In another project, ensemble meteorology is used to create a prototype probabilistic forecast product. More research is needed to determine the applicability of ensemble dispersion products.

INTRODUCTION

The Hybrid-Single Particle Lagrangian Integrated Trajectories (HYSPLIT) model was developed at the NOAA Air Resources Laboratory beginning in the early 1980s (Draxler and Taylor, 1982). Draxler and Hess (1998) describe the last major upgrade and compare HYSPLIT-calculated concentrations to measurements from field experiments, calculated Cs-137 deposition to that from the 1986 Chernobyl accident, and calculated volcanic ash to satellite imagery for the Rabaul, September, 1994 eruption. Results from recent model upgrades (see http://www.arl.noaa.gov/ready/hynew.html) are compared against a database of tracer measurements from field experiments, the "Data Archive of Tracer Experiments and Meteorology" (DATEM - see http://www.arl.noaa.gov/datem/). HYSPLIT was implemented at NCEP in 1998 (see http://www.nws.noaa.gov/om/tpb/458.htm) for radiological applications. The planned NOAA National Centers for Environmental Prediction (NCEP) installation of ARL's current version of HYSPLIT will include the ability to run HYSPLIT for volcanic ash transport and dispersion forecasting and produce output in the same format as VAFTAD.

Evaluation of volcanic ash dispersion forecasts includes two main components: the dispersion model and the meteorological forecast. To evaluate the dispersion model, model calculations using analysis meteorology are compared to volcanic ash observations, typically satellite analyses. To evaluate the meteorological forecast, the model calculations using forecast and analysis meteorology are compared. Current research at ARL is focused on the meteorological component, to provide more useful volcanic ash dispersion guidance products. Two ongoing projects will be described: one to assess the reliability of a forecast, the other to assess the possible use of ensemble dispersion forecasts.

FORECAST PATTERN RELIABILITY

The reliability of a forecast pattern is based on past patterns with similar meteorological situations. We hypothesize that forecasts are more reliable in some situations and less reliable in other situations. Forecasters aware of this differentiation may be able to better interpret forecast model output and thereby assign a degree of reliability to the forecast. Seven volcanoes were chosen for this study, in or near areas of responsibility of the Volcanic Ash Advisory Centers (VAACs) located at Washington and Anchorage.

Area	Volcano
1. Alaska	Augustine
2. N. Atlantic	Hekla
3. Mexico	Popocatepetl
4. NW United States	Rainier
5. Kamchatka	Sheveluch

[1]Corresponding author: Barbara.Stunder@noaa.gov, NOAA Air Resources Laboratory (R/ARL), 1315 East-West Highway, Silver Spring, MD, 20910, USA

6. Caribbean	Soufrierre Hills
7. South America	Tungurahua

A daily archived database is being created for hypothetical eruptions of each volcano listed above. The data include: a forecast trajectory, a forecast pattern, and an "offset" forecast pattern. The offset forecast pattern is the mean of the 8 forecast patterns using meteorology offset by one degree of latitude and longitude surrounding the volcano (Draxler, 2003), and the forecast pattern from the volcano without offset meteorology. All forecasts are run out to +18 hours. For reference, an analysis pattern is run using analysis meteorology for the days corresponding to the forecasts. In summary, the archived database contains, for each volcano, on each day, a trajectory, a forecast pattern, an offset forecast pattern, and an analysis pattern.

When corresponding forecast and analysis patterns are compared (Fig. 1), a forecast region that overlaps an analysis region is called a "hit", a forecast region that extends beyond an analysis region is called "excess", and the region of the analysis that was not forecast is called a "miss". For the aviation community, some degree of an excess region (false alarms) may be acceptable, but even a small degree of a miss region may be dangerous to aircraft safety

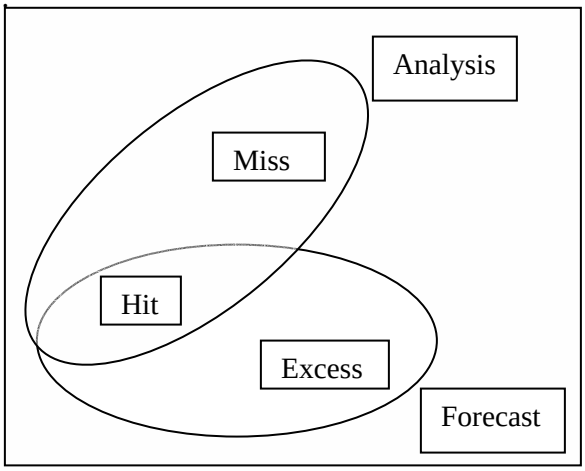

Figure. 1. Illustration of terminology with a forecast and analysis pattern: hit, miss, and excess.

The meteorological conditions for each forecast are categorized by the trajectory quadrant, trajectory distance, and the ratio of the offset forecast pattern area to the forecast pattern area, the "offset excess ratio" (Fig.2).

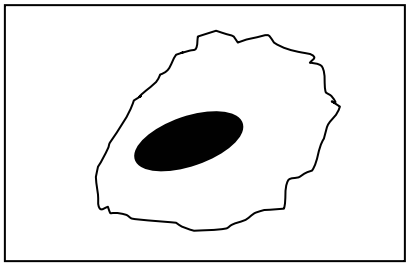

Figure 2: Offset excess ratio is the ratio of the forecast pattern area (solid oval) to offset forecast pattern area (irregular shape).

When an operational forecast is run, the database is searched for cases with meteorological conditions (trajectory quadrant and distance, and offset excess ratio) closely matching those for the forecast. A FOPARE (FOrecast PAattern REliability) chart that displays the percent of excess, hits, and misses for the matching cases, and their mean, can be created (Fig. 3). Preliminary results suggest that FOPARE charts with a small proportion of misses (<30%, 100% - 70%) and a small proportion of excesses (<30%) indicate the forecast is "reliable". When the misses are greater than 30% the forecast should be used with caution, since a significant percent of the ash pattern may extend beyond the forecast pattern. The above thresholds for misses and excesses have yet to be verified for operational use.

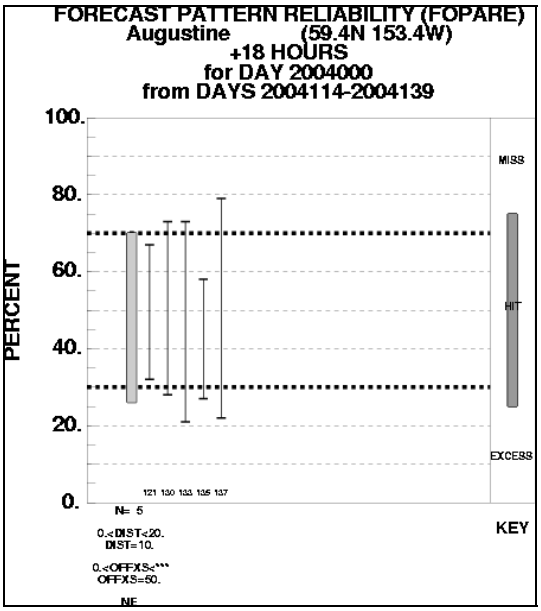

Figure 3. Example FOPARE chart.

ENSEMBLE DISPERSION FORECASTS

Uncertainties with volcanic ash dispersion forecasts have not been quantified. Servranckx and Chen (2004) describe some of the uncertainty as arising from uncertainties in the source term, meteorology, and transport and dispersion parameterizations. Current models, such as VAFTAD, and the planned NCEP implementation of HYSPLIT, use pre-determined ash particle specifications and vertical distributions, a given 3-dimensional meteorology dataset, certain transport and dispersion algorithms, and for real-time forecasting, an estimate of the eruption column height and eruption duration. A collection of dispersion forecasts using a range of realistic inputs and/or model algorithms/parameterizations, can be called an "ensemble" to show the range of forecast possibilities and the corresponding probabilistic forecast.

As an example, if the eruption column height is determined to be in a range between 20,000 ft and 25,000 ft, the model can be run for both heights, i.e. a 2-member ensemble. If the results are similar, then knowing the exact height is not important. If the results are different, perhaps because wind speeds vary significantly from 20,000 ft and 25,000 ft, the forecaster would need to use both model outputs to produce a forecast. The combined forecast product would then account for the uncertainty in the eruption column height.

Another dispersion ensemble can be created from the NCEP ensemble global meteorology forecast, which is based on an estimate of the uncertainty in the meteorological analyses (Szunyogh and Toth, 2002). For each of the 10 NCEP ensemble members, the model is run with a different analysis, which leads to different meteorological forecasts.

To illustrate an ensemble dispersion forecast, based on the NCEP ensemble meteorology, we chose a hypothetical 40,000 ft (about 12,200 m) eruption of Pavlof, Alaska, at 00 UTC 21 May 2004. Figure 4 shows the forecast pattern 18 hours after the eruption, for the layer from the surface to about FL550. The concentrations shown (units per cubic meter), spanning four orders of magnitude, are with respect to the mass (one unit) in the initial eruption column. In an operational setting, the mass of an eruption is not known so one unit is typically assumed.

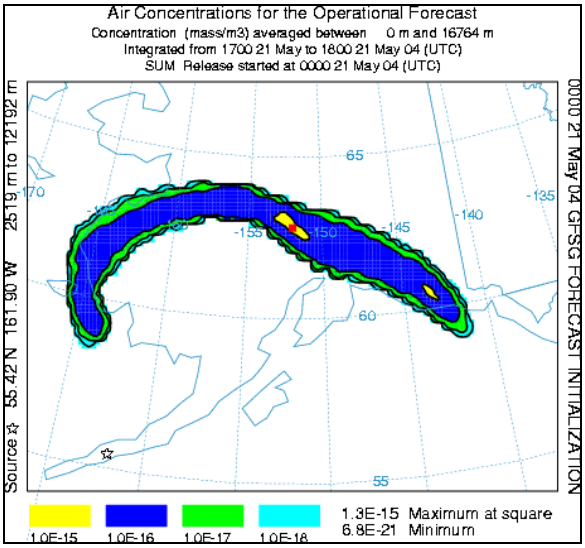

Figure 4. HYSPLIT 18-h forecast using operational NCEP GFS meteorology for a hypothetical 40,000 ft eruption of Pavlof at 00 UTC 21 May 2004.

To illustrate the differences in the meteorology, trajectories were computed using the ensemble members' meteorology beginning at the

time of the hypothetical eruption (Fig. 5). At 18 hours downwind from Pavlof, the trajectory endpoints span about 400 km in the crosswind and alongwind directions.

The individual dispersion forecast patterns based on the ensemble members (not shown) are generally similar to that of the operational forecast (Fig. 4), but show differences as suggested by the ensemble trajectories (Fig. 5). Calculating the mean dispersion forecast (Fig. 6) from the ensemble member forecasts shows a larger area of ash than the operational forecast.

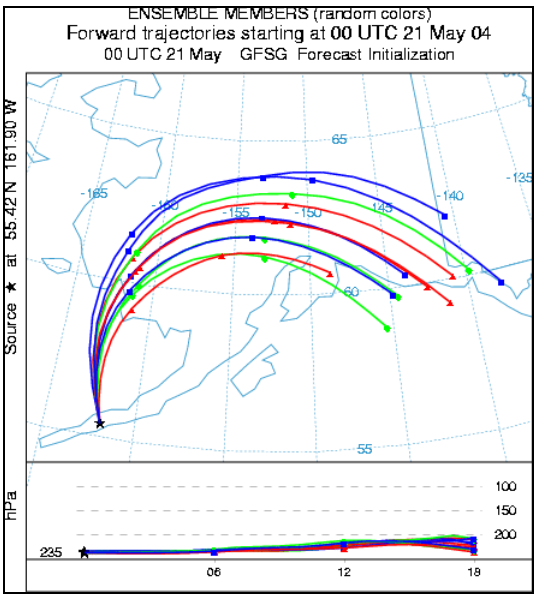

Figure 5. The ensemble of 18-hour duration HYSPLIT trajectories from Pavlof, beginning at 00 UTC 21 May 2004.

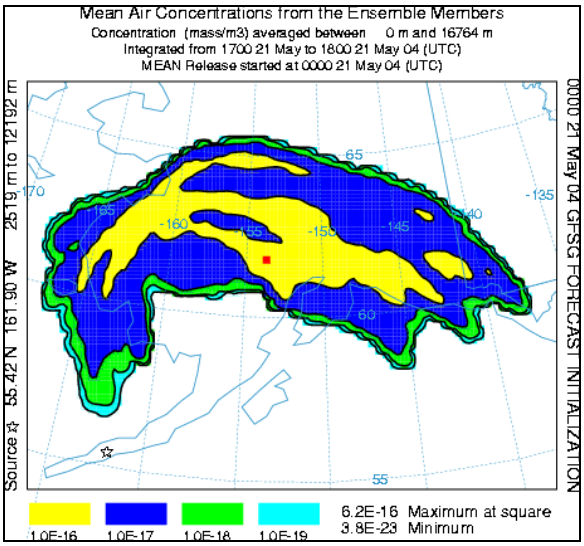

Figure 6. Mean dispersion forecast from the ensemble member dispersion forecasts.

Statistics other than the mean may also be computed from the ensemble member dispersion forecasts (Draxler, 2003). For example, the probability that the ash concentration exceeds 1.0 x 10^{-17} (arbitrarily chosen) is shown in Figure 7. The area with probability greater than 0%, as expected, is similar to the area with ensemble mean concentrations greater than 1.0 x 10^{-17} (Fig. 6). The area with probability greater than 25% is a small region. We do not have enough data yet to determine the usefulness of a product similar to this, or how a forecaster would use it. To speculate, a forecaster receiving a product such as Figure 7 might then develop a forecast that ash is likely in the area around the 25% probability area, but is possible in the area with non-zero probabilities. Forecasts such as this are somewhat analogous to current weather forecasts with probability of precipitation.

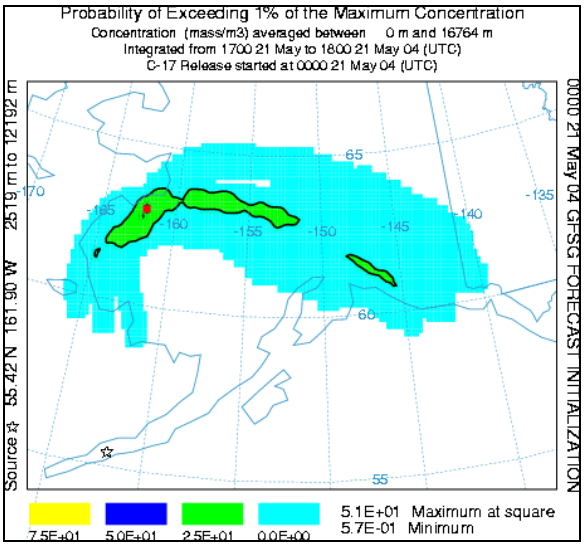

Figure 7. Forecast probability that ash concentrations are greater then 1.0E^{-17}.

Figure 8 shows the actual, but hypothetical, dispersion pattern based on analysis meteorology. Comparison to the operational forecast (Fig. 4) shows a generally similar pattern, but the analysis pattern is slightly farther north, within the ensemble mean pattern (Fig. 6). This suggests that, for this case, though the forecast was good (similar to that with analysis meteorology), use of the ensemble dispersion information may have provided additional useful information.

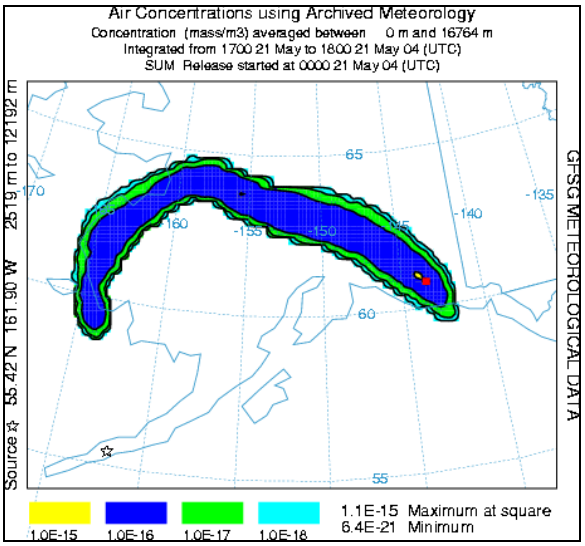

Figure 8. HYSPLIT analysis using analysis GFS meteorology corresponding to the forecast in Fig. 4.

Further research is needed beyond this case study in the dispersion application of the NCEP ensemble meteorology. More traditional use of the NCEP ensembles, such as 500 hPa height contours and quantitative precipitation forecasts, has focused on the mid- to long-range forecasts, i.e. greater than about 3 days. Use for short-term forecasts, as done here, needs to be assessed.

SUMMARY

Dispersion modeling research projects using the HYSPLIT model are being conducted at NOAA to provide more useful volcanic ash forecast guidance. In one project, the goal is to provide a qualitative assessment of the reliability of a forecast. In another project, the applicability of the NCEP ensemble meteorology forecast to improve dispersion forecasts is being studied. Results of both projects may lead to additional information of use to the forecaster.

REFERENCES

Draxler, R.R., 2003: Evaluation of an ensemble dispersion calculation, J. Applied Meteorology, 42, 308-317.

Draxler, R.R. and G.D. Hess, 1998: An Overview of the Hysplit_4 Modeling System for Trajectories, Dispersion, and Deposition, Aust. Met. Mag., 47, 295-308.

Draxler, R.R. and A.D. Taylor, 1982: Horizontal dispersion parameters for long-range transport modeling, J. of Applied Meteorology, 21, 367-372.

Heffter, J.L., 1996: Volcanic ash model verification using a Klyuchevskoi eruption. Geophy. Res. Letters, 23-12, 1489-1492.

Heffter, J.L. and B.J.B. Stunder, 1993: Volcanic ash forecast transport and dispersion (VAFTAD) model, Weather and Forecasting, 8, 533-541.

Servranckx, R. and P. Chen, 2004: Modeling volcanic ash transport and dispersion: Expectations and reality, 2nd International Conference on Volcanic Ash and Aviation Safety, Alexandria, VA, this volume.

Szunyogh, I., and Z. Toth, 2002: The effect of increased horizontal resolution on the NCEP global ensemble mean forecasts. Mon. Wea. Rev., 130, 1125-1143

OPERATIONAL VOLCANIC ASH PLUME PREDICTION MODEL PUFF AT THE JAPAN AIRLINES

H. L. Tanaka (Geoenvironmental Sciences, University of Tsukuba, Tsukuba 305-8572 Japan), Saburo Onodera (Japan Airlines, Tokyo Japan), and DAISUKE NOHARA (Meteorological Research Institute, Tsukuba Japan)

1. Introduction

Volcanic ash cloud floating and traveling in the air is a great concern to airline pilots. If a commercial jet aircraft encounters ash cloud, the damage could be serious enough to cause an engine failure (Hobbs et al., 1991; Casadevall, 1994; Onodera, 1997). In order to avoid serious accidents of commercial aircrafts, real-time volcanic plume prediction models have been developed by some agencies.

A 3-D turbulent diffusion model was developed by Armienti and Macedonio (1988) using an observed upper air wind data and applied to stronboli eruption of Mt. St. Helens in 1980. Glaze and Self (1991) constructed a turbulent diffusion model considering the vertical wind shear and applied to Usu volcano in 1977 to see distributions of ash fall. Hurst and Turner (1999) developed a 3-D turbulent diffusion model called ASHFALL to predict volcanic ash fall for operational use. In this model, the regional distribution of upper air wind is prepared by RAMS (Regional Atmospheric Modeling System). Turner and Hurst (2001) further combined HYPACT (Hybrid Particle and Concentration Transport Model) with RAMS to improve the model. Heffter and Stunder (1993) developed a transport dispersion model called VAFTAD (Volcanic Ash Forecast Transport and Dispersion) to predict ash plume floating in the air.

A group of worldwide volcanic ash advisory services was organized to form volcanic ash advisory centers (VAACs) by nine organizations under the auspice of the International Civil Aviation Treaty (ICAO). The Tokyo VAAC is one of the nine VAACs, which was established in April 1997 at the Tokyo Aviation Weather Service Center. The Tokyo VAAC operates the Lagrangian and Eulerian models to forecast the position of the volcanic ash clouds (Tokyo Aviation Weather Service Center, 2001).

In parallel with those activities, a real-time volcanic ash plume tracking model called PUFF was developed for the purpose of real-time aviation safety in northeastern Pacific rim including Alaska volcanoes (Tanaka, 1991; Kienle et al., 1991; Dean et al., 1993; Tanaka, 1994; Searcy et al. 1998). It is noted that the PUFF model is the earliest ash tracking model applied for the aviation safety purpose in a real-time operation (Tanaka et al., 1993; Akasofu and Tanaka, 1993). The model is operational under the Alaska Volcano Observatory (AVO) at the Geophysical Institute of the University of Alaska Fairbanks (GI/UAF) since the eruption of Redoubt volcano in 1990. The PUFF model at the University of Tsukuba was applied to the actual eruption of Usu volcano on 31 March 2000 in Hokkaido (Endoh et al., 2001; Tanaka and Yamamoto, 2002) and Miyake-jima Volcano on August 18 2000.

The research product of the PUFF prediction system, including the model simulation and animation graphics of the simulation results, was transplanted to Japan Airlines with the assistance by the Japan Weather Association (JWA). This report describes the latest improvements installed in the PUFF model operational at the Japan Airlines.

2. Description of the model

The volcanic plume prediction model PUFF was constructed in 1991 and reported in detail by Tanaka (1994) and Searcy et al. (1998) as an application of pollutant dispersion models. The model is based on the three-dimensional (3-D) Lagrangian form of the transport-diffusion equation. In the Lagrangian framework, a realization of the stochastic process of plume particles may be described by a random walk process (e.g., Chatfield, 1975). Here, the diffusion is simulated by a sufficiently large number of random variables $r_i(t)$, $i=1 \sim M$, representing position vectors of M particles from the source S of the volcanic crater. The diffusion is superimposed on convective transport and gravitational fallout.

With a discrete time increment, (t=5 minutes), the Lagrangian form of the governing equation may be written as

$$\begin{cases} r_i(0) = S, & i = 1 \sim M, \ for\ t = 0, \\ r_i(t + \Delta t) = r_i(t) + V\Delta t + D\Delta t + G\Delta t, & i = 1 \sim M, \ for\ t > 0, \end{cases} \quad (1)$$

where $r_i(t)$ is a position vector of an i-th particle at time t, V is the local wind velocity to transport the particle, D is a vector containing three Gaussian random numbers for diffusion, and G is the gravitational fallout speed approximated by Stokes Law.

For the computation of convective transport, the wind velocity $V= (u,v,w)$ is obtained from the global Grid Point Values (GPV) provided by Japan Meteorological Agency (JMA). The gridded data are first interpolated in time onto the model's time steps of every 5 minute. A cubic spline method (see Burden et al., 1981) is used to interpolate the wind data from 6 hour interval to the model's time step. Then, the wind velocity at an arbitrary spatial point is evaluated using the 3-D cubic-splines from the nearby gridded data.

The diffusion of the ash particles $D=(c_h, c_h, c_v)$ is parameterized by the random walk process, where the horizontal and vertical diffusion speeds c_h, c_v may be related to the horizontal and vertical diffusion coefficients K_h, K_v. We have repeated diffusion tests with various values of diffusion coefficients, and the resulting dispersals are compared with satellite images of actual dispersals for several volcanic eruptions in the past (Yamagata, 1993; Yamamoto 2000; 2002). With these diffusion tests, we find that the appropriate horizontal and vertical diffusion coefficients are K_h=150 and K_v=1.5 (m^2 s^{-1}), respectively. Note that the values may be different for different volcanoes and for different weather conditions.

The gravitational settling is based on Stokes Law as a function of the particle size r. The fallout velocity $G=(0,0,-v_t)$ is approximated by the terminal speed v_t of plume particles below:

$$\frac{v_t}{v_o} = \frac{r_o}{r}\left[\left\{\left(\frac{r}{r_o}\right)^2 + \frac{1}{4}\right\}^{\frac{1}{2}} - \frac{1}{2}\right]^{\frac{3}{2}} \quad (2)$$

where v_0 (=1.0 m/s) is a reference velocity, and r_0 (=150 μm) is the particle size that separates the inertial range and viscosity range. In the viscosity range, the frictional force of the particle is proportional to v_t, so the terminal velocity becomes a function of r^2. Whereas, in the inertial range, the frictional force is proportional to v_t^2, so the terminal velocity becomes a function of $r^{1/2}$. In the present formulation, the terminal velocity v_t shifts smoothly from the former to the latter separated by r_0.

The actual eruption contains large fragments up to few meters in size as well as fine ash over a continuous particle size to less than 1 μm. Large particles settle out within a short time, so the particle size spectrum shifts toward the smaller particles as time proceeds. Because we are interested in the particles which can travel for several hours, we have assumed that the initial particle size distribution obeys a logarithmic Gaussian distribution centered at 100 μm with its standard deviation 1.0. Thus, about 95% of particles are supposed to have their size between 1 μm and 1 cm. In practice, the particles larger than 1 cm drop quickly within a few time steps of the simulation. The particles less than 100 μm can travel far from the source providing important information of the plume dispersion.

Sufficiently large numbers of particles are contained within the initial vertical column above the crater of the erupting volcano. During the 5 min of a time step, the particles are released constantly in time from the crater in the model.
A simple buoyancy model is considered with initial upward motion w_0 and a constant damping rate λ (=1/60s). When the equilibrium plume height z_2 is given, the initial speed w_0 may be evaluated from z_2, and the vertical plume distribution z may be calculated from the following form:

$$Z = Z_2 - \frac{\omega_o}{\lambda} e^{-\lambda t} \quad (3)$$

Random numbers are generated uniformly in time t for the time step of 5 min, which produces dense plume particles near the top of the plume. The gravitational fallout and convective transport during the 5 min are calculated for a given time t superimposed on the vertical distribution to generate the plume source $S=(x,y,z)$.

In a case of a short-time explosive eruption puff, the ash particles are generated only for the initial time of the time integration. When the eruption continues for certain period of time, the model generates new particles over the same vertical column for every time step during the specified eruption period. For a steady eruption, the particle number tends to increase in the model atmosphere before the plume particles have dropped or crossed the vertical wall of the model domain. Therefore, the number of particles

released at every time step is adjusted in order to draw optimal statistical information from the model products. For this reason, we set the number of the particles released for a time step as 100 in this study. Although it is possible to increase the number toward the limit of the computer capability, the time integration will then be considerably slower, which is a disadvantage for the urgent case. An excessive complication and sophistication are not recommended in the application to the real-time operational prediction.

3. Results

Figure 1 illustrates an example of the ash plume distribution simulated for a hypothetical eruption of Etna Volcano. The simulation started from 21:00 UTC, 28 July 2004, and the ash distribution is for 9 hours after the beginning of the eruption. Plume height in feet is designated by different colors. The model simulation takes about 2 min and the graphics takes about 3 min using the SUN Workstation Ultra 60. After the 5 min of the computation time, we can observe the 3-D animation of the ash plume dispersal during the first 10 hours of the volcanic eruption.

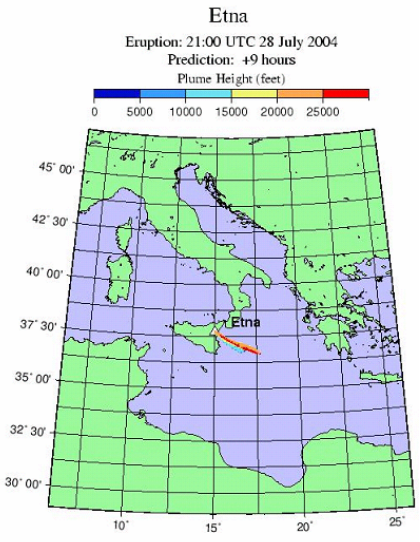

Figure 1. An example of the ash plume distribution simulated for a hypothetical eruption of Etna Volcano. The simulation started from 21:00 UTC, 28 July 2004, and the plot is for 9 hours after the eruption.

The 5 min is the critical time for the aviation safety purpose. The model simulation can be repeated many times whenever a new information, such as the accurate plume height, is reported. The model is applicable to any volcano in the world, and is routinely running for hypothetical eruptions of Sakura-jima, Usu Volcano, Miyake-jima, Mt. Asama, Mt. Fuji in Japan, Redoubt volcano, Augustine volcano in Alaska, and Etna volcano in Italy. Those PUFF model simulations may be seen at the following web site.
(http://air.geo.tsukuba.ac.jp/puff/index.html)

4. Concluding Summary

Volcanic ash cloud floating and traveling in the air is a dangerous object for commercial and non-commercial aircrafts. In order to avoid encounters with ash cloud, a real-time volcanic plume prediction model, called PUFF, has been developed in 1991 and reported by Tanaka (1994) and Searcy et al. (1998) for Alaska volcanoes. The performance of the ash tracking accuracy has been checked whenever actual eruptions occur in the world. The demonstration to real eruptions of Usu volcano and Miyake-jima are reported to assess the performance of the model for tracking the airborne ash clouds for the aviation safety purpose (Tanaka and Yamamoto, 2002). The PUFF model has been updated, and the latest version as described in this report is installed at the flight operation system in the Japan Airlines.

Since the establishment of ICAO's VAACs, volcanic plume tracking becomes operational in the world, providing useful information to aviation industry. Along with the VAACs, we need further to improve the accuracy of the PUFF model by accumulating experience in the flight operations and by establishing timely notification system to pilots with much user-friendly graphic interface.

Acknowledgments

The authors are grateful to the support rendered by Drs. S. Akasofu, K. Dean, J. Dehn of the University of Alaska. Thanks are extended to Mr. S. Shimoda and Ms. S. Yamagata of JWA for their technical support. The authors appreciate Ms. K. Honda for her technical assistance. This research was supported by the IARC/NASDA research project: Modeling the dynamics of volcanic eruption cloud, and by Asahi Breweries Foundation.

References

Akasofu, S.-I. and H. L. Tanaka, Urgent issue of developing volcanic ash tracking model, *Kagaku Asahi*, **5**, 121-124 (in Japanese), 1993.

Armienti, P. and G. Macedonio, A numerical model for simulation of tephra transport and deposition: Application to May 18, 1980, Mount St. Helens eruption, *J. Geophys. Res.*, **93**, 6463-6476, 1988.

Burden, R. L., J. D. Faires, and A. C. Reynolds, *Numerical analysis*, Prindle, Weber and Schmidt, 598 pp, 1981.

Casadevall, T. L., The 1989-1990 eruption of Redoubt volcano, Alaska: Impacts on aircraft operations, *J. Volcanol. Geotherm. Res.*, **62**, 301-316, 1994.

Chatfield, C., *The analysis of time series: An introduction,* Chapman and Hall, 286 pp, 1975.

Dean, K. G., S. I. Akasofu, and H. L. Tanaka, Volcanic hazards and aviation safety: Developing techniques in Alaska, *FAA Aviation Safety Journal*, Vol. 3, No. 1, 11-15, 1993.

Endoh, K., M. Ohno, M. Kunikita, M. Morohoshi, M. Suzuki, Y. Nishimura, D. Nagai, T. Chiba, and I. Tohno, Pheatomagmatic explosions of the 2000 eruption of Usu volcano, *Natural Science Reports, Nihon University*, **36**, 65-73 (in Japanese), 2001.

Glaze, L. S. and S. Self, Ashfall dispersal for the 16 September 1986, eruption of Lascar, Chile, calculated by a turbulent diffusion model, *Geophys. Res. Let.*, **18**, 1237-1240, 1991.

Heffter, J. L. and B. J. B. Stunder, Volcanic ash forecast transport and dispersion (VAFTAD) model, *Computer Techniques*, **8**, 533-541, 1993.

Hobbs, P. V., L. F. Radke, J. H. Lyons, R. J. Ferek, D. J. Coffman, and T. J. Casadevall, Airborne measurements of particle and gas emissions from the 1990 volcanic eruption of Mount Redoubt, *J. Geophys. Res.*, **96**, 18735-18752, 1991.

Hurst, A. W. and R. Turner, Performance of the program ASHFALL for forecasting ashfall during the 1995 and 1996 eruptions of Ruapehu volcano, New Zealand, *J. Geol. and Geophys.*, **42**, 615-622, 1999.

Kienle, J., A. W. Woods, S. A. Estes, K. Ahlnaes, K. G. Dean, and H. L. Tanaka, Satellite and slow-scan television observations of the rise and dispersion of ash-rich eruption clouds from Redoubt volcano, Alaska, *EOS*, Vol. 72, 2, 748-750, 1991.

Onodera, S., Volcanic activity and flight operations, *Aviation Meteorological Notes*, **45**, 13-30, 1997.

Searcy, C., K. Dean, and B. Stringer, PUFF: A volcanic ash tracking and prediction model, *J. Volc. and Geophys. Res.*, **80**, 1-16, 1998.

Suck, S. H., E. C. Upchurch, and J. R. Brock, Dust transport in Maricopa county, Arizona, *Atmos. Environ.*, **12**, 2265-2271, 1978.

Tanaka, H. L., Development of a prediction scheme for the volcanic ash fall from Redoubt volcano, First Int'l. Symp. on Volcanic Ash and Aviation Safety, Seattle, Washington., U.S. Geological Survey Circular 1065: 58, 1991.

Tanaka, H. L., K. G. Dean, and S. I. Akasofu, Predicting the movement of volcanic ash clouds, *EOS*, Vol. 74, No .20, 231-231, 1993.

Tanaka, H. L., Development of a prediction scheme for volcanic ash fall from Redoubt volcano, Alaska, Proc. First International Symposium on Volcanic Ash and Aviation Safety. U.S. Geological Survey, Bulletin 2047, 283-291, 1994.

Tanaka, H.L., and K. Yamamoto, Numerical Simulations of volcanic plume dispersal from Usu volcano in Japan on 31 March 2000. *Earth, Planets and Space*, **54**, 743-752, 2002.

Tokyo Aviation Weather Service Center, Volcanic ash advisory service, Japan Meteorological Agency, *Geophys. Maga. Ser. 2*, Vol. 4, No. 1-4, 2001.

Turner, R. and T. Hurst, Factors influencing volcanic ash dispersal from the 1995 and 1996 eruptions of Mount Ruapehu, New Zealand, *J. Appl. Meteor.*, **40**, 56-69, 2001.

Yamagata, S., *Development of volcanic plume prediction scheme for aviation safety,* Graduation Thesis, Natural Science, University of Tsukuba, 136 pp, 1993.

Yamamoto. K., *Numerical experiment of the volcanic ash cloud dispersion and the justification by satellite image,* Graduation Thesis, Natural Science, University of Tsukuba, 87 pp, 2000.

Yamamoto, K., *Numerical experiments and the assessment for the probability of the volcanic ash dispersal,* Master thesis, Graduate School of Life and Environmental Sciences, University of Tsukuba, 70 pp, 2002.

DETECTING ASH CLOUDS IN TROPICAL ATMOSPHERES

I.M. Watson, W.I. Rose, G.J.S. Bluth.
Dept. of Geological Mining Engineering and Sciences, Michigan Technological University, Houghton, MI, 49931, USA

Abstract

Current mapping and retrieval algorithms applied to volcanic ash are susceptible to interference from atmospheric water vapor. Whilst this interference is well documented and understood in an operational context, quantification of the effect has remained elusive. A forward model has been developed that calculates the effects water vapor has on the 'split-window' ash signal using a combination of a Mie-scattering code embedded in a MODTRAN-based atmosphere (Watson et al., in prep). Initial results from the model suggest a brightness temperature difference 'cost' of 1-3 degrees K when considering an ash cloud from a Northern latitude in a tropical atmosphere.

There is a strong dependence of the effect of water vapor on the optical depth of the cloud: thicker, higher clouds, transmitting less of the contribution of radiance from the underlying surface are less strongly affected than thinner, lower clouds where the surface contribution is more significant. This discovery has important ramifications in terms of ash cloud detection and tracking. (1) Initial stages of eruptive activity are relatively independent of atmospheric conditions, and (2) ash clouds in tropical atmospheres will become less detectable much more quickly as the water vapor signal swamps the negative brightness temperature difference signal.

Theory

A forward model has been developed (Watson et al., in prep.) that embeds a Mie-scattering aerosol model within a MODTRAN atmosphere. The model facilitates investigation of the sensitivity to key parameters that are typically either assumed or acquired from data external to the satellite image. These parameters can include (1) the volcanic ash's chemical composition and particle size distribution (defined by its effective radius, variance and total number of particles) (2) the atmosphere's temperature, pressure and relative humidity profile as a function of height (3) the ash clouds height and depth and (4) the underlying surface's temperature and emissivity (figure 1).

Figure 1.

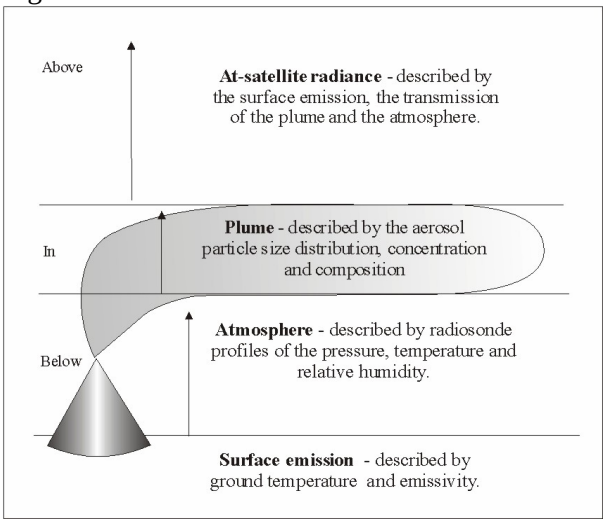

Radiative transfer is treated by the model in three stages; (1) the ground-leaving radiance (defined by the ground temperature and emissivity) is passed through the atmosphere to the base of the plume. The atmospheric contribution to the upwelling radiance is added to yield the radiance at the cloud base; (2) this radiance is transmitted through the cloud, using both the transmission of the atmosphere (MODTRAN-derived) and the plume (Mie model derived) and again atmospheric upwelling radiance is added to yield the cloud-top radiance; (3) finally, the cloud top radiance is the then transmitted

through the portion of the vertical path above the plume and again path-added upwelling radiance from the atmosphere added to yield the at-satellite radiance. This model was tested against a single layer MODTRAN model (without the presence of volcanic aerosol in the 'in' layer) in order to validate the three-layer assumption.

Methodology

The model can be used to determine the effects of water vapor on current detection (Prata 1989 a and b) and retrieval algorithms (Wen and Rose, 1994; Rose et al., 1995, 2000, 2001 and 2003; Yu and Rose 2003) and validate previous atmospheric correction attempts (Yu et al., 2002).

Figure 2.

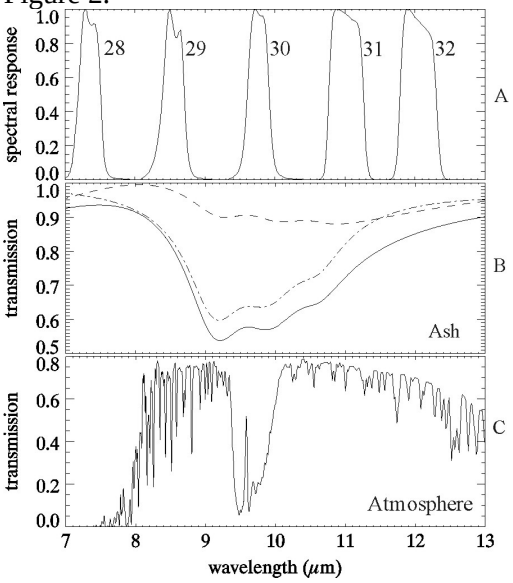

Figure 2. (after Watson et al., 2004) (A) the spectral response functions of the MODIS instrument (B signature of andesitic ash and (C) an example atmospheric transmission spectrum

The forward model is operated through a graphical user interface, allowing the user to input the ash, cloud and atmospheric data into the model. The model then calculates the at-satellite radiance for the given parameters. Separate transmission spectra for just andesitic ash and a clear atmosphere can be seen in figure 2.

The split window algorithm calculates the brightness temperature difference channels 31 and 32 of the Moderate Resolution Imaging Spectroradiometer (MODIS), which are analogous to channels 4 and 5 of the Advanced Very High Resolution Radiometer (AVHRR) and the Geostationary Operational Environmental Satellite (GOES). It can be seen from figure 2 that between 11 and 12 μm the slopes of the two transmission spectra are in opposition. Therein lies the answer to how the split window algorithm is affected by water vapor; if the two spectra are convolved (multiplied together) the ash's spectral signature, what we are using to detect the presence of ash, is washed out by water vapor. The more water vapor is added the more the ash signal is hidden.

Example results were derived using a Northern latitude and tropical atmosphere for comparison. At-satellite radiances were derived for both cold, dry and warm, wet atmospheres. In both cases 2.0 μm andesite ash particles in a lognormal distribution (with a variance of 0.74) were used to represent loading of the atmosphere at a height of 10 km and a cloud thickness of 1 km. Preliminary results are shown below.

Results

All other things being equal (including ground temperature and emissivity) the presence of water vapor reduces the positive slope of the at-satellite radiance spectrum. This effect can be more strongly seen if the radiance value is converted to brightness temperature using the Planck function (figure 3.). Here, the wavelength range is reduced to highlight the area between 10 and 13 μm that the split window retrieval uses to locate ash – the brightness temperature difference (BTD) algorithm (Prata et al., 1989 a and b; Wen and Rose, 1994). In this example the change in BTD is about 1.8 K. This has a significant effect on the detectability of volcanic ash as much of the fringes of typical volcanic ash

clouds have BTD values of this order or less.

Figure 3.

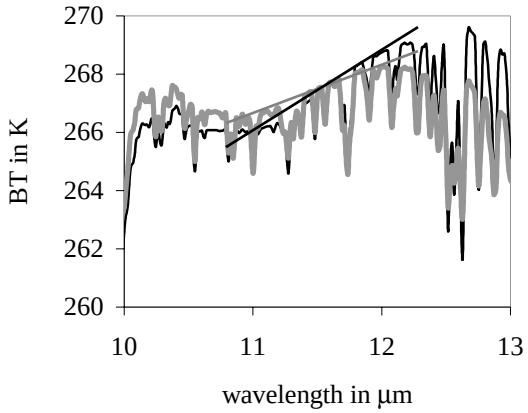

Figure 3. Brightness temperature (BT) spectra for 2.0 µm andesitic ash in a wet (grey line) and dry (black line) atmosphere. Note again the change in gradient between 11 and 12 µm for the two examples, as indicated by the straight lines.

It is possible to show how significant a ~ 2K effect on the detection of volcanic ash by taking a known northern latitude eruption and 'moving it' to the tropics (figure 4). Such an example has been calculated for the September 1992 Mt. Spurr eruption (Watson et al., in prep). Figure 4 shows the Spurr eruption cloud captured by AVHRR at 1700 UT on 17th September 1992 (see Schneider et al., 1995 for more details) in (a) an atmosphere that represents, as accurately as possible, the Aleutian atmosphere into which the cloud was injected and (b) a tropical atmosphere above Guadeloupe that causes a 2K suppression of the brightness temperature difference signal. What is immediately apparent is that the are of the detectable part of the cloud is dramatically reduced (by the order of 50 %). A 2 K cost is by no means extreme (3.5 K has been observed in some model runs) and, can clearly be seen to remove significant fringes from the cloud when using zero as a BTD cut off.

Figure 4.

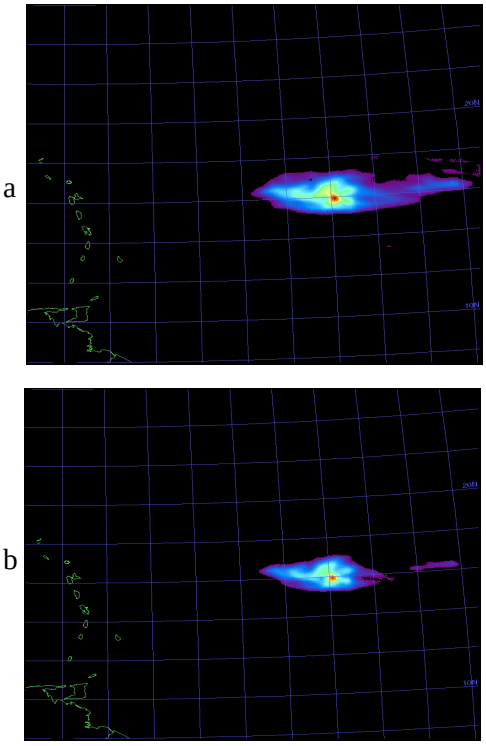

Figure 4. Example ash map indicating the change in area for the September 1992 Mt. Spurr eruption cloud (above the Caribbean volcanic arc) with enough water vapor in the atmosphere to change the BTD by (a) 0 and (b) -2 K respectively.

Preliminary conclusions

Forward modeling can be used to quantitatively determine the effects of different water vapor concentrations on the 'split-window' signal. Water vapor more strongly affects clouds that are optically thinner as relative proportions of signal from the underlying ground (and water vapor) increase. Lower (optically thick) clouds with larger particles (per constant volume) will be more strongly affected than higher clouds with smaller particles. Clouds with larger particles (of equivalent mass/volume) will be more strongly affected than clouds with smaller particles. Thus, water vapor effects are a complex function of water vapor content, cloud height, cloud opacity and

particle size and *must* be treated as such. The 'cost' in BTD varies from -0.8 (atypical) to 3.5 K and usually ranges from +1 to +3 K in clouds of optical depth 0.2 to 0.9. Cloud areas and tonnages can be reduced to 10% or less of their high latitude analogues (Watson et al., in prep).

References

Prata, A.J., Infrared radiative transfer calculations for volcanic ash clouds, *1989a Geophysical Research Letters, Vol. 16, pp. 1293-1296*

Prata, A.J., Observations of volcanic ash clouds in the 10-12 m window using AVHRR/2 data, *1989b, International Journal of Remote Sensing, Vol. 10, pp. 751-761*

Rose, W I, D. J. Delene, D. J. Schneider, G. J. S. Bluth, A. J. Krueger, I. Sprod, C. McKee, H. L. Davies and G. G. J. Ernst, 1995, Ice in the 1994 Rabaul eruption cloud: implications for volcano hazard and atmospheric effects, *Nature, 375: 477-479*.

Rose, W I, G J S Bluth and G G J Ernst, 2000, Integrating retrievals of volcanic cloud characteristics from satellite remote sensors--a summary, *Philosophical Transactions of Royal Society, Series A, vol. 358 no 1770, pp. 1585-1606.*

Rose, W I, G J S Bluth, D J Schneider, G G J Ernst, C M Riley and R G McGimsey 2001, Observations of 1992 Crater Peak/Spurr Volcanic Clouds in their first few days of atmospheric residence, *Journal of Geology, 109: 677-694.*

Rose, W I, Y Gu, I M Watson, T Yu, GJS Bluth, A J Prata, A J Krueger, N Krotkov, S Carn, M D Fromm, D E Hunton, G G J Ernst, A A Viggiano, T M Miller, J O Ballentin, J M Reeves, J C Wilson, B E Anderson D Flittner, 2003, The February-March 2000 eruption of Hekla, Iceland from a satellite perspective, *AGU Geophysical Monograph 139: Volcanism and the Earth's Atmosphere, ed by A Robock and C Oppenheimer, pp. 107-132. ISBN 0-87590-998-1*

Schneider, D. J., W. I. Rose and L. Kelley, 1995, Tracking of 1992 eruption clouds from Crater Peak/Spurr Volcano using AVHRR, *U. S. Geol. Surv. Bull. 2139 (Spurr Eruption, edited by T. Keith), 27-36.*

Watson, I.M., Realmuto, V.J., Rose.,W.I., Bluth G.J.S., Forward modeling of volcanic cloud transmissions through different atmospheres, *in preparation for Journal of Geophysical Research – Atmospheres*

Watson, I.M., Realmuto, V.J., Rose, W.I., Prata, A.J., Bluth, G.J.S., Gu, Y., C. E. Bader, Yu, T., 2004 Thermal infrared remote sensing of volcanic emissions using the Moderate Resolution Imaging Spectroradiometer (MODIS), *Journal of Volcanology and Geothermal Research, Vol. 135, pp. 75-89*

Wen, S and W I Rose, 1994, Retrieval of Particle sizes and masses in volcanic clouds using AVHRR bands 4 and 5, *Journal of Geophysical Research, 99:5421- 5431.*

Yu, T W I Rose and A J Prata, 2002, Atmospheric correction for satellite-based volcanic ash mapping and retrievals using "split window" IR data from GOES and AVHRR, *Journal of Geophysical Research, 106: No D16, 10.1029.*

Yu, T and W I Rose, 2000, Retrieval of sulfate and silicate ash masses in young (1-4 days old) eruption clouds using multiband infrared HIRS/2 data, *AGU Monograph 116 --Remote Sensing of Active Volcanism, ed by P Mouginis-Mark, J Crisp and J Fink, pp. 87-100.*

ERUPTION CLOUD ECHO MEASURED WITH C-BAND WEATHER RADAR

Yoshihiro Sawada
Faculty of Science, Hokkaido University, Sapporo, Japan

Abstract

Careful inspections of radar echo-data in Japan showed that eruption clouds by fairly smaller sized eruptions can be registered with C-band weather radars. Aggregation of fine ash particles and water-coated ash particles inside eruption clouds are considered as the reason of detection.

Introduction

C-band weather radars are commonly operated for weather observation in many countries having active volcanoes, and eruption clouds by strong volcanic eruptions have been registered as radar echoes. However, almost no observation is reported for smaller eruption cloud. Radar data of C-band weather radars in Japan were inspected and several echoes were obtained (Sawada, 2003b). The reason of detection is considered.

Report of Eruption Cloud with Weather Radar

According to the database of Smithsonian Institution during a period since 1970 through 2003, observations of eruption clouds as echoes with weather radars are reported. In addition to the data, the author inspected and gathered radar data in Japan obtained with weather radars of Japan Meteorological Agency (JMA). Results in papers are inspected, too. The volcanoes of which eruption clouds were detected as radar echoes counted 13 with 23 eruptions as shown in Table 1.

Wavelength of C-band radar (wavelength of 5 cm) is basically too long to detect fine ash particle (mm-μm in size) of eruption cloud. In general, it is considered that major portion of eruption cloud composed with accumulated large sized particles, high distribution-density of particles and high content of water/ ice particles can be detected as echoes. Actually, the big eruption columns such as 1980 Mount St. Helens, 1991 Pinatubo and 1992 Spurr were well detected, and major extents & top altitudes were well monitored with time (Smithsonian Institution Web site, Harris et al.,1981 and Oswald et al.,1996). Doppler radar system can measure movements of ash/ water particles, and is very effective to monitor small eruption clouds. Small & not so dense ash plumes lower than 5 km in heights from Popocatepetl, Mexico were well detected (Table 1).

Observation Result in Japan

ECE (Eruption Cloud Echo) by Large-Sized Eruption

JMA operates 29 C-band weather radars in Japan; 20 stations with wavelength of 5.7cm, power of 250 - 300 kW & detection range of 300 km, and 9 airport stations with power of 200 kW & detection range of 100 km.

Eruption clouds higher than 9 km by four strong eruptions of 1973 Tyatya, 1977 Usu, 1986 Izu-Oshima and 2000 Miyake-jima were obtained as clear ECEs by the radars (Table 1).

1973 July 14 Tyatya Eruption

ECEs were observed with Kushiro radar (ca. 220 km SW of the volcano). Eruptions simultaneously occurred from two craters (Abdurakmanov et al., 1999) and the double ECEs were clearly monitored (Photo 1, Japan Meteorological Agency, 1974)).

1977 August 7, 8 & 9 Usu Eruption

ECEs were observed with radars of Sapporo (ca. 70 km NE of the volcano) and Hakodate (ca. 80 km SSW). Analysis of PPI (Plan-Position Indicator) and RHI

Photo 1 Double eruption cloud echoes (white arrows) of July 14, 1973 Tyatya Eruption tracked with Kushiro weather radar (Japan Meteorological Agency, 1974)

Table 1. List of volcanoes of which eruption clouds were detected with radars during 1970 - 2003
*: Visual Measurement; ** : Doppler Radar; *** : X-band Radar

Observation Date	Volcano	Max. Height of Eruption Cloud
1970 May 5	Hekla, Iceland	15 [(1)] km
1973 July 14, 17, 18	Tyatya (Kunashir)	9 [(2)]
1976 Jan. 23	Augustine, Alaska	14 [(1)]
1977 Aug. 7, 8, 9	Usu, Hokkaido	9.7 [(3)]
1980 May 8, June, July	Mt St. Helens (Washington)	>25 [(4)]
1981 Apr. 9	Hekla (Iceland)	6.6 [(1)]
1981 May 15	Pagan (Mariana Islands)	18 - 20 [(1)]
1984 July 7	Sakura-jima (Kyushu)	2.1* [(5)]
1986 Nov. 21	Izu-Oshima (Izu Islands)	10 - 12 [(6)]
1991 Jan. 17	Hekla (Iceland)	11.5 [(1)]
1991 June 12, July 27, Aug. 5 - 11	Pinatubo (Philippines)	16.5 [(1)(7)]
1991 June 3, 8, 12	Unzen (Kyushu)	6.5 [(8)(9)]
1992 June 27, Aug. 18 - 21, Sep. 17	Spurr (Alaska)	18 [(1)]
1992 Aug. 20, 21, Sep.	Pinatubo (Philippines)	9 [(1)]
1992 Feb. 5	Unzen (Kyushu)	Not obs.* [(8)]
1993 May 21	Unzen*** (Kyushu)	4* [(10)]
1996 July 16	Sakura-jima** (Kyushu)	0.6* [(11)]
1996 Dec. 14	Sakura-jima (Kyushu)	Not obs.* [(12)]
1998 Feb. 11, Sep. 8, 22, Oct. 17	Popocatepetl** (Mexico)	4* [(1)]
1999 Mar. 11, 18, Apr. 4, 11	Popocatepetl** (Mexico)	Not obs.* [(1)]
2000 Feb. 26 – 27	Hekla (Iceland)	12* [(13)]
2000 Mar. 31	Usu (Hokkaido)	3.5* [(14)]
2000 Aug. 10, 18, 29	Miyake-jima (Izu Isls.)	16 - 17* [(15)]

(1) Smithsonian Institution, (2) JMA (1974), (3) JMA (1980), (4) Harris et al. (1981), (5) Uehara et al. (1985), (6) Seis. & Volc. Dep. (1987), Takano (1987), (7) Oswalt et al. (1996), (8) Niina (1992), Fukuoka DMO (1996), (9) Tanegashima WS (1992), (10) Arao et al. (1996), (11) Fukui et al. (1997), (12) Tanegashima WS (1998), (13) Lacasse et al. (2004), (14) by the courtesy of Sapporo DMO, Sawada (2003b), (15) by the courtesy of Tokyo DMO, Sawada (2003b) Where, JMA: Japan Meteorological Agency, Seis. & Volc. Dep.: Seismological and Volcanological Department, DMO: District Meteorological Observatory and WS: Weather Station.

(Range Height Indicator) data showed horizontal moving velocities and approximate vertical profiles of eruption columns, respectively (Japan Meteorological Agency, 1980).

1986 November 21 Izu-Oshima Eruption

ECEs were observed with 4 radars; Fuji (wavelength of 10.4 cm & detection range of 500 km, ca. 100 km NW of the volcano, operated by 1999), Tokyo (ca. 110 km NNE), Haneda airport (ca. 100 km NNE) (Seismological and Volcanological Department, 1987) and Nagoya (ca. 220 km WNW) (Takano, 1987). Extent of the ECE v.s. that with satellite image was under the ratio of one : several tens (Sawada, 2003a).

2000 August 18 Miyake-jima Eruption

ECEs were tracked with Shizuoka radar (ca. 145 km NW of this volcano) (by the courtesy of Tokyo District Meteorological Observatory, Sawada、2003b).

ECE by Small-Sized Eruption

7 ECEs by small eruptions with cloud-top lower than 4 km were detected in Japan (Table 1), while 2 ECEs of 1993 Unzen & 1996 July Sakura-jima are with X-band and Doppler radars, respectively.

Sakura-jima (South of Kyushu)

Kagoshima airport radar (ca. 25km NNE of the volcano) detected ECE on July 7, 1984 as shown in Fig. 1 (Uehara et al., 1985). Its cloud top was 2.1km and extent of ECE was about 3 km x 3km over the crater.

Weak & small ECEs were obtained on December 14, 1996 with Tanegashima radar (ca. 102 km SSE of the volcano) (Fig. 2). The eruption occurred before dawn, and its cloud-top was not observed due to darkness. However, the size of eruption was at ordinary level (Tanegashima Weather Station, 1998).

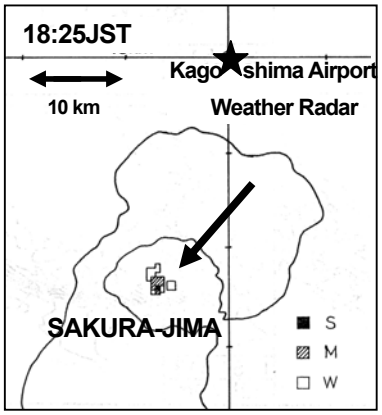

Fig. 1 Eruption cloud echo (solid arrow) of Sakura-jima eruption on July 7, 1984 obtained with Kagoshima airport weather radar (Uehara et al., 1985 (modified))

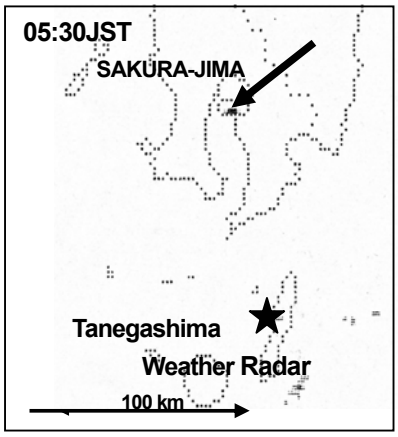

Fig. 2. Eruption cloud echo (solid arrow) of Sakura-jima eruption on December 14, 1996 with Tanegashima radar (Tanegashima Weather Station, 1998 (modified))

Unzen (SW of Kyushu)

ECEs accompanied by pyroclastic flows on June 3 & 8, 1991 and by eruptions with lapilli-ejections on June 12 were obtained with Fukuoka radar (about 80 km N of the volcano). ECEs in February, 1992 were very weak ones. (Niina, 1992, Fukuoka District Meteorological Observatory, 1996). The ECEs on June 8 were also registered with Tanegashima weather radar (ca. 235 km SSE) of the volcano (Tanegashima Weather Station, 1992). The ECEs on June 3 drifted eastward and could be tracked across the Ariake Inland Sea reaching over Kumamoto City, ca. 36km ENE of the volcano (Fig. 3).

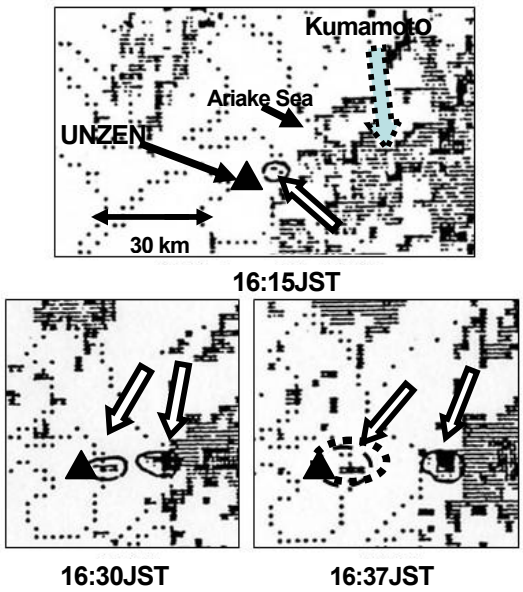

Fig. 3. Eruption cloud echoes of pyroclastic flows (white arrows) at Unzen on June 3, 1991 tracked with Fukuoka weather radar (Niina, 1992, Fukuoka District Meteorological Observatory, 1996 (modified))

Usu (SW of Hokkaido)

Phreatomagmatic eruptions occurred with 3.5 km high eruption clouds on March 31, 2000. Only possible small echoes (one-two pixels) moving eastward were detected twice on the day with Hakodate weather radar (ca. 70 km S of the volcano) (by the courtesy of Sapporo District Meteorological Observatory, Sawada, 2003b).

Discussion

Why can C-band weather radar observe ECEs of small volcanic eruptions ?

Cloud top of June 8, 1991 Unzen ECE with RHI was 6.5 km and radar reflection from the upper ECE was weaker than that from the lower (Niina, 1992). He considered that weaker reflection was due to fall out of ash particles from the upper cloud, while those fallen particles accumulated at the lower ECE causes stronger radar reflections.

Arao et al. (1996) observed about 4 km tall ash clouds accompanied by pyroclastic flows with X-band radar (wavelength of 3.2 cm) at Unzen on May 21 1993. The radar reflection from the upper ECE was stronger than that from the lower. They discussed that ash particles in the upper cloud were aggregated and were coated with water due to cooling of water-vapor under high humidity in eruption cloud & upper surrounding air. At the lower cloud, fallen ash particles dispersed due to low humidity conditions in and outside the ECE. They showed that radar reflections from water-coated particles increase compared with those from dry particles.

ECEs of February, 2000 Hekla Eruption were very well and for long time tracked with C-band radar, and the effects with high contents of water or ice particles are discussed for the reason (Lacasse et al., 2004).

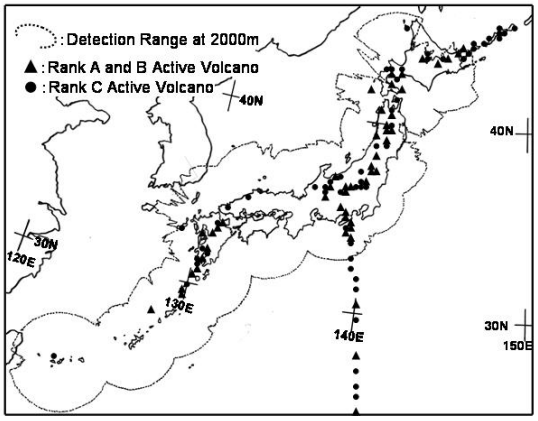

Fig. 4. Overlay of the detection range at 2000m of JMA's weather radar network and active volcanoes in Japan. (after instruction data of Japan Meteorological Agency)

Small and possibly thin ECEs of ash clouds by pyroclastic flows at Unzen on June 3, 1991 could be tracked at east-side around Kumamoto city , about 34 km from the volcano (Fig. 3). There were rain clouds in the area, and high humidity may cause water-coatings & aggregation of fine ash particles in the small ECEs.

In addition to water vapor content in eruption clouds, high water contents due to phreatomagmatic eruptions, existence of underground water, and high humidity conditions of surrounding air may accelerate to generate water-coated ash particles and to aggregate ash particles in eruption clouds. These eruption clouds will be detected and tracked with C-band weather radars.

Conclusion

Not only ECEs by large-sized eruptions, but also by small volcanic eruptions could be detected by C-band weather radars. It is considered that water coatings and aggregations of ash particles enabled to be detected as ECEs. However, it is hard to discriminate ECEs from rain clouds.

The detection range of JMA's radar network can cover most of active volcanoes in Japan (Fig. 4). Recently, airport weather radars are being reinstalled as doppler type systems. By the network, it is expected to observe ECEs by not only radars near volcanoes but also those far from eruption sites. Detection capability of ECEs by the network is up to the strength of eruption, weather condition and topographical condition between radar sites and volcanoes, but further high detection rate is expected with the combinations of weather radars. It will be possible to detect ECEs of eruption clouds higher than 5 km except insular volcanoes in the ocean with JMA's C-band weather radar network under good conditions.

Acknowledgement

The author gratefully acknowledges to the personnel at radar observatories of Japan Meteorological Agency for providing of the radar data for this research work.

References

Abdurakmanov, A. I. and Steinberg, G. S. (1999): Tyatya volcano – Morphology and geological structure of the volcano. Institute of Volcanology and Geodynamics Russian Academy of Natural Science, 1-20

Arao, K., Iwasaki, H., Fukui, K., Hayakawa, Y. and Takeda, T. (1996): A case study of structure and evolution of the ash cloud derived from Unzen pyroclastic flow using radar data. Bulletin of Volcanological Society of Japan, v. 41, 149-158 (in Japanese with English abstract and captions)

Fukuoka District Meteorological Observatory (1996): Pyroclastic flow on June 8, 1991 of Unzen observed with weather radar. Memoirs of Fukuoka Meteorological Observatory, v. 51, 71-75 (in Japanese)

Fukui, K., Mori, T. and Churei, M. (1997): Observation of volcanic plume from Sakura-jima with doppler radar. Abstract of Session of Meteorological Society of Japan, v. 71, 226 (in Japanese)

Harris, D. M., Rose W. I. Jr., Roe R. and Thompson M. R. (1981): Radar observations of ash eruptions at Mount St. Helens volcano, Washington. The 1980 Eruptions of Mount St. Helens, Washington: U. S. Geological Survey Professional Paper, v. 1250, 323-333

Japan Meteorological Agency (1974): Volcanic activities after the 1973 June 17 Earthquake off Nemuro Peninsula. Technical Report of Japan Meteorological Agency, v. 87, 3, 17-18 & 101-102 (in Japanese)

Japan Meteorological Agency (1980): The 1977 August – 1978 December Eruption of Usu. Technical Report of Japan Meteorological Agency, v. 99, 7-14 & 193 (in Japanese)

Lacasse, C., Karlsdottir, S., Larsen, G., Soosalu, H., Rose, W. I., and Ernst, G. G. J. (2004): Weather radar observations of the Hekla 2000 eruption cloud, Iceland. Bulletin of Volcanology, v. 66, 457 – 473

Niina, Y. (1992): Radar echoes obtained by Fukuoka weather radar, of eruption clouds with pyroclastic flows at Fugen-dake, Unzen. Radar-Kansoku-Gijutsu-Shiryou of Japan Meteorological Agency, v. 41, 41-52 (in Japanese)

Oswalt, J. S., Nichols W. and O'hara J. F. (1996): Meteorological observations of the 1991 Mount Pinatubo Eruption. Fire and Mud: Newhall, C. G. and Punongbayang R. S. edt., Philippine Institute of Volcanology and Seismology and University of Washington Press, 625-636

Sawada, Y. (2003a): Study on observation and analysis of eruption cloud with imagery of Geostationary Meteorological Satellite (HIMAWARI). Journal of Meteorological Research of Japan Meteorological Agency, v. 55, 57-152 (in Japanese with English abstract and captions)

Sawada, Y. (2003b): Eruption cloud echo observed with JMA's C-band weather radar. Sokko-jihou of Japan Meteorological Agency, v. 70, 119-169 (in Japanese)

Seismological and Volcanological Department (1987): The 1986 Eruption of Izu-Oshima. Special Report Series of Natural Disasters of Japan Meteorological Agency, v. 1 in 1987, 90-91 & 148-152 (in Japanese)

Smithsonian Institution Website: http://www. volcano. si.edu (accessed 2004-07-17)

Takano, S. (1987): Recent Radar Observations (84)— Echoes by the Izu-Oshima Eruption Clouds. Geophysical Notes of Tokyo District Meteorological Observatory, v. 88, 1 (in Japanese)

Tanegashima Weather Station (1992): Echoes by the large pyroclastic flows of Fugen-dake, Unzen (1991 June 8). Radar-Gijutu-Uchiawasekai- Shiryou of Japan Meteorological Agency in 1991, 74 & 77 (in Japanese)

Tanegashima Weather Station (1998): Radar echoes possibly by eruptions of Sakura-jima. Radar-Gijutsu-Uchiawasekai-Shiryou of Japan Meteorological Agency in 1997, 27-28 (in Japanese)

Uehara, M., Taira, T. and Fukunaga, S. (1985): Weather radar system at Kagoshima airport station. Radar-Kansoku-Gijutsu-Shiryou of Japan Meteorological Agency, v. 34, 28-32 (in Japanese)